THE CONTRIBUTION OF SOMATOSTATIN-EXPRESSING (SOM+) INTERNEURONS TO THE PTEN MODEL OF AUTISM SPECTRUM DISORDER

By

Timothy W. Holford

A Dissertation Submitted to the Faculty of the

Charles E. Schmidt College of Science

In Partial Fulfillment of the Requirements for the Degree of

Doctor of Philosophy

Florida Atlantic University

Boca Raton, FL

August 2021

THE CONTRIBUTION OF SOMATOSTATIN-EXPRESSING (SOM+)

INTERNEURONS TO THE PTEN MODEL OF AUTISM SPECTRUM DISORDER

by

Timothy W. Holford

This dissertation was prepared under the direction of the candidate's dissertation advisor, Dr. M. McLean Bolton, Department of Biological Sciences, and has been approved by all members of the supervisory committee. It was submitted to the faculty of the Charles E. Schmidt College of Science and was accepted in partial fulfillment of the requirements for the degree of Doctor of Philosophy.

SUPERVISORY COMMITTEE:

M. McLean Bolton, Ph.D.
Dissertation Advisor

Ken Dawson-Scully
Ken Dawson-Scully (Jul 17, 2021 11:11 EDT)

Ken Dawson-Scully, Ph.D.

Robert W. Stackman Jr.
Robert W. Stackman Jr. (Jul 18, 2021 08:18 EDT)

Robert W. Stackman Jr., Ph.D.

G.T. Macleod
G.T. Macleod (Jul 24, 2021 12:39 EDT)

Gregory MacLeod, Ph.D.

SL Milton
Sarah Milton (Jul 24, 2021 12:54 EDT)

Sarah Milton, Ph.D.
Chair, Department of Biological Sciences

Teresa Wilcox

Teresa Wilcox, Ph.D.
Interim Dean, Charles E. Schmidt
College of Science

Robert W. Stackman Jr.
Robert W. Stackman Jr. (Jul 18, 2021 08:18 EDT)

Robert W. Stackman Jr., Ph.D.
Dean, Graduate College

July 26, 2021

Date

ACKNOWLEDGEMENTS

I have many people to thank for their assistance during my Ph.D. First, my mentor, Dr. McLean Bolton, has been so supportive from the very beginning. From her acceptance and inclusion the first time rotating through her lab, through graciously adopting me even after I had joined a different lab then needed to switch halfway through my second year, all the way until now, she has been a strong advocate for me and my science. She directed me when needed and gave me the space to discover at other times. She trusted me with equipment and techniques so much that gave me the opportunity to teach and mentor others, which I greatly appreciated. All the while, she had treated me as person first, with compassion and understanding, and not primarily as a data gatherer. Dr. Bolton has fostered an environment of excellence and inclusion in her lab, and I am excited to continue my post doc here to see it continue to blossom.

Next, my committee members, Drs. Ken Dawson-Scully, Robert Stackman, and Greg MacLeod, were instrumental to my success. They were more than simply members of my committee; rather, each was interested in my work and my development as a scientist. They did their best to make themselves available to me for encouragement and advice, and though I did not give them the opportunity to provide this support as many times as I may have liked, at each occasion they were more than willing to offer guidance and wisdom, for which I am very grateful. I look

forward to continuing to rely on their experience and knowledge, and intend to make the most of their kindness and support in the future.

Finally, the environment created by the partnership of Florida Atlantic University and the Max Planck Florida Institute for Neuroscience was of incredible value. Indeed, the wealth of scientific discussion and interaction with other neuroscientists within and between institutes, as well as among the invited speakers and visiting scientists, inspired and directed my thoughts on multiple occasions toward better research. This is especially the case within the Bolton lab, as the other members our lab continually support and inspire one another, and I am tremendously grateful for the assistance in experiments that I received from multiple lab members. All of these factors have had such a positive impact and created an experience so enticing that I find myself not even wanting to leave after graduation.

ABSTRACT

Author:	Timothy W. Holford
Title:	The Contribution of Somatostatin-Expressing (SOM+) Interneurons to the PTEN Model of Autism Spectrum Disorder
Institution:	Florida Atlantic University
Dissertation Advisor:	M. McLean Bolton, Ph.D.
Degree:	Doctor of Philosophy
Year:	2021

Autism spectrum disorder (ASD) is a complex disorder with large individual variability, where every case has differences in the type and severity of symptoms. Despite the recent increase in diagnoses, scientists have advanced considerably less in their understanding of the mechanisms of ASD because few individual genes that are implicated in ASD are mutated in much more than 1% of patients. One proposed mechanism is that the dysfunction of GABAergic interneurons may play a role in the development and progression of the disorder by interrupting the excitatory and inhibitory balance of neural networks. In our research, we elucidate the role of one class of interneurons in ASD by knocking out a high-risk gene (phosphatase and tensin homologue on chromosome ten, or PTEN) selectively in somatostatin-expressing (SOM+) interneurons. Since many symptoms of autism spectrum disorder present themselves as social anxieties, we test our mouse model in a

variety of settings to observe social interaction and social preference, anxiety-like behavior, and repetitive stereotyped behavior. We found that in the SOM+ conditional knockout of PTEN, mice had elevated levels of anxiety and fear recall, suggesting a potential disruption of amygdala function. We then investigated potential dysfunction at the cellular and circuit levels using confocal microscopy, electrophysiology, and 2P local circuit mapping. We found that SOM+ cells lacking PTEN were overgrown morphologically, with larger cell bodies and larger, more complex dendritic arbors. Additionally, SOM+ cells in the central amygdala (CeA) lacking PTEN had elevated levels of excitatory drive from the basolateral amygdala (BLA) as well as a drastic disruption of lateral inhibition within the CeA, seen by decreased connection probability and reduced inhibitory post synaptic currents. Given what is known about central amygdala circuitry, these deficits in CeA SOM+ neuron activity conceivably underlie the fear and anxiety-related phenotype observed in mice with a conditional SOM+ PTEN knockout.

DEDICATION

All of my work is primarily dedicated to the Lord Jesus, the Messiah, without whom I would certainly not be here today. I am grateful to Him for the ability to think and reason, and I am honored to be able to steward the gifts and talents I have been given and put them to good use. His peace has been an invaluable comfort through many difficult seasons and the endurance that I have found in Him allowed me to push forward through many failures. I thank God for science and I am excited to continue pursuing understanding.

Next, it is dedicated to my girls. My beautiful, patient, supportive and encouraging wife, Ashley, and sweet, spirited, lovely baby child, Emery, have been a welcome respite following long days and nights at the lab. Ashley has graciously and patiently put up with my graduate student salary for many years, and she has endured many of nights and weekends of taking care of herself and a baby alone while I work until after midnight, especially in the last year. She is a hard worker and a selfless caregiver, and I am extremely grateful to her. My daughter has been a tiny bundle of joy with a natural curiosity that will flourish inside a beautiful child. I have loved the easy stuff and the hard stuff, and I look forward to spending even more time with her as I pray that all my effort here will serve to benefit her as well.

Additionally, this is dedicated to my family who have stood by me my whole life and been helpful and encouraging even in the times when it looked like I was

squandering my abilities and throwing away my chances. They believed in me and kept me going to do something worthwhile and explore my creativity and curiosity. All of my siblings are simply amazing and we all think that the others have the cooler and more impressive jobs, with an empathy, compassion, and work ethic that we learned from our parents as they raised us to grow into all that God made us to be. My family-in-law has also been tremendously supportive, and they have been in my corner from the beginning, assisting Ashley and I in more ways than I will ever be able to repay, all out of their love and generosity rooted in Christ.

Finally, all of my friends whose loyal love has made the whole process still a great part of a fun life. Even when things were difficult, I was able to relax and enjoy it as part of my story. All of my friends at Christ Fellowship, and especially those in the middle and high school student ministries, reminded me of my ultimate purpose and made every Wednesday night a great way to give back and live a life that truly makes a difference for students. The high school guys I mentored for 5 years looked up to me and allowed me to be an example of a Christian with a brain. Similarly, I have gotten tons of opportunities to volunteer with amazing people at Christ Fellowship to directly benefit the community and add value to countless individuals. They all kept me grounded and focused on what is really most important, all while encouraging me to work hard and finish strong.

THE CONTRIBUTION OF SOMATOSTATIN-EXPRESSING (SOM+)

INTERNEURONS TO THE PTEN MODEL OF AUTISM SPECTRUM DISORDER

LIST OF FIGURES

LIST OF EQUATIONS

CHAPTER 1: INTRODUCTION

Overview of Project

Scientific studies into the molecular, cellular, and behavioral consequences of neurological disorders are critical for better understanding the progression and expression of disorders as well as for the ability to develop and implement therapeutic interventions. Studies that coordinate behavioral experiments with molecular and cellular dysfunction are needed to establish greater connections between neuronal circuitry and behavioral phenotypes. Without investigating and identifying the underlying cellular and circuit-level aberrations that result from mutations associated with neurological disorders, attempts at therapeutic interventions may end up exacerbating some circuit dysfunction or creating dysfunction elsewhere. In this project, we chose to focus on a particular subtype of neurons and their role in a mouse model of a neurological disorder. Specifically, we explore the contribution of somatostatin (SOM)-expressing interneurons to the phosphatase and tensin homolog (PTEN) model of autism spectrum disorder (ASD).

While autism spectrum disorder is very complicated, and many genes have been shown to affect the development and progression of the disorder, we chose to focus on the mouse model of PTEN due to its established behavioral phenotype and PTEN's specific role in regulating other ASD candidate genes. We began by breeding mice to conditionally knock out the expression of PTEN only in SOM-expressing

interneurons using a Cre:lox system. Mice in which Cre recombinase was expressed under the SOM promoter were bred with mice in which loxP sites were inserted on both sides of the PTEN gene, so that only in cells that expressed somatostatin (SOM), the expression of PTEN would be silenced. Additionally, we included a Cre-dependent TdTomato reporter gene, so that SOM-expressing cells would fluoresce red when illuminated with green light, in order to identify them.

The first aim was to identify the behavioral consequences of knocking out PTEN from SOM-expressing interneurons, to see which aspects of the aberrant behavior observed in the PTEN mouse model were dependent on PTEN's function specifically in somatostatin-expressing neurons. We ran the mice through a battery of tests that are commonly used for assessing behavioral phenotypes, especially those associated with autism spectrum disorders, including sociability-, restricted/repetitive motion-, sensory integration-, contextual fear-, and anxiety-related behaviors. We found that, unlike the PTEN mouse model where all cell types are affected by PTEN dysfunction, the conditional SOM-cell PTEN knock out mice only showed deficits in fear- and anxiety-related behaviors.

Our second aim was to identify the circuit-level disruptions that may underlie the behavioral phenotype observed in the conditional PTEN knock out mice. As brain areas with large populations of SOM-cells would likely be more disturbed by a SOM-specific mutation, and because of the detected fear and anxiety-related deficits, we focused our physiological investigations in the central amygdala (CeA) since it is a dense cluster of inhibitory interneurons, including SOM-expressing neurons, that helps gate the output of the amygdala and regulates

aspects of fear and anxiety-related behaviors. We found that SOM-cells lacking PTEN in the CeA were enlarged morphologically and showed disrupted patterns of synaptic connectivity and synaptic strength compared to wild-type SOM neurons.

Taken together, our work shows that the deletion of PTEN from SOM-expressing interneurons results in disruptions to local inhibitory signaling in the central amygdala and gives rise to fear and anxiety-related deficits that are common in autism spectrum disorder. These projects, and future studies following the same lines, will help to differentiate the roles of specific cell-types and local circuits in neurological disorders, and may pave the way for future therapeutic interventions that can more accurately target isolated behavioral phenotypes.

This thesis will provide much more detail surrounding autism spectrum disorder and how it is studied, the phosphatase and tensin homolog on chromosome ten (PTEN) and its role in health and disorder states, and somatostatin-expressing (SOM+) interneurons and how they fit into the milieu of neuronal subtypes and their importance for everyday function or their disturbance in neurological disorders. Finally, we will present the details of our experiments with their results and implications, as well as conclusions and a direction for future research in this topic.

CHAPTER 2: AUTISM SPECTRUM DISORDER

Autism Spectrum Disorder in Humans

Autism spectrum disorder (ASD) is a complex neurological disorder that affects millions of children, adults, and caregivers across the world, and diagnoses are continuing to rise. In the United States, the average prevalence is 1in 54 (1.85%) for children at the age of 8 according to 2016 data from the Autism and Developmental Disabilities Monitoring (ADDM) Network (Maenner, 2020), or 1 in 40 (2.5%) for children between 3 and 17 years old according to the 2016 National Survey of Children's Health (NSCH). Focusing on the ADDM data collected by medical professionals, prevalence has increased dramatically and steadily since 2002 (it was 0.66%, or 1 out of 150, in 2002 and 1.13%, or 1 out of 88, in 2008).

Some of the increased prevalence may be due to increased awareness and improvement in screening and diagnostic standards, but it is difficult to parse the reasons for the rise. In data from the National Health Interview Survey (NHIS), for example, parents reported ASD at a rate that rose from 1.1% in 2009-2011 to 2.5% in 2015-2017 (Zablotsky et al., 2019). Interestingly, children were more likely to be diagnosed with any developmental disability (including ASD) if they had public or private insurance compared to those with no insurance, perhaps giving evidence to the importance of awareness and diagnostic practices, or perhaps reflecting the idea that parents who could afford it and were more aware of the signs and symptoms

were more likely to seek a medical diagnosis. On the other hand, children in more rural areas were more likely to be diagnosed with a developmental disability (including ASD) than those in urban areas, where presumably there would be more access to screening and medical professionals, so attempts at defining the causes of increased cases have been lacking. Additionally, it has been suggested that historical levels of ASD are under-represented, and though some of the rise in cases may be due to the re-characterization to ASD, especially among patients with intellectual disabilities (Fombonne et al., 2009; Shattuck, 2006) this does not account for the full rise in cases, and a truly increasing prevalence of ASD is probable.

While the diagnoses have risen and the screenings have improved, there is still considerable individual variability in the type and severity of symptoms. The three main characteristics of ASD that are most common and have been used for identification and diagnostic purposes are difficulties with social interaction, language or communication deficits, and restricted interests or repetitive behaviors. However, in addition to these, many other symptoms or medical co-morbidities may exist, including increased anxiety, sensitivity to sensory stimuli, ADHD, cognitive or developmental delays, macroencephaly, and difficulty regulating emotions (Gillberg & Billstedt, 2000; Hatton et al., 2006; Hollander et al., 2003; Lainhart et al., 1997; Maenner, 2020; Zablotsky et al., 2019).

Genetics and Circuitry of Autism Spectrum Disorder

While the rates of autism are nearly identical across ethnicities (though slightly lower in Hispanic children), there are clear sex-linked differences, as boys

are more than 4 times as likely as girls to be diagnosed (Zablotsky et al., 2019), which gives evidence of some critical biological or genetic factors that affect the development or progression of ASD. Additionally, twin studies starting in the 1990s showed a strong genetic influence for the progression of autism, as 60% of identical twins both had autism, while none of the studied fraternal twins both had an autism diagnosis (Bailey et al., 1995). When the data was expanded to look at ASD-related cognitive and social disruptions, the genetic influence was even more obvious, with 92% concordance in identical twins compared to 10% in fraternal twins.

In light of the clear genetic links for this disorder, many attempts have been made to identify the candidate genes involved in its development and progression since there are thousands of genes with the potential to influence the nervous system in such a way that an ASD-like phenotype may arise. Consequently, genome-wide association, whole exome sequencing, and targeted sequencing studies have identified hundreds of genes that are more commonly mutated in humans with ASD (Betancur, 2011; De Rubeis et al., 2014; O'Roak et al., 2011, 2012; O'Roak & State, 2008). While this is a big step forward in attributing genetic causes to ASD, through these studies hundreds of genes have been implicated in ASD, and as such, no individual gene is associated with more than ~1% of autism cases. However, smaller lists that include genes more likely to be over-represented in ASD, compared to one would expect by chance, have been identified (De Rubeis et al., 2014; O'Roak et al., 2012).

Though there are many genes that are thought to be associated with ASD, they tend to fall into clusters based on their role in the cell with some of the most

commonly mutated genes being involved in transcription, protein synthesis/cellular signaling, synapse maintenance, and synaptic transmission.

There are also researchers who suggest that, given the diversity of potential genetic factors, a common underlying disruption in neural circuitry or communication may be present in many cases. Some conceivable hotspots of circuit dysfunction include sensory areas such as the temporal cortex, executive areas such as the medial prefrontal cortex, and regulators of emotion and affect such as the amygdala. Similarly, various attempts at synthesizing the variability of genetic functions with the convergence of behavioral phenotypes have resulted in multiple "whole-brain" theories of dysfunction in ASD. For example, some propose a general neural processing deficit, where attention and perceptual inputs are misinformed or sensory stimuli are exaggerated in the brain (Belmonte et al., 2004; Markram & Markram, 2010), while others suggest a circuitry-related deficit centered around abnormal connectivity among brain regions or disrupted inhibition in local networks giving rise to an imbalance in neural circuits (Rippon et al., 2007; Yizhar et al., 2011).

Animal Models of Autism Spectrum Disorder

Given the increasing number of people affected by autism spectrum disorders, including family members, educators, and caretakers of the individuals with the disorder, it is increasingly important to intensify the efforts of scientific research into understanding ASD and potential therapeutic interventions. As it is not ethical, nor desirable or feasible, to experiment on human patients, the development of animal models of ASD has been instrumental in the advancement of

our knowledge. Several mouse models of ASD candidate gene mutations have been generated and studied to provide this type of insight. However, among these genetic models, there are a few that have been studied considerably more than others, such as FMR1, SHANK3, and CNTNAP2 and they represent a wide variety of molecular functions within the cell, demonstrating the diversity of the genes linked to autism spectrum disorder.

Fragile X syndrome is associated with mutations to the FMR1 gene on the X chromosome that is involved in protein translation, and it has been closely linked to ASD (Hatton et al., 2006; McCary & Roberts, 2013). Accordingly, mouse models of FMR1 mutations have exhibited ASD-related behavioral deficits similar to human patients, including hyperactivity, social deficits, and sensitivity to sensory stimuli (Chen & Toth, 2001; Sørensen et al., 2015).

SHANK3 is part of a family of scaffolding proteins that stabilize important post synaptic molecules such as ion channels and G-protein coupled receptors and play a role in the development and maintenance of the synapse (Boeckers et al., 2002). It is an ASD candidate gene (Abrahams & Geschwind, 2008) and mouse models with SHANK3 mutations show impacted social behavior and elevated anxiety, as well as restricted repetitive motion, which is mediated by striatal dysfunction (Peça et al., 2011). Interestingly, these deficits can be reversed by re-introducing SHANK3 in adult mice, indicating that there are not detrimental developmental effects of the mutation (Mei et al., 2016).

CNTNAP2 is a member of the neurexin family of transmembrane proteins that serves to cluster and stabilize K+ channels in axons (Poliak et al., 2003) and it

has been identified as an ASD candidate gene in humans (Alarcón et al., 2008; Arking et al., 2008). Mouse models of CNTNAP2 mutations also exhibit decreased social interaction as well as hyperactivity and restricted repetitive motion (Peñagarikano et al., 2011).

Clearly there is strong evidence for genetic mutations as the leading factor in ASD; mutations in many of the genes identified result in demonstrably increased risk in humans and animal models of the mutations can replicate many of the behavioral deficits. Yet, there is some evidence that non-genetic interactions may play a part in the development of some forms of ASD. For example, while the erroneously reported relationship between vaccines and ASD has been reliably refuted (Madsen et al., 2002; Nelson & Bauman, 2003), there exists real increased risk of ASD for children with prenatal exposure to opioids (E. Rubenstein et al., 2019), valproic acid (Nicolini & Fahnestock, 2018), and maternal immune activation (Careaga et al., 2017; Patterson, 2011) and animal models exist to probe these relationships as well.

Nevertheless, our work focuses on the implications of genetic and circuitry-related dysfunction for autism spectrum disorders, and to that end, we have chosen to study the disruption of a protein that has been identified as a higher-risk candidate of the intracellular signaling/protein synthesis category, namely PTEN.

CHAPTER 3: PHOSPHATASE AND TENSIN HOMOLOG (PTEN)

What is PTEN? Structure and Function

We have chosen to focus the current project on a candidate gene that is very important, but is less studied in an ASD context, PTEN. PTEN stands for phosphatase and tensin homolog and is a potent regulator of cell cycle, growth, and proliferation through its activity as a phosphatase upstream of the AKT/mTOR pathway.

PTEN's name is a result of its interesting structure. When the crystal structure of PTEN was resolved, it surprisingly revealed a phosphatase domain that had homology not just to other phosphatases, but also to proteins that are not similar to phosphatases at all, such as the actin binding protein, tensin 1 (J.-O. Lee et al., 1999; D.-M. Li & Sun, 1997; J. Li et al., 1997). While PTEN's catalytic domain is similar to other protein tyrosine phosphatases (PTPs), the class of enzymes to which it belongs, and it has the ability to remove a $[PO_4]^{3-}$ group from acidic tyrosine-phosphorylated peptides as the name suggests, it has a much larger catalytic pocket with many positively charged residues which enables it to bind its main substrate, phosphatidylinositol (3,4,5) triphosphate (PIP3) (J.-O. Lee et al., 1999; Maehama & Dixon, 1998).

Additionally, PTEN has two structural domains that allow it to anchor itself in the cell. It has a C2 structural domain, similar to phospholipase C1 and protein

kinase C, that is not common to other phosphatases, which enables PTEN to bind to the phospholipid membrane and has been shown to affect cell migration (Raftopoulou et al., 2004). It also has a PDZ domain, similar to post synaptic density proteins, that allows it to bind to the actin cytoskeleton, which is necessary for proper function (Wu et al., 2000). The combination of these two structural domains allow it to be trafficked easily and anchored near the cell membrane for activity-dependent signaling mechanisms, especially in response to cellular activation via growth factors and insulin (Tamburini et al., 2008; Wan et al., 2007).

PTEN is a regulator of internal cell signaling and functions in multiple ways, but its primary catalytic activity is to remove a phosphate from phosphatidylinositol (3,4,5) triphosphate (PIP3) to make phosphatidylinositol (4,5) bisphosphate (PIP2) (Maehama & Dixon, 1998). PIP3 is an important signaling molecule involved in numerous molecular pathways, however, one major function of PTEN is regulating the interaction of PIP3 and AKT, also known as protein kinase B. Since PTEN converts PIP3 into PIP2, when PTEN is missing from the cell, there is a buildup of PIP3, leading to a recruitment of AKT, which is then phosphorylated by PDK1 and the mTOR2 complex (Sarbassov et al., 2005; Zoncu et al., 2011). Thus activated, AKT regulates numerous downstream proteins that are involved in proliferation and cell survival (Manning & Cantley, 2007; Song et al., 2012), including other proteins known to be mutated in ASD patients, such as TSC1/TSC2 (P. Baker et al., 1998; Manning et al., 2002). This interaction with TSC1/TSC2 leads to activation of the mTOR1 complex, which modulates protein synthesis related to cell growth, axon elongation, and dendritic morphology (Inoki et al., 2002; Potter et al., 2002). The

PIP3/AKT/mTOR pathway, which is inhibited by normal PTEN function, has several feedback loop mechanisms to prevent over-activation (Carracedo et al., 2008; Kinkade et al., 2008). However, loss of PTEN can also disrupt the feedback mechanisms, which brings about further dysfunction, and can lead to the maladjusted cellular metabolism that is common in many types of tumors (Fang et al., 2010; Sancak et al., 2007).

Though PTEN is a potent regulator of this important molecular pathway, it also has cellular functions outside its role as a phosphatase of PIP3. The loss of PTEN has been shown to disrupt the cellular microenvironment and extracellular matrix in ways that make it easier for tumors to proliferate (Bronisz et al., 2012; Trimboli et al., 2009). PTEN has also been shown to have activity in the nucleus of the cell where it promotes genetic stability by upregulating housekeeping proteins to aid in repairing DNA breaks (Bai et al., 2007; Puc & Parsons, 2005; Shen et al., 2007) so that PTEN dysfunction can also increase the chance of DNA damage and instability.

PTEN in Humans

With so much of PTEN's function associated with growth, development, and regulation of cell cycle and metabolism, it is not surprising that PTEN has been studied for decades for its role as a tumor suppressor in tissues throughout the body. It was first identified as a potential tumor suppressor gene in 1997 by two different labs when they reported it to be downregulated or missing from numerous types of tumors (J. Li et al., 1997; Steck et al., 1997). It was simultaneously discovered in a third lab that was looking for novel tyrosine phosphatases, since

they were already thought to be potential tumor suppressors (D.-M. Li & Sun, 1997). Beginning in 1997, an explosion of papers began to identify PTEN as a commonly mutated gene and potent regulator of many types of tumors in humans. Notable studies on human tissues have shown increased mutations or decreased expression of PTEN in tumors and cancers in the breast (J. Li et al., 1997; Steck et al., 1997), endometrium (Risinger et al., 1997), thyroid (Alvarez-Nuñez et al., 2006; Dahia et al., 1997), prostate (Cairns et al., 1997), leukocytes/lymphnodes (Grønbæk, 1998; Gutierrez et al., 2009), glia (Huse et al., 2009; S. I. Wang et al., 1997), lung (Soria et al., 2002; Zhang et al., 2010), and liver (Dong-Dong et al., 2003; Yao et al., 1999).

Within months of its discovery, PTEN began to be associated with two familial diseases that resulted in tumors in various regions of the body, namely, Cowdens Disease and Bannayan-Zonana Syndrome (BZS), or Ruvalcava-Riley-Smith Syndrome (RRS), and other related disorders that didn't fit all the criteria for either of these two (Liaw et al., 1997; Marsh, Dahia, et al., 1998; Marsh et al., 1997; Nelen et al., 1997). Though they are still distinct diseases, they are largely affected by PTEN and reports have shown that up to 80% of people with Cowdens disease have a PTEN mutation (Marsh, Coulon, et al., 1998). A few tumor-inducing diseases are now grouped under the umbrella of PTHS, or PTEN hamartoma tumor syndrome, that is defined by the growth of multiple benign tumors. Although PTEN mutations don't necessarily lead directly to cancer, it drastically increases the probability of cancerous tumors, especially in the breast (J. Li et al., 1997; Steck et al., 1997).

Although PTEN's role in cancers is very important and well documented, we were more interested in the effects of PTEN that relate to autism spectrum disorder.

As PTEN was being discovered and its role in cancer described, others were noticing the large overlaps between autism and aspects of PTEN function. For example, macrocephaly/macroencephaly is a common symptom of patients with PTEN mutations, and macroencephaly occurs in 15-37% of individuals with ASD (Fombonne et al., 1999; Lainhart et al., 1997). Additionally, intellectual disability and speech delays occurred in 15-20% and ~50% of BZS patients with PTEN mutations, respectively (Parisi et al., 2001), and according to CDC assessments from 2000, intellectual disability has been reported in 40-62% of ASD cases.

Accordingly, as researchers began to look for a connection between PTEN and ASD, case studies reported patients with combinations of PTEN mutations, macroencephaly, and ASD (Goffin et al., 2001; Zori et al., 1998). In 2005, PTEN mutations were reported in 17% of ASD patients with macroencephaly (Butler et al., 2005). Larger surveys also found overrepresentation of PTEN mutations individuals with ASD, especially among those with macroencephaly (McBride et al., 2010; Varga et al., 2009). Given the fact that hundreds of genes have been implicated in the development of ASD, and no individual gene is mutated in more than 1% of cases, it is striking that PTEN mutations are over-represented in ASD cases, and shows that the role of PTEN in ASD warrants further investigation (Abrahams & Geschwind, 2008; O'Roak et al., 2012).

Animal Models of PTEN Mutations

Given the importance of understanding how PTEN causes this dysfunction in living organisms necessitated the creation of animal models of PTEN mutations.

The types of mutations mainly fall into two categories: the global haploinsufficient model and conditional knockout/knockdown models.

The global haploinsufficient model refers to mice with a germline mutation in one chromosomal copy of PTEN that renders it non-functional in all cells in all areas of the animal's body. This can also be thought of as a mouse heterozygous (+/-) for a working PTEN enzyme. Haploinsufficiency simply means that if one copy of the gene is disrupted, the other single copy (haplo-) is not capable of (-insufficiency) producing the necessary level of catalytic action present in an organism with both copies and results in the cellular dysfunction responsible for the PTEN mutation's phenotype. The first PTEN (+/-) mouse models were generated independently in multiple labs, as the full knockout was lethal during embryonic development, and they showed multiple tumors consistent with human PTEN mutations (Di Cristofano et al., 1998; Podsypanina et al., 1999; Suzuki et al., 1998). Many researchers confirmed the presence of tumors that are associated with human PTEN mutations in their mouse models and were able to help identify some of the molecular pathways involved (Abate-Shen et al., 2003; Backman et al., 2001; Di Cristofano et al., 2001; Guigon et al., 2009; G. Li et al., 2002; H. Wang et al., 2002; Yanagi et al., 2007).

In contrast to heterozygous PTEN deletions, conditional knockout/ knockdown models disrupt the function of PTEN only in a subset of cell-types or regions which allow for more specific investigation of PTEN function, especially as it relates to the brain. Many versions of these mice have been generated and, unsurprisingly, they have some effects that are common to all and some that are

more specific. Notable conditional mutation models for experiments in the function of PTEN in the brain include a modified GFAP-Cre that expresses in neurons and granule cells (Kwon et al., 2001), CamKII-Cre (Sperow et al., 2012), Nse-Cre (Kwon et al., 2006), Nkx-Cre (Vogt et al., 2015), and PV-Cre (Baohan et al., 2016). Similarly, region-specific mutations or knockdowns have investigated the localized effects by injecting Cre (Gutilla et al., 2016; Liu et al., 2010; Williams et al., 2015) or shRNA (Singh et al., 2014; Zukor et al., 2013). The specific results of these types of manipulations will be discussed further and compared to the results of our experiments in the chapters that follow.

While many labs have been investigating various aspects of PTEN function for more than two decades, there is still a surprising lack of data available for how different neuronal cell types are affected by PTEN mutations, and even fewer pair behavioral consequences of PTEN loss with cellular and circuit dysfunction. As stated earlier, the contribution of the scientific community to the understanding of PTEN's role as a tumor suppressor is impressive and important, however, those experiments have dominated the field of PTEN research and we are more interested in the role of PTEN in neurological function, specifically applied to autism spectrum disorder. To this end, we set out to investigate a large hole in the field, namely how PTEN function in inhibitory somatostatin-expressing (SOM+) interneurons is linked to ASD behaviors and how the relevant circuitry is affected by PTEN deletion.

CHAPTER 4: SOMATOSTATIN- EXPRESSING (SOM+) INTERNEURONS

Inhibition in Neuronal Circuits

Inhibitory interneurons make up roughly 30% of the cells in the brain, and they are a crucial part of brain function through their activity in local circuits. Contrary to excitatory projection neurons that send axons to very distant targets throughout the brain, most inhibitory neurons make synapses within a small local region, and though there are some inhibitory populations that influence distant targets (Tomioka et al., 2005), the majority of them do not. Interneurons have a direct effect on shaping neuronal communication in three main ways: feed-forward inhibition, feedback inhibition, and lateral inhibition.

Feed-forward inhibition is an important mechanism for regulating the strength of information coming into a local circuit from excitatory projection neurons. In general, this is accomplished through axons projecting onto principal neurons that send branches to local interneurons as well. The inhibitory neurons then feed forward onto the same principal neurons and limit the signal via GABA-mediated hyperpolarization of the target cells. In this way, strong excitatory projections can be dampened in certain cells, which can lead to a sharpening of the incoming signal or a reduction in the response, where necessary. For example, the infralimbic (IL) prefrontal cortex sends excitatory connections to the basolateral amygdala (BLA) that assist in the extinction of fear memories. These IL projection

neurons are themselves subject to feed-forward inhibition via neurons from the ventral hippocampus synapsing onto local parvalbumin-expressing interneurons in the IL, which provides a mechanism for fear renewal (Marek et al., 2018).

Alternatively, feedback inhibition provides a way for the signals of principal neurons to be reflexively reduced. Here, the interneurons synapse back onto the original principal neurons, or other nearby principal neurons in the case of regional feedback inhibition, and directly inhibit their activity as a result of their own spiking. This can be a powerful mechanism for dampening recurrent activation, or reducing the drive of neurons that are over stimulated since the inhibition received is a result of the overactive cell's own spiking. Feedback inhibition has been shown to exist in the cortex as well as the amygdala (Ünal et al., 2020; Yavorska & Wehr, 2016), and to be specifically reduced in the BLA after stress-inducing stimuli (Isoardi et al., 2007).

Finally, lateral inhibition is a mechanism for local circuits to fine-tune information or process inputs from multiple brain areas. Here, excitatory afferents synapse onto inhibitory neurons that form interconnected networks with one another as well as principal neurons. Thus the activation of some interneurons can inhibit or disinhibit other signals within the local circuit. This can serve to enhance contrast of signals or to broaden signals to be more generalized. For example, in the somatosensory cortex, interneurons show vast interconnectivity between multiple subtypes, with some preferring to synapse onto dendrites and others onto cell bodies of parvalbumin-expressing interneurons (Hioki et al., 2013).

Interneuron Classes and Somatostatin- Expressing Interneurons

Inhibitory neurons in the brain are themselves a set of multiple cell types, most often identified by the expression of various (generally) non-overlapping genetic markers. Somatostatin-expressing (SOM+) neurons comprise one such distinct class of interneurons alongside other cell types, such as parvalbumin- (PV+), vasoactive intestinal peptide- (VIP+), cholecystokinin- (CCK+), and protein kinase c delta- (PKC-δ+) expressing interneurons. Each class of interneurons has been associated with specific functions within different circuits and brain regions, as well as distinct wiring patterns and physiological properties.

Parvalbumin-expressing interneurons form the largest and most studied group of inhibitory cells. About 40-50% of interneurons are PV+ and they are widely distributed throughout the cortex as well as subcortical structures. They tend to make inhibitory synapses on the cell bodies of principal neurons, also known as perisomatic inhibition, especially in the hippocampus (Megías et al., 2001; Papp et al., 2001), but have also been shown to form networks with other interneurons, for example in a disinhibitory circuit in the amygdala (Wolff et al., 2014). PV+ cells have been implicated in all forms of circuit inhibition including lateral inhibition in the cortex (Baohan et al., 2016; Hioki et al., 2013) and feed-forward and feedback inhibition in the hippocampus (Freund & Katona, 2007).

VIP+, CCK+, and PKC-δ+ neurons comprise of a much smaller proportion of inhibitory cells, making up roughly 20-30% of interneurons all together, however, each class has been associated with specific important functions within cortical and subcortical circuits. VIP+ neurons make up roughly 15% of all GABAergic neurons,

and they have been shown to primarily synapse onto other interneuron types, making disinhibitory local circuits specifically in the cortex (S. Lee et al., 2013; Pfeffer et al., 2013; Pi et al., 2013). CCK+ neurons, on the other hand, have been shown to synapse onto the somas of both excitatory and inhibitory cells, and they may be important for regulating social behaviors, fear and anxiety, and memory (Bowers & Ressler, 2015; Freund & Katona, 2007; Schmidt et al., 2014; Whissell et al., 2019). Additionally, PKC-δ+ neurons are an overlapping subset of GABAergic neurons that are specifically important for regulation of amygdala-related functions such as fear acquisition and expression (Haubensak et al., 2010; Yu et al., 2017) and feeding suppression (Cai et al., 2014).

The final, and most important for our purposes, class are the SOM+ cells, which make up about 30% of all inhibitory neurons. The origins of the group of cells began in the late 1800s when a strange cell-type was originally described by Carlo Martinotti, a pupil of Camillo Golgi, as neurons that had axons which ascended the neocortex, from lower layers to higher layers (Scarani et al., 1996), and they were later referred to as "Martinotti" cells. These cells have now been joined others with different morphological characteristics to be absorbed into the class of SOM+ interneurons, which are nearly ubiquitously distributed across cortical regions, although not uniformly so (Tremblay et al., 2016).

SOM+ neurons tend to make synapses to the distal dendrites of pyramidal cells in the cortex to control excitatory inputs and dendritic integration, but have also been shown to make some axo-axonic synapses that modulate the firing output of post synaptic cells (Gonchar et al., 2002; Kepecs & Fishell, 2014). SOM+ neurons

also form disinhibitory networks with other interneuron types, such that activity in different neuron classes can provide the circuit with opposing responses. For example, PV+ and SOM+ neurons can encode different behavioral events in the anterior cingulate cortex (Kvitsiani et al., 2013) as well as control the increase or decrease of fear through disinhibition in the basolateral amygdala (Letzkus et al., 2011; Wolff et al., 2014). Additionally, SOM+ neurons have been shown to perform lateral inhibition in both the visual and auditory cortex to suppress the surroundings of receptive fields and serves to increase the contrast of the neural representation of sensory stimuli (Lakunina et al., 2020; Nienborg et al., 2013).

While these genetic markers are usually sufficient to pick out distinct populations of inhibitory neurons, some researchers go further to characterize cell types based on morphological and physiological differences as well, especially in SOM+ neurons (Halabisky et al., 2006; Kawaguchi & Kubota, 1996). However, for our purposes, we focused our experiments on neurons expressing the genetic somatostatin marker rather than morphology or physiology. This benefited us in two ways: first, it enabled us to use the Cre-specific drivers to conditionally knock out PTEN in all SOM+ neurons, and second, we were able to do so without being concerned with post-hoc analysis of every cell, as identifying sub-classes of SOM+ interneuron cell types was neither of interest to us, nor in the scope of this project. Instead, we focused on the role of inhibition as a whole, and SOM+ neurons specifically, in neurological disorders.

Inhibition and SOM+ in Neurological Disorders and ASD

Since inhibition plays such a crucial role in the proper function of many types of circuits in the brain, it is no wonder that disruptions in inhibitory signaling have been implicated in many neurological disorders, including ASD. While some have suggested a broad association of numerous neurological disorders with an excitation/inhibition imbalance in different brain regions (Lewis et al., 2005; J. L. R. Rubenstein & Merzenich, 2003), and in general we believe that proper balance of circuit dynamics in necessary for proper brain function, we also believe it is possible to be more specific about the circuitry and behavioral deficits that exist.

Some of these types of specific, circuit-related experiments on interneuron function have been conducted in association with autism spectrum disorder, as well other neurological disorders. For example, experiments using combinations of opsins that can be active for extended periods of time (stable step-function opsins, SSFOs) in social behavioral tests have shown that an increase in excitation/ inhibition ratio in the medial prefrontal cortex can cause social deficits that are often seen in ASD (Yizhar et al., 2011). They showed that increasing principal neuron activity reduced social interactions, but was rescued by a simultaneous increase in inhibitory activity (to restore the balance). However, they did not test to see if a decrease in interneuron activity produced the same deficits as the elevated excitation (conceivably they would both result in elevated E/I ratio). Another group found that in another model of ASD, FMR1 knockout mice showed drastic changes to the number and distribution of PV+ neurons in circuits of the somatosensory cortex

but not hippocampal circuits, implying a difference in the processing of sensation, but not memory (Selby et al., 2007).

Finally, PTEN mutations have also been shown to affect interneuron function in a few papers. Deletion of PTEN from interneuron progenitors in Nkx2.1-Cre and Dlx-Cre mice resulted in a disruption of interneuron populations beginning *in-utero*. Since Nkx2.1 is expressed in progenitors from the medial ganglionic eminence, from which interneurons arise and migrate to the cortex, this allowed them to explore the effect of PTEN mutations in interneuron development. Specifically, the ratio of PV+ to SOM+ neurons was increased, and the social behavior of these mice was disrupted. Similarly, the deletion of PTEN from Dlx-expressing progenitors in the subventricular zone resulted in an increased PV+ to SOM+ ratio, potentially disrupting interneuron networks in the cortex (Vogt et al., 2015). Additionally, another group experimented with PV-Cre mice to generate PTEN (+/-) PV+ cells in the visual cortex. These experiments revealed a decrease in lateral inhibition onto pyramidal cells and reduced connection probability from SOM+ to pyramidal cells in the visual cortex as a result of PTEN loss (Baohan et al., 2016).

These are important experiments, but there are few that deal specifically with PTEN, and even fewer that investigate SOM+ neurons' involvement, and our research will fill gaps in the understanding of interneuron function in animal models of PTEN mutations. Though they compose a large proportion of inhibitory neurons, SOM+ neurons have been studied with less scrutiny than PV+ cells, especially in regards to their role in neurological disorders, so to further investigate the effect of SOM+ specific mutations of PTEN on mouse behavior and physiology, we conducted

our experiments in SOM-Cre mice bred with PTEN floxed mice. In this way, PTEN will only be knocked out from all SOM+ neurons and allow us to parse out these cells' important role within the PTEN model of autism spectrum disorder.

CHAPTER 5: CONDITIONAL KNOCKOUT OF PTEN IN SOM+ INTERNEURONS RESULTS IN ELEVATED FEAR AND ANXIETY IN MICE

Introduction

The large variability of the phenotypic expression of autism spectrum disorder (ASD) can make it difficult to study the underlying genetic and neural mechanisms. Honing in on specific genes, brain circuits, and cell types can help to elucidate important functions and potential disruptions. Here, we are investigating the role of a singe gene, PTEN, in a single cell type, SOM-expressing interneurons, to better understand the disruption of inhibitory circuitry in a mouse model of ASD. In order to determine the specific effect of PTEN's activity in SOM+ interneurons, we first ran a battery of behavioral tests on mice lacking PTEN only in SOM interneurons.

While genetic factors are known to play a role in the development of ASD, and some researchers encourage increased genetic testing for patients and family members in hopes of better identifying cases (McBride et al., 2010; Varga et al., 2009), ASD is still primarily diagnosed using behavioral criteria. Therefore, it is important to investigate links between our genetic manipulations and the behavior of our mice to ascertain links between PTEN function in SOM+ neurons and the behavioral phenotypes of ASD. Although it is difficult to directly probe the affect of our mice, efforts have been made to build up a set of behavioral assays to phenotype

ASD in mice (Crawley, 2007; Silverman et al., 2010), and we tested our subjects in an array of tasks developed for murine model systems that are relevant to ASD-related behaviors in humans .

The three-chamber apparatus is used to evaluate the sociability of the wild type and mutant mice, as well as their affinity for novel or familiar social partners, because of ASD's known role in limiting voluntary social interactions in human patients since at least the 1970s (Bartak et al., 1977; Lindley et al., 1977). Mice are extremely social creatures and are known to seek interactions with other mice, form complex hierarchies, and engage in behaviors that may even be considered play, especially in a more ecologically-relevant housing apparatus (Puścian et al., 2016; Shemesh et al., 2013), and though some doubt has been expressed as to the validity of the classic three-chamber test, it still allows robust examination of sociability (Kondrakiewicz et al., 2019; Nadler et al., 2004). In a three-chambered test, wild type mice will prefer to spend time near another mouse rather than an inanimate object and other mouse models of ASD have shown that some mice with mutations in ASD-related genes lose their affinity for social interactions (Clipperton-Allen & Page, 2014; Nadler et al., 2004; Vogt et al., 2015).

Humans diagnosed with ASD sometimes engage in repetitive behaviors or have restricted interests, and analogs of some of these behaviors can be tested in mouse models of ASD (Crawley, 2007; Hollander et al., 2003). We used an open field chamber to assess the animals' general activity levels when exploring a new space as well as to measure repetitive behaviors such as excessive rearing or grooming. We then used a hole-board insert to further test exploratory behavior and restricted

interest or repetitive motion. By seeing how widely a mouse explores an array of holes in the floor, or if they get focused on investigating one hole over and over, we can compare these practices to their wild type littermates.

Since many ASD patients also often experience elevated levels of anxiety (Gillberg & Billstedt, 2000; Gillott et al., 2001), we tested the mice to see how the SOM-Cre PTEN knockout affected anxiety-like behaviors in a light/dark chamber and an elevated plus maze . In the light/dark test, half of the chamber is exposed to the light in the room while the other half is shielded from the light by means of opaque plastic walls and an opaque lid. This allows the mouse to strike a balance between spending time in the relative "safety" of the covered, dark side of the chamber and the open "vulnerable" side. Mice are naturally curious and will explore the whole box, but the more "anxious" a mouse is, the more time it will spend in the dark side of the chamber. The elevated plus maze tests a similar preference for safety vs. exploration. It is raised above the ground and has two arms with walls, in which a mouse cannot see its elevation or the ground, and two arms with no walls, on which their perilous position is revealed. Mice will generally explore the whole maze and look over the edges, but more "anxious" mice prefer to stay in the walled arms.

Sensory sensitivity is another common phenotype of ASD in humans, where affected people may be more overwhelmed by lights, sounds, or sensations that seem innocuous to others (Markram & Markram, 2010). This has also been demonstrated in ASD models of mice (Chen & Toth, 2001). To investigate this type of behavior in our model, we tested startle responses to acoustic stimuli as well as

sensory integration using a pre-pulse inhibition protocol. By playing a burst of sound at different levels of intensity and measuring the mouse's startle response with an accelerometer, we are able to determine the threshold for acoustic startle and the intensity of their reactions. Pre-pulse inhibition is a variant of acoustic startle that is widely used to measure unconscious sensory integration in humans and mice, and it has been shown to be disrupted in ASD patients (Braff et al., 1978; Perry et al., 2007; Powell et al., 2009). By playing a milder, sub-threshold sound immediately before a louder, startling sound, the jumping reaction of the subject is reduced. It is important to note that the sub-threshold "pre-pulse" is sufficiently close to the startling tone, temporally, that there is not time for conscious expectation or bracing, therefore it is a reflection of how sensory information is brought together in the brain.

Finally, given the association between ASD and emotional deregulation as well as the involvement of SOM-expressing cells in the amygdala (Krabbe et al., 2018; Wolff et al., 2014), we assessed fear conditioning and rear recall. Fear conditioning is a classic behavioral technique that seeks to pair an innocuous sensation such as a light, tone, or smell (conditioned stimulus, CS) with a noxious sensation, most often a mild foot shock (unconditioned stimulus, US). Differential auditory fear conditioning uses two different acoustic stimuli, one paired with the foot shock (CS+) and one not paired with the foot shock (CS-) to have the animal differentiate between the two stimuli and learn to associate one as fearful and the other as benign. The mouse is then re-introduced to the tones, usually hours to days later and either in the same context or a different context, to see if they exhibit a fear

response (freezing) when the sounds are played. There are many possible variations in these types of experiments to try to assess how of fearful memories are learned, consolidated, recalled, and forgotten, but here we focus on differential fear learning and recall.

In order to really understand the role of PTEN in SOM-expressing cells, a behavioral phenotype has to be established. In doing so, we can parse out the contribution of a single gene and single cell-type. Even though PTEN is expressed in other cell-types, this approach will let us hone in on the specific aspects of the PTEN model that are affected by local inhibitory signaling in SOM-expressing neurons.

Methods

Animals - All animals were bred, housed and maintained in accordance with protocols approved by the IACUC at MPFI. We generated conditional knockouts of PTEN by triple crossing *PTEN-Flox*, *SOM-Cre*, and *Ai14-RosaTdTomato* mice. This ensured that PTEN would only be missing from cells expressing somatostatin, and those cells would also express the genetically encoded fluorescent marker, TdTomato. Littermate controls were used in all experiments as the PTEN Flox/+ parents generated +/+, FL/+, and FL/FL pups.

All animals were pair- or group- housed for social, open field, hole board, light/dark, and elevated plus maze (EPM) tasks and single-housed for acoustic startle, pre-pulse inhibition (PPI) and fear conditioning/recall. Mice were handled for three days prior to testing and allowed to habituate to the testing room for one hour prior to each behavioral experiment. We tested one behavior on consecutive days for social, open field, hole board, light/dark, and elevated plus maze tasks. We

then allowed two days between EPM and PPI, and between PPI and fear conditioning/recall (Figure 1).

Social Preference/Novelty – Mice were tested in a custom-made plastic three-chamber arena (24" x 16" x 9") to study their propensity for social interaction and social novelty. Each chamber was (8" x 16" x 9") with doors to allow free access between chambers. The center chamber remained empty throughout the test, but each of the sides contained an overturned pencil cup in one of the corners. The experiments were conducted in three phases, each being recorded by video for animal tracking and analysis. First, the mouse was allowed to investigate the whole apparatus in a 10 minutes habituation phase. Next, during the social preference phase, an age-matched, conspecific, non-familiar mouse was placed inside one of the overturned pencil cups in a side chamber while the other pencil cup remained empty. The test mouse was reintroduced to the apparatus and allowed to freely explore the three chambers for 10 minutes. Finally, the social novelty phase consisted of placing a second age-matched, conspecific, non-familiar mouse in the opposite pencil cup in the other side chamber and observing the test mouse for another 10 minutes. Each video was analyzed off-line using AnyMaze animal tracking software by Stoelting. Social preference for the first mouse stage was measured as the total time the test mouse spent interacting with the mouse-in-a-cup compared to the empty cup as follows:

Equation 1 - Social Preference Ratio

$$SPR = \frac{(t_m - t_e)}{(t_m + t_e)}$$

where *SPR* is the social preference ration, t_m is time spent interacting with the mouse-in-a-cup, and t_e is time spent interacting with the empty cup. The preference ration for social novelty was measured as the time spent in the chamber with the new mouse compared to the chamber with the mouse that was introduced in the previous phase as follows:

Equation 2 - Social Novelty Ratio

$$SNR = \frac{(t_n - t_f)}{(t_n + t_f)}$$

where *SNR* is the social novelty ratio, t_n is the time spent interacting with the novel mouse, and t_f is the time spent interacting with the familiar mouse (from the previous stage).

We also looked at the time each mouse spent grooming as a measure of restrictive-repetitive behavior. Videos were played back and manually scored for duration of grooming during each phase of the social test.

Open Field Test – General locomotion and activity were tested in a clear plastic open field chamber (18" x 18" from AnyBox by Stoelting, Woods Dale, IL). Mice were placed in the apparatus and allowed to freely explore for 10 minutes. All trials were recorded on video then analyzed off-line using AnyMaze animal tracking software by Stoelting. We measured the total distance traveled by the mice as well as the number and duration of rearing bouts and whether the mice preferred the "safer" edges of the chamber or wandered into the center.

Hole Board Test – To test restrictive or repetitive motion, a hole board (from AnyBox by Stoelting) was inserted into the open field chamber. The board covered

the entire 18" x 18" box and consisted of 16 holes (1" in diameter) equally spaced in a 4x4 grid. A mouse was placed in the chamber and allowed to freely explore for 10 minutes. Infrared beam motion detectors were set up just below the level of the holes to detect investigative nose-pokes into a particular hole. All trials were recorded on video then analyzed off-line using AnyMaze animal tracking software by Stoelting. We measured the total number of holes explored/poked, the total number of nose pokes, and the propensity to return to a previously poked hole, and the number of holes poked in the center vs. the perimeter.

Light/Dark Test – One test for anxiety-like behaviors is the light/dark test. The 18" x 18" light/dark chamber (from AnyBox by Stoelting) is divided into two sections. One side (9" x 18") has four opaque black walls and an opaque black lid which blocks the light from the room and stays quite dark while the other adjoining side (9" x 18") has three clear walls, sharing one of the black opaque walls, and is illuminated fully. A small opening in the joining wall allows for the mouse to freely move between the light portion and the dark portion of the box. Mice were placed in the light side of the box and allowed to freely explore for 10 minutes. All trials were recorded on video then analyzed off-line using AnyMaze animal tracking software by Stoelting. We measured the number of entries into the light portion as well as the total time spent in the light and dark sides.

Elevated Plus Maze – Another test for anxiety-like behavior is the elevated plus maze. A custom-built plus sign maze with two open arms (2" x 10") and two walled arms (2" x 10" x 6.5") stands 20" above the ground. Mice were placed on an open arm and allowed to freely explore the maze for 10 minutes. All trials were

recorded on video then analyzed off-line using AnyMaze animal tracking software by Stoelting. We measured the number of entries into and the total time spent in the open and closed arms.

Acoustic Startle Response – Acoustic startle tests were conducted to test for increased or decreased sensitivity to sensory cues. We purchased the SR-LAB startle response system from San Diego Instruments and set it up according to the manufacturers instructions. It consists of a control box with multiple IO ports for lights and cues, a 12" x 12" x 12" sound reducing chamber (for external noise) with a built in speaker, and tube-like enclosure for mice with an accelerometer attached to the bottom. We calibrated the analog output from the system to the speaker using a sound level meter (Extech Instruments, Waltham, MA) to generate a curve of acoustic stimuli at appropriate noise levels. Mice were first habituated to the chamber during a 5-minute session with background 65 dB white noise. Next, they were introduced to a series of 40 ms acoustic stimuli consisting of 8 pulses each of 70 dB, 75 dB, 80 dB, 90 dB, 100 dB, and 110 dB white noise as well as 12 pulses each of 65dB and 120 dB white noise interleaved in randomized order with randomized inter-pulse intervals. Startle responses measured by the accelerometer were averaged for each of the dB levels in order to build an input/output curve of acoustic sensitivity for each mouse. Four pulses of 120 dB noise were introduced at the beginning and end of the test to measure startle desensitization.

Pre-Pulse Inhibition – A pre-pulse inhibition protocol was used to measure any abnormalities in sensorimotor integration. PPI tests were conducted with the SR-LAB startle response system (San Diego Instruments, San Diego, CA). Mice were

allowed to habituate to the chamber with 65 dB background noise for 5 minutes prior to testing. Mice were then introduced to a series of acoustic stimuli interleaved in randomized order with randomized inter-pulse intervals. Test pulses were 40 ms of 120 dB white noise that were preceded by pre-pulses of 20 ms long white noise at 70 dB, 75 dB, or 80 dB with either a 50 ms or 100 ms delay between the pre-pulse and the test pulse. Each pulse condition was introduced 6 times in random order, along with 12 test pulses with no pre-pulse condition and 12 background noise pulses of 65 dB, for a total of 60 acoustic stimuli. Four pulses of 120 dB noise were introduced at the beginning and the end of the test to measure startle desensitization. The accelerometer measured startle responses to each stimuli condition and was averaged for each mouse and the ratio of startle to the noise without a pre-pulse vs those with a pre-pulse was used to find the level of pre-pulse inhibition at each sound level according to the formula:

Equation 3 - Pre-Pulse Inhibition

$$PPI = 1 - \frac{r_i}{r_m}$$

where r_i is the average startle response to the inhibiting pre-pulse stimuli and r_m is the average startle response to the maximum startling stimuli (120 dB with no pre-pulse).

Fear Conditioning – Differential auditory fear conditioning tests were conducted using a Med Associates (Fairfax, VT) fear conditioning chamber (10" x 11.5" x 8.5") inside a sound attenuating box (25" x 30" x 17"). During conditioning, two different acoustic stimuli were played to the mice and one was paired with a mild foot shock. The tone that was not paired with the shock (CS-) was a constant

30 sec pure tone of 5000 Hz at a level of 85 dB. The conditioned stimulus paired with the foot shock (CS+) was a series of 5 ms pure tone "pips" of 12000 Hz at a level of 85 dB that occurred once a second for 30 seconds. This CS+ was co-terminated by a mild 1-second electric current of 0.8 mA (US) delivered through the grated floor of the chamber. Both the CS- and CS+/US were interleaved and delivered 7 times with randomly variable inter-stimulus delays. The behavior of the mice was recorded in the dark with an infrared camera (Basler, through MedAssociates) and analyzed using Med Associates' Video Freeze software. We measured the percentage of time the mouse spent freezing during each of the 30-second epochs in which the tones were played.

Fear Recall – Differential fear recall was conducted in the same Med Associates apparatus as the fear conditioning; however, to isolate the fear memory related to the acoustic stimulus alone and not the context of the box, we slightly modified the chamber. A plastic insert was laid on the floor of the chamber over the metal grating to change the tactile stimuli presented to the mouse, a plastic "tent" was placed above the mouse that spanned the whole of the chamber so that the shape of the box became a triangle, and all pieces were cleaned using 0.1% Alconox detergent (Alconox, White Plains, NY) instead of 70% ethanol so that the olfactory signals would also be different. Mice were then re-presented with 3 each of the CS+ (without the US shock) and CS- acoustic stimuli interleaved at random inter-stimulus intervals and their freezing was recorded in the dark with the same infrared camera and Med Associates Video Freeze software. We measured the

percentage of freezing that occurred during each of the 30-second epochs in which the tones were played.

Results

We found that the conditional knockout of PTEN in SOM+ neurons affected mouse behavior in a profile that had both similarities and differences to other mouse models of ASD, with the overall effect being increases in the expression of fear and anxiety among the various tests.

Social Interaction and Social Novelty are not disrupted by knockout of PTEN in SOM+ neurons – Many mouse models of ASD show deficits in an individual's propensity to interact with other mice, or to recognize and spend more time with more novel mice they have not interacted with. These two phenomena are referred to here as "social preference" and "social novelty." While previous studies have shown social interaction deficits in mice with various PTEN mutations, we found that in the conditional knockout of PTEN from SOM+ neurons, social interaction was not affected (Figure 2). SOM+ PTEN KO (Floxed, or FL) mice showed similar patterns in the amount of time they spent in social interactions across all stages of the social test compared to their wild type littermates (n=10 WT, 12 FL, 2-way ANOVA: $F(3,120)=2.107$, $p=0.103$). They showed a significant difference in the amount of time they spent interacting with a stranger mouse-in-a-cup compared to an empty cup (111.2 seconds vs. 54.65 seconds, on average, n=12, Tukey's test: $p<0.0001$). This was comparable to their wild type littermates, who spent an average of 115.6 seconds interacting with the stranger mouse compared to 41.01 seconds interacting with an empty cup (n=10, Tukey's test: $p<0.0001$).

In terms of social novelty, no deficits were observed in the floxed mice either (Figure 2). They were able to recognize the second stranger mouse as being new, and they spent significantly more time interacting with the second stranger compared to the first, whom they had already met in the previous stage (110.0 seconds vs 45.20 seconds, on average, n=12, Tukey's test: $p<0.0001$). Interestingly, the floxed mice actually showed a higher preference for social novelty than the wild type mice, who, though they did spend more time with the second stranger than the first mouse, failed to reach a level of significance in this measure (78.14 seconds vs. 51.90 seconds, on average, n=10, Tukey's test: $p=0.2526$).

The social similarities between wild type and SOM+ PTEN KO mice are further illustrated in the social preference ratio (SPR) and social novelty ratio (SNR). Here, the difference between the amount of time each mouse interacted with the target mouse or cup was normalized by the total amount of time they spent interacting with either. This measure limits some of the variability present between animals based on how much time they spend exploring other zones of the apparatus. It also emphasizes differences in a non-linear fashion, so that smaller values are weighted more heavily. If a mouse spends equal time with the social vs non-social target, the SPR is 0, if they spend 50% more time with the social target than with the non-social target, the SPR is 0.2, twice the time gives an SPR of 0.33, thrice the time gives an SPR of 0.5, and so on, up to an infinite time difference yielding an SPR of 1. Overall, no significant effect as a result of the conditional knockout of PTEN was observed (n=10 WT and 12 FL mice, 2 way ANOVA: $F(1,60)=0.1119$, $p=0.7392$) but there was a robust effect for each genotype due to the

stage of the test (n=10 WT and 12 FL mice, 2 way ANOVA: $F(2,60)=11.40$, $p<0.0001$) indicating that they both showed higher preference for the social target than during the habituation phase (Figure 3).

SOM+ PTEN KO mice are less active and exploratory in the open field apparatus – We found that our SOM+ PTEN KO mice performed differently in the open field apparatus compared to their wild type littermates. Floxed mice showed reduced activity and exploration compared to wild type. Overall, floxed mice travelled a shorter distance throughout the duration of the test, spent more time immobile, and had fewer bouts of rearing, which is an exploratory behavior (Figure 4). Both genotypes travelled less in the second half of the test compared to the first half, and floxed mice travelled less than wild type in both halves (n=10 WT and 13 FL mice, 2 way ANOVA – Genotype effect: $F(1,42) = 6.793$, $p=0.0126$, Half effect: $F(1,42) = 8.601$, $p=0.0054$). Floxed mice were more immobile than wild type mice (n=10 and 13 FL mice, 2 way ANOVA – Genotype effect: $F(1,42) = 4.381$, $p=0.0424$). Floxed mice also showed fewer bouts of exploratory rearing behavior (n=10 and 13 FL mice, 2 way ANOVA – Genotype effect: $F(1,42) = 6.156$, $p=0.0172$).

The open field test can also be used as an analogue for anxiety-related behavior by analyzing a mouse's activity in the center of the apparatus compared to the sides of the apparatus, where a more anxious mouse will tend to spend more time in the sides and corners and be less active there. We looked at these measures for our experiments and found that there were not differences between our genotypes for entries into each zone or the time spent in each zone, but saw reduced rearing in the sides and corners in floxed mice. Both genotypes entered the center

zone fewer times during the second half of the test, with each spending a comparable amount of time in the center, but the floxed mice trended toward fewer rearing bouts (n=10 WT and 13 FL, 2 way ANOVA – Center Entries (Half effect): $F(1,42) = 10.97$, $p=0.0019$, Time in Center (Genotype effect): $F(1,42) = 0.7147$, $p=0.4027$, Figure 5). Similarly, both genotypes entered the side zones fewer times in the second half of the test and spend comparable amounts of time there, but the floxed mice reared less in the side zones compared to wild type mice (n=10 WT and 13 FL, 2 way ANOVA – Side Entries (Half effect): $F(1,42) = 11.43$, $p=0.0016$, Time in Side Zone (Genotype effect): $F(1,42) = 0.7147$, $p=0.4027$, Rearing Bouts (Genotype effect): $F(1,42) = 10.61$, $p=0.0022$, Figure 6).

All together, these open field data indicate that the SOM+ PTEN KO mice were less active and exploratory in the this new environment, and they preferred the relative "safety" of the sides of the apparatus just like their wild type littermates.

SOM+ PTEN KO mice do not show restricted interest or repetitive motion – The hole board test serves as a proxy for restricted repetitive motion and can be used to discriminate between the reactions of mice of different genotypes' when they experience new environments with opportunities to investigate. We measured the number of holes poked, as detected by infrared beams below the surface of the board, as well as the mouse's location in the apparatus when they peeked in each hole. Similar to the open field test, information about activity in the center of the apparatus vs the sides or corners of the apparatus can be linked to anxiety-related phenomena.

Only a subset of our mice were tested in the hole board apparatus, however, in our hands, floxed mice and wild type mice each spent more time in the sides and corners than in the center zone, but the difference was more pronounced in floxed mice, as indicated by the interaction effect, which means that the mice of different genotypes had different reactions to the separate zones (n=3 WT and 6 FL, 2 way ANOVA – Zone effect: $F(2,21) = 91.05$, $p<0.0001$, Interaction: $F(2,21) = 4.503$, $p=0.0236$, Figure 7). One can see in figure 10A that floxed mice spent less time in the center and sides, but more time in the corners compared to the wild type mice.

Conversely, there was not evidence of a restricted-repetitive motion phenotype in the SOM+ PTEN KO mice in this test (as seen in Figure 7B) as both wild type and floxed mice nose poked a similar number of holes in total (85.33 for WT vs 76.833 for FL), and showed similar patterns in where they preferred to explore the holes (n=3 WT and 6 FL, 2 way ANOVA – Zone effect: $F(2,21) = 36.92$, $p<0.0001$, Genotype effect: $F(1,21) = 0.7473$, $p=0.3971$). A mouse with restricted interest or repetitive motion would have poked holes in a more exclusive area of the apparatus or had significantly more nose pokes.

We also evaluated the grooming behavior of our mice, as a further measure of restricted repetitive motion, during the social tests. Similar to the hole board test, we found no evidence of restricted repetitive motion in our mice, as both genotypes spent the same amount of time self-grooming (stats, Figure 8)

Mice with PTEN knockout in SOM+ neurons show elevated levels of anxiety in a light/dark chamber – We used the light/dark test as an analogue of anxiety-related behavior in accordance with the fact that mice from other models of

ASD and anxiety disorders show a stronger preference for the safety of the dark side of the apparatus compared to wild type mice.

We found that both our genotypes spent more time in the dark side of the light/dark test, but floxed mice spent significantly less time in the light and more in the dark compared to their wild type littermates (n=10 WT and 13 FL, 2 way ANOVA – Zone effect: $F(1,42) = 463.6$, $p<0.0001$, Interaction: $F(1,42) = 18.29$, $p=0.0001$, Figure 9). Again, here the interaction effect indicates that the two genotypes showed opposing patterns in their responses to each zone, i.e. more time in one zone and less time in the other compared to WT, whereas a pure "genotype" effect would see and increase or decrease across both zones. Floxed mice spent less time in the light (118.9 seconds vs 174.9 seconds, Sidak's test: $p=0.0133$) and more time in the dark (477 seconds vs 414.3 seconds, Sidak's test: $p=0.0053$) compared to WT mice.

A more detailed look at the light side of the apparatus (Figure 10) revealed that neither genotype showed a difference in light time based on the segment of the test (the first 5 minutes vs the last 5 minutes), but floxed mice spent less time in the light than WT mice throughout (n=10 WT and 13 FL mice, 2 way ANOVA – Segment effect: $F(1,42) = 0.6010$, $p=0.4425$, Genotype effect: $F(1,42) = 9.417$, $p=0.0038$, Figure 10A). Conversely, both genotypes showed an increase in exploratory rearing during the second half of the test, but floxed mice reared significantly less overall than WT, further illustrating the lower levels of rearing seen in the open field (n=10 WT and 13 FL mice, 2 way ANOVA – Segment effect: $F(1,42) = 8.405$, $p=0.0059$, Genotype effect: $F(1,42) = 6.489$, $p=0.0146$, Figure 10B).

Further investigation into the activity of our mice in the dark side of the apparatus gave more evidence to the anxiety-related phenotype of the SOM+ PTEN KO. Neither genotype showed a difference in time spent in the dark side based on the segment of the test, but floxed mice spent more time in the dark than WT mice throughout (n=10 WT and 13 FL mice, 2 way ANOVA – Segment effect: $F(1,42) = 0.2468$, $p=0.6220$, Genotype effect: $F(1,42) = 10.84$, $p=0.0020$, Figure 11A). They showed that the average visit to the dark zone was much longer for floxed mice compared to wild type mice (n=10 WT and 13 FL mice, 2 way ANOVA – Segment effect: $F(1,42) = 0.4607$, $p=0.5010$, Genotype effect: $F(1,42) = 10.70$, $p=0.0021$, Figure 11B).

SOM+ PTEN KO mice show patterns of anxiety-like behavior in the elevated plus maze – We used the elevated plus maze as a further measure of anxiety-related behavior, which has been shown to reveal information about anxiety levels based on the amount of time spent in the open vs closed arm of a small plus-shaped maze raised a few feet off the ground.

SOM+ PTEN KO mice showed increased levels of anxiety compared to wild type mice (Figure 12). Both genotypes spent much more time in the closed arm of the EPM compared to the open arm, but the floxed mice had a more extreme preference for the closed arm (n=10 WT and 13 FL mice, 2 way ANOVA – Arm effect: $F(1,42) = 468.4$, $p<0.0001$, Interaction: $F(1,42) = 6.671$, $p=0.0134$). Similar to the light/dark test, the interaction effect shows that the floxed mice preferred the "safer" closed arm to the open arm in a stronger manner than the wild type mice. Accordingly, SOM+ PTEN KO mice spent less time in the open arm (115.53 seconds

vs 93.82 seconds) and significantly more time in the closed arm (378.6 seconds vs 428.2 seconds, Sidak's test: p=0.0295) compared to wild type mice.

We also looked closer at the elevated plus data to evaluate any differences in arm exploration in the first or second half of the test (Figure 13), which would be expected if the interest in novelty gives way to the desire for comfort or safety over time. While the trends are still clear, the relatively low values compared to the variability in time spent in the open arm failed to show differences related to the segment of the test or genotype (n=10 WT and 13 FL mice, 2 way ANOVA – Segment effect: $F(1,42) = 3.056$, $p=0.0878$, Genotype effect: $F(1,42) = 2.450$, $p=0.1251$, Figure 13A). However, with a more representative amount of the total testing time spent in the closed arm, both genotypes showed increased time in the closed arm during the second half of the test, and the preference was stronger in floxed mice (n=10 WT and 13 FL mice, 2 way ANOVA – Segment effect: $F(1,42) = 7.540$, $p=0.0088$, Genotype effect: $F(1,42) = 4.995$, $p=0.0308$, Figure 13B).

SOM+ PTEN KO mice have increased startle responses to loud acoustic stimuli – In order to evaluate sensitivity to acoustic stimuli, we tested our mice in an SR-LAB chamber. A small tube equipped with an accelerometer was placed inside a sound proof chamber with an internal speaker so that we could measure startle responses to different intensity levels of white noise since sensitivity to sensory information is common in human patients with ASD as well as some animal models of ASD.

We found that SOM+ PTEN KO mice exhibited stronger startle responses to loud acoustic stimuli. Fitting a sigmoidal dose-response curve to the intensity of

accelerometer deflection revealed an increase in the maximum startle response evoked by louder stimuli while the baseline, EC50, and slope were only marginally affected (n=10 WT and 13 FL mice, EC50: 99.10 dB vs 99.91 dB, Slope: 0.060 vs 0.053, Max Response: 500.4 vs 732.3, Comparison of Fits – $F(4,176) = 3.378$, $p=0.0108$, Figure 14). Since the profile of the curves for WT and floxed mice only diverged as the stimuli got louder, they don't seem to be universally more sensitive, but their responses grow to stronger levels as the tone intensity increases.

Pre-Pulse Inhibition was not affected by knockout of PTEN in SOM+ neurons – We measured pre-pulse inhibition to investigate the sensory integration of our mice since it is a common test in many models of neurological disorders to reveal deficits in unconscious sensory processing. Humans as well as mice will show a reduced startle response to a loud tone if it is preceded by a softer tone at intervals of 50-100 ms. The tones are sufficiently close in time such that the reduction in startle response is not the result of a conscious expectation or preparation, but rather has to do with the way sensory signals are integrated and interpreted.

In our experiments, both genotypes show reduced startle amplitude to stimuli with pre-pulses of 70, 75, and 80 dB at 100 ms and 50 ms intervals (Figure 15A). Both genotypes show a strong decrease in startle amplitude to stimuli with a pre-pulse compared to their responses to the 120 dB noise but floxed mice still startle more than their wild type littermates (n=9 WT and 13 FL mice, 2 way ANOVA – PPI effect: $F(7,160) = 9.637$, $p<0.0001$, Genotype effect: $F(1,160) = 4.237$, $p=0.0412$, Figure 15B).

However, this difference in pre-pulse inhibition seen between the floxed mice and wild type mice is due to the general increase in startle amplitude to loud noises exhibited by the floxed mice rather than a lack of pre-pulse inhibition. This can be seen clearly when the responses for each mouse have been normalized to the maximum startle amplitude for the 120 dB pulse with no pre-pulse. Here we can see that both genotypes show strong PPI and are not significantly different from each other (Figure 16A). The pre-pulse inhibition ratio is intact for floxed mice, with both genotypes showing increasing response inhibition to louder pre-pulses, which is expected (n=9 WT and 13 FL mice, 2 way ANOVA – PPI effect: $F(5,120) = 4.436$, $p=0.0010$, Genotype effect: $F(1,120) = 1.289$, $p=0.2585$, Figure 16B).

SOM+ PTEN KO mice show increased freezing during auditory fear conditioning – Auditory fear conditioning is a staple experiment for investigating fear learning in wild type mice as well as many models of neurological disorders. The acquisition of fear memory is important because learning to avoid cues associated with danger is a necessary trait for survival, and malfunctions in this process could lead to disruptions in a mouse's, or person's, ability to pair environmental cues to potential threats. In our experiments, we use differential auditory fear conditioning, where two tones are used, one that is paired with a mild foot-shock (CS+) and one that is not (CS-).

We found that both genotypes were clearly able to acquire fear memory and their freezing increased with the number of pairings of tone and foot-shock (Figure 19). However, mice with SOM+ PTEN knockouts show elevated levels of freezing to the tone paired with a mild foot shock (CS+) throughout conditioning compared to

their wild type littermates (n=10 WT and 13 FL mice, 2 way ANOVA – Conditioning effect: $F(6,147) = 12.01$, $p<0.0001$, Genotype effect: $F(1,147) = 4.480$, $p=0.0360$, Figure 17). Eventually, the wild type mice reached the same level of freezing as the floxed mice, but the floxed mice exhibited a higher freezing response with fewer pairings.

Mice with PTEN knocked out in SOM+ neurons have increased freezing during fear recall – Fear recall is a simple experiment to test whether a mouse exposed to a fear conditioning protocol can remember the cue associated with the foot-shock and respond accordingly. Most often this is recorded as freezing, although some researchers look at more complex behaviors that may be analogous to fearful avoidance. We tested our mice 24 hours after conditioning, and we presented them with both the tone that was previously paired with a shock and the benign tone. Comparing their responses to the CS+ and CS- tones gives us an idea of how specific the fear memory is, with higher freezing to the CS- tone indicating more fear generalization.

We found that both genotypes freeze when presented with the tone previously paired with a foot shock, but the floxed mice show increased freezing behavior across all three recall trials (n=10 WT and 13 FL mice, 2 way ANOVA – Genotype effect: $F(1, 63) = 5.683$, $p=0.0202$, Figure 18A). We also show that both genotypes are able to differentiate between the tone previously paired with a foot shock (CS+) and the tone that was not paired with a shock (CS-), and again we see the floxed mice still froze to the CS+ tone more than WT mice (n=10 WT and 13 FL mice, CS+ Freezing: 57.17% vs 68.91%, t-test – $p=0.0364$, Figure 18B).

Discussion and Conclusions

Many models of ASD have been evaluated behaviorally and exhibit phenotypes with disruptions across the whole range of ASD-related behaviors. Some genetic models show behavioral profiles that mirror human ASD patients in many ways, while other models have more specific behavioral deficits that don't cover the full spectrum of the human ASD phenotype or are focused on cell-type or regional effects of disorder-related mutations.

The PTEN gene has also been evaluated along these lines, using multiple models to better understand the variety of impacts that aberrant function can have on animal behavior, neuronal morphology, and cellular physiology. However, here we have created a cell-type specific mutation in order to investigate the contribution that SOM+ neurons have to the overall PTEN model of ASD for the first time. Our results indicate that proper SOM+ function is a crucial determining factor for success in some behaviors related to the elevated fear and anxiety often seen in patients with ASD, while it does not strongly disrupt the animal's ability to perform other tasks.

Social deficits have been shown in other mouse models with ASD-related mutations, such as SHANK3 (Peça et al., 2011), TSC1/TSC2 (Goorden et al., 2007), Fragile X (Spencer et al., 2005), and CNTNAP2 (Peñagarikano et al., 2011). Various PTEN models have also shown altered social behavior, including the PTEN +/- haploinsufficient mice (Clipperton-Allen & Page, 2014) and mice with a neuron-specific deletion of PTEN (Kwon et al., 2006). In contrast to these models, our mice did not show altered social behavior. They spent more time with social vs non-

social targets and accurately identified novel mice to interact with. This seems to indicate that SOM+ neurons are not directly responsible for the maintenance of social interactions. It may be that their role in social behavior is limited by the nature of their involvement in cortical circuits related to these tasks, or that the dysfunction associated with PTEN deletion from SOM+ is compensated for in socially relevant circuits.

Excessive grooming and restrictive repetitive motions have also been documented in other mouse models of ASD, including SHANK3 (Peça et al., 2011) and CNTNAP2 (Peñagarikano et al., 2011), however we did not observe these phenomena in SOM+ PTEN KO mice. These behaviors are often associated with disruptions in striatal circuitry function, especially in the SHANK3 model. Our results indicate that the removal of PTEN from SOM+ neurons does not significantly affect the way that striatal neurons communicate and their contribution more strongly associated with other behaviors.

Our mice did show lower exploratory behavior in the form of rearing and mobility in the open field test. This may be due to an increased level of anxiety in the mice, or lack of interest in exploring the environment, however they did spend the same amount of time in the center of the arena compared to wild type mice. Interestingly, when the hole board was introduced to the open field arena, for a subset of mice on a separate day, the SOM+ PTEN KO mice did spend significantly less time in the center and side zones and more time in the corners compared to wild type mice, though they did not poke significantly fewer holes. These results together seem to indicate a susceptibility to increased levels of anxiety when there

is more going on (hole board vs open field), and a weaker motivation for investigating their environment, which is in line with the "intense world" theory that proposes patients with ASD are overwhelmed with complex and changing environments and tend to prefer situations they have more control over (Markram & Markram, 2010).

Anxiety is a common comorbidity with ASD among human patients (Gillberg and & Billstedt, 2000; Gillott et al., 2001) and mouse models (Kwon et al., 2006; Peça et al., 2011; Peñagarikano et al., 2011). Accordingly, we found that SOM+ PTEN KO mice showed elevated levels on anxiety in multiple different tests. The light/dark test showed that the lack of PTEN in SOM+ neurons resulted in floxed mice spending more time in the dark side of the chamber and less in the light when compared to wild type mice. They also were less exploratory in the light side, showing fewer bouts of rearing. Similarly, when they entered the dark chamber, they tended to stay longer, as seen in the increased average visit to the dark side of the chamber. Additionally, the elevated plus maze provided further evidence that floxed mice are more anxious than their wild type littermates, as they spent more time in the closed arms of the apparatus and less time exploring the "dangerous" open arms. All together, the results of the anxiety-related behavioral tests clearly indicate a role for proper SOM+ neuron function in brain areas and circuits that are important for regulating the balance between curiosity and safety. Disruptions in SOM+ cells result in elevated anxiety across multiple different evaluations.

Sensitivity to sensory stimuli is another commonly reported symptom in patients with ASD and mouse models (Chen & Toth, 2001; Perry et al., 2007). We

found that our SOM+ PTEN KO mice had larger startle responses to the same levels of acoustic stimuli compared to wild type mice, indicating that PTEN dysfunction in SOM+ neurons contributes to sensory sensitivity. As the intensity of the acoustic stimuli increased, so did the difference between wild type and floxed mice, showing that there may be a non-linear response to the way SOM+ neurons affect sensory sensitivity.

While floxed mice had a larger response to louder presentations of white noise in general, their sensorimotor integration was not altered, as seen by the similarity of their responses during pre pulse inhibition. Wild type mice and floxed mice both reduced their startle amplitude when pre-pulses of different intensities and inter-event intervals were played. This means that although the floxed mice were more jumpy, they did not seem to have an underlying integration issue that is common in other neurological disorders.

Finally, our fear conditioning experiments showed that floxed mice have differences in the acquisition and recall of fear memories, which is in line with other neurological disorder models and the observed comorbidity between fear and anxiety and ASD. Both genotypes were able to associate the tone and shock during conditioning, but SOM+ PTEN KO mice acquired fear memories more rapidly, measured by their increased freezing to fewer presentations of the CS+ and foot shock. This may indicate that they have stronger drive onto fear-related circuitry. Similarly, they had stronger freezing responses to the tone previously paired with a foot shock in a separate context, 24 hours later. Stronger recall may indicate more robust storage of fear memories, or more efficient retrieval of the tone-shock

pairing. In both instances, the contribution of SOM+ interneurons to the circuitry involved in creating and maintaining fearful memories has been disrupted by the loss of PTEN in those cells.

Altogether, our data show that the role that SOM+ neurons play in the broader context of the PTEN model of ASD is more specific than more global manipulations. Clearly, the contribution of SOM+ neurons has more to do with anxiety and fear-related behaviors in general than it does with social interactions and restricted-repetitive motion. Here, we can see the effects of a single cell-type and begin to further understand how mutations in different groups of cells can play different parts in the expression of disrupted behavior in animal models of neurological disorders. It is important to attempt to parse out how separate regions or cell types give rise to the different layers of the behavioral phenotype observed in a neurological disorder in order to better understand how they all work together, and to potentially target different symptoms more directly. With this information, we can contribute to the ongoing efforts to alleviate some discomfort from those who are afflicted with more disruptive forms of ASD.

A)

B)

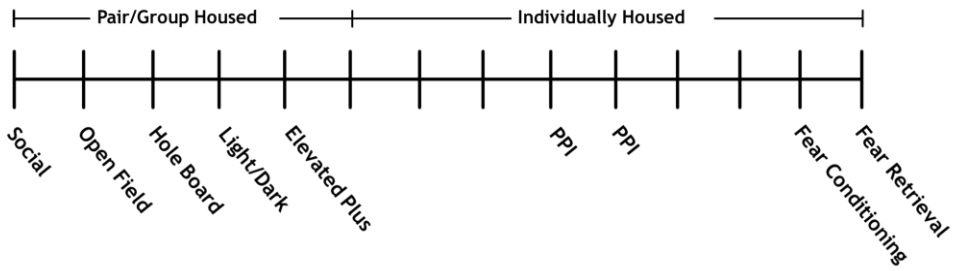

Figure 1: Overview of behavioral experiments

A) Pictures of behavioral chambers, clockwise from top right: Pre-pulse inhibition and acoustic startle, three chamber social, elevated plus maze, light/dark, hole board (remove insert for open field). B) Schedule of experiments for a behavioral run.

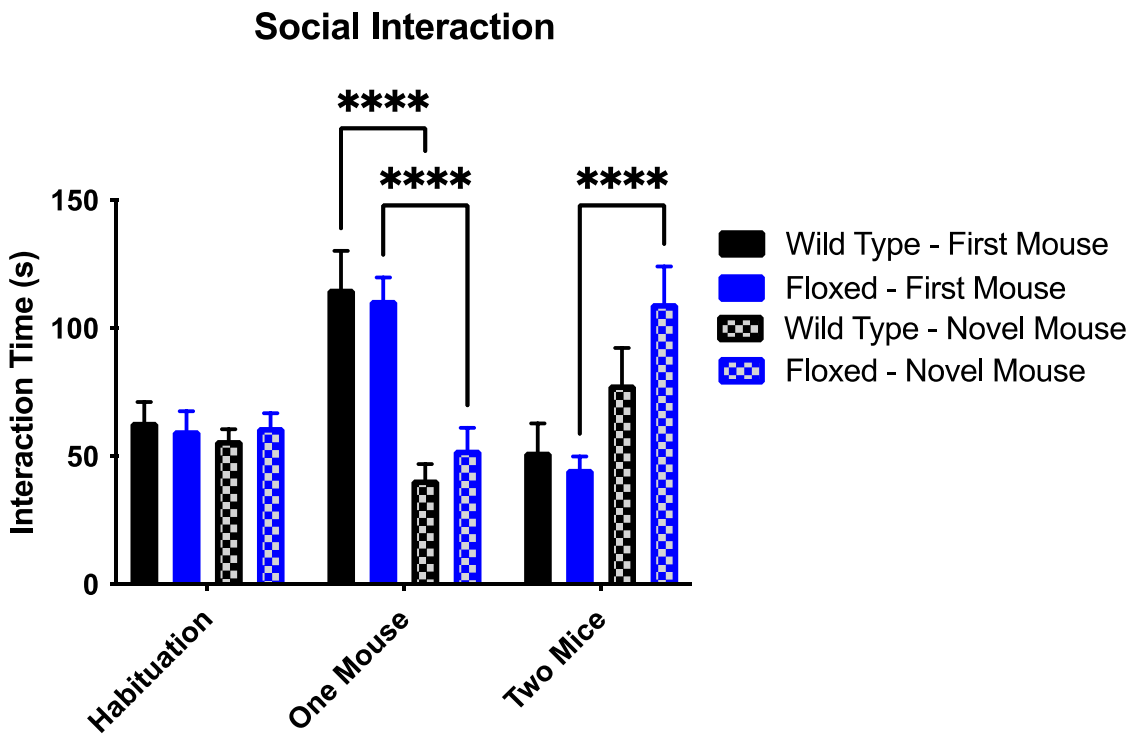

Figure 2: Floxed mice show a similar social interaction profile to wild type littermates

Both sets of mice interacted significantly more with social targets than with non-social targets (the empty cup) in the One Mouse stage (WT: n=10, 115.6s vs 41.01s, Tukey's test: $p<0.0001$, Floxed: n=12, 111.2s vs 54.65s, Tukey's test: $p<0.0001$). Floxed mice showed a higher preference for social novelty than wild type mice in the Two Mice stage (WT: n=10, 78.14s vs 51.90s, Tukey's test: $p=0.2526$, Floxed: n=12, 110.0s vs 45.20s, Tukey's test: $p<0.0001$). All data are presented as mean +/- SEM.

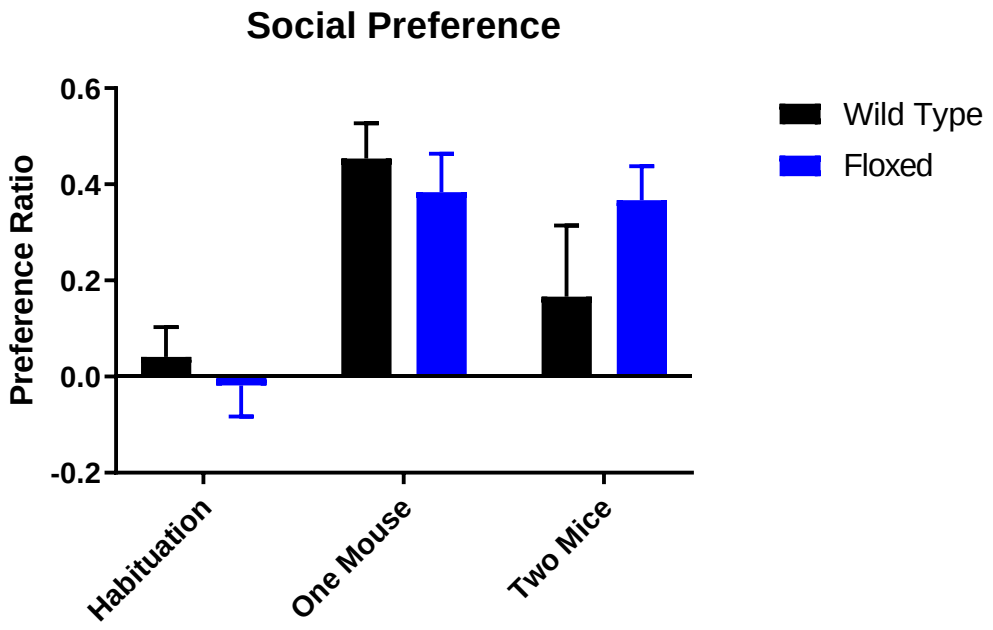

Figure 3: Wild type and floxed mice have intact social preference

Wild type and floxed mice both show increased preference ratios for social preference and social novelty but were not significantly different from each other (n= 10 WT and 12 FL mice, 2 way ANOVA: Stage Effect – $F(2,60)=11.40$, $p<0.0001$, Genotype Effect – $F(1,60)=0.1119$, $p=0.7392$). All data are presented as mean +/- SEM.

A)

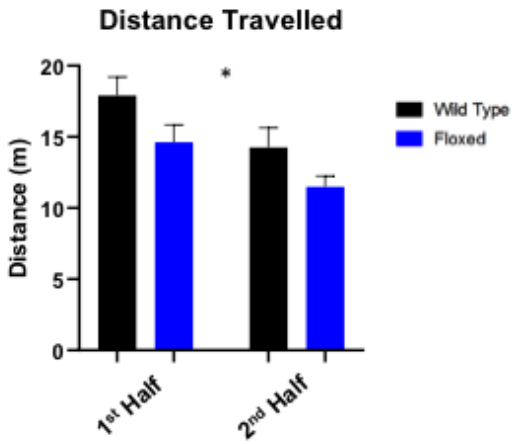

B)

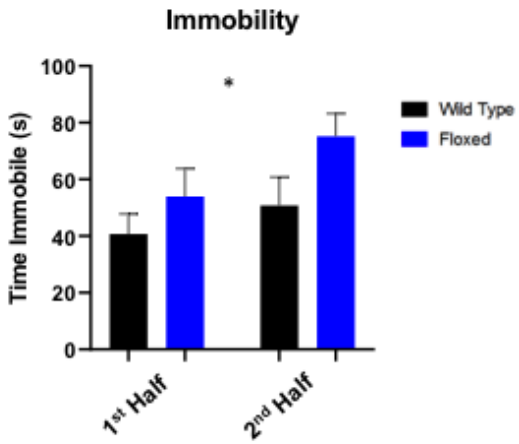

C)

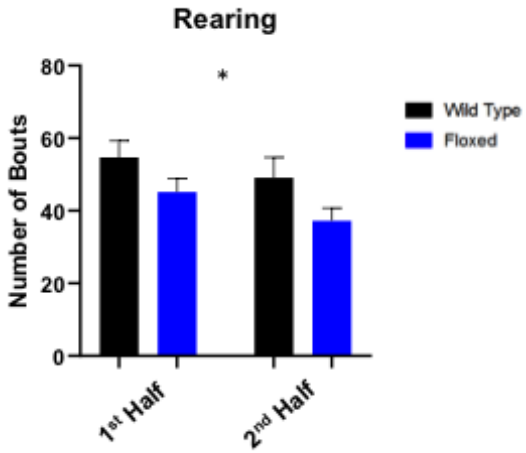

Figure 4: Floxed mice show indications of anxiety in the open field test

A) Both genotypes travelled less in the second half of the test compared to the first half, and floxed mice travelled less than wild type in both halves (n=10 WT and 13 FL mice, * indicates 2 way ANOVA – Genotype effect: $F(1,42) = 6.793$, $p=0.0126$, Half effect: $F(1,42) = 8.601$, $p=0.0054$). B) Floxed mice spent more time immobile than wild type mice (n=10 and 13 FL mice, * indicates 2 way ANOVA – Genotype effect: $F(1,42) = 4.381$, $p=0.0424$). C) Floxed mice also showed fewer bouts of exploratory rearing behavior (n=10 and 13 FL mice, * indicates 2 way ANOVA – Genotype effect: $F(1,42) = 6.156$, $p=0.0172$). All data are presented as mean +/- SEM.

A)

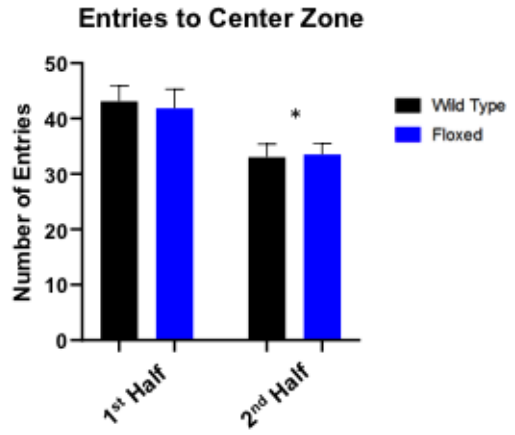

B)

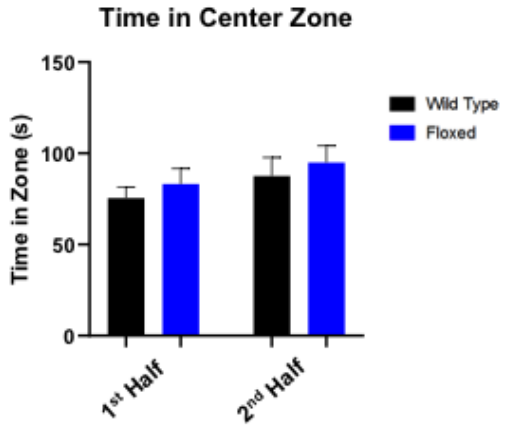

C)

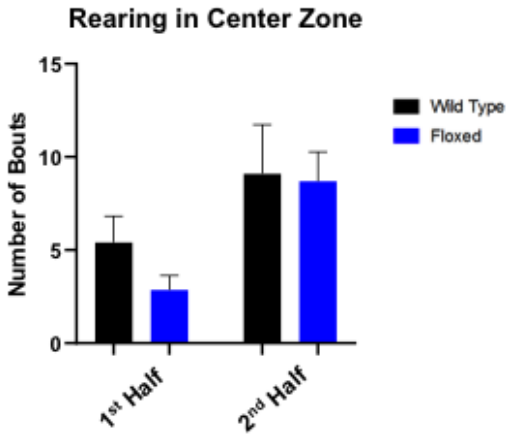

Figure 5: Floxed mice do not show differences from wild type mice in the center zone

A) Both genotypes entered the center zone fewer times during the second half of the test (n=10 WT and 13 FL, * indicates 2 way ANOVA –Half effect: $F(1,42) = 10.97$, $p=0.0019$). B) Both genotypes spent a comparable amount of time in the center (n=10 WT and 13 FL, 2 way ANOVA - Genotype effect: $F(1,42) = 0.7147$, $p=0.4027$). C) The floxed mice trended toward fewer rearing bouts compared to wild type littermates, especially in the first half of the test. All data are presented as mean +/- SEM.

A)

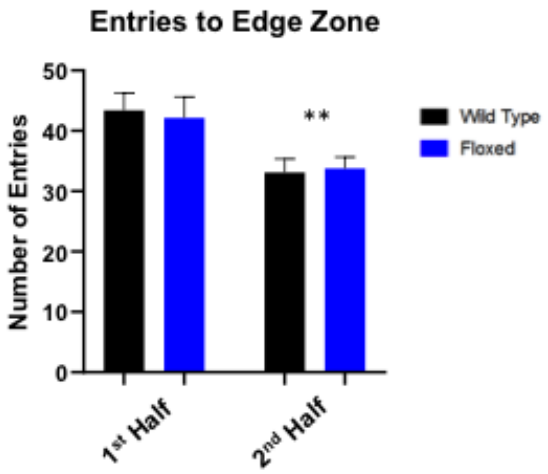

B)

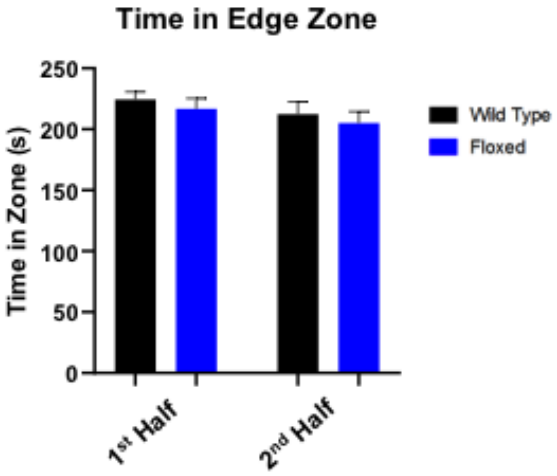

C)

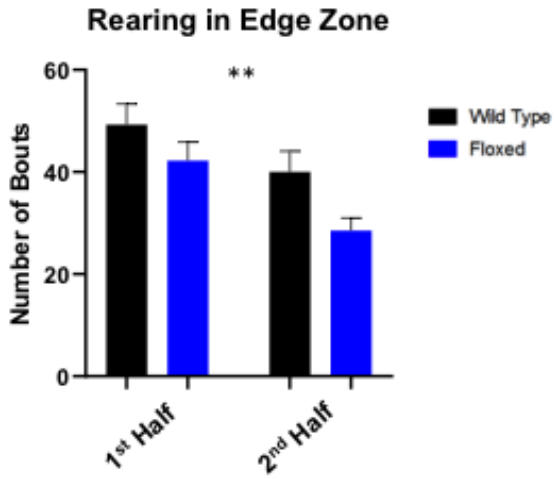

Figure 6: Both genotypes spent more time in the edge zone, but floxed mice reared less

A) Both genotypes entered the side zones fewer times in the second half of the test (n=10 WT and 13 FL, ** indicates 2 way ANOVA – Half effect: F (1,42) = 11.43, p=0.0016). B) Both genotypes spend comparable amounts of time in the edge zones (n=10 WT and 13 FL, 2 way ANOVA - Genotype effect: F (1,42) = 0.7147, p=0.4027). C) The floxed mice reared less in the side zones compared to wild type mice (n=10 WT and 13 FL, ** indicates 2 way ANOVA - Genotype effect: F (1,42) = 10.61, p=0.0022). All data are presented as mean +/- SEM.

A)

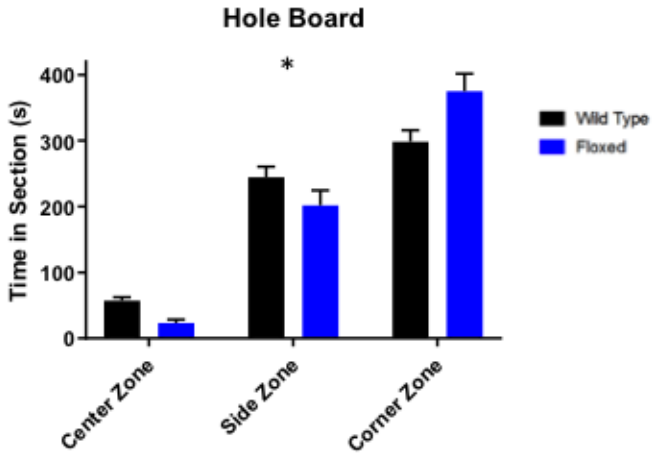

B)

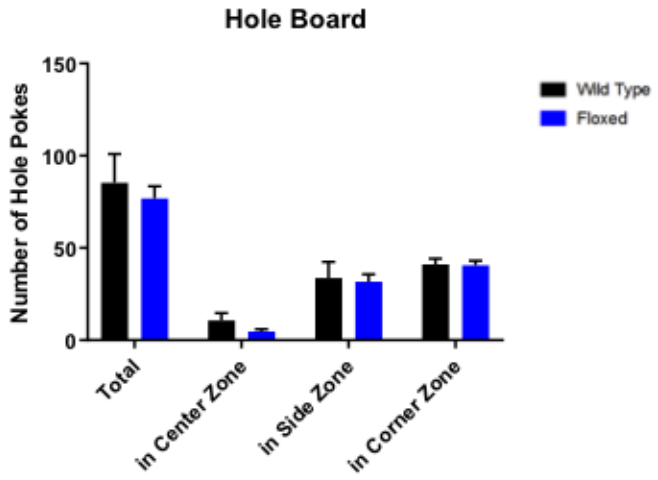

Figure 7: Wild type and floxed mice show similar behavior patterns in the holde board test

A) Floxed mice and wild type mice spent more time in the sides and corners than the center zone, but the difference was more pronounced in floxed mice (n=3 WT and 6 FL, 2 way ANOVA – Zone effect: $F(2,21) = 91.05$, $p<0.0001$, * indicates Interaction: $F(2,21) = 4.503$, $p=0.0236$). B) Wild type and floxed mice nose poked a similar number of holes in total, and showed similar patterns in where they preferred to poke (n=10 WT and 13 FL, 2 way ANOVA – Zone effect: $F(2,21) = 36.92$, $p<0.0001$, Genotype effect: $F(1,21) = 0.7473$, $p=0.3971$). All data are mean +/- SEM.

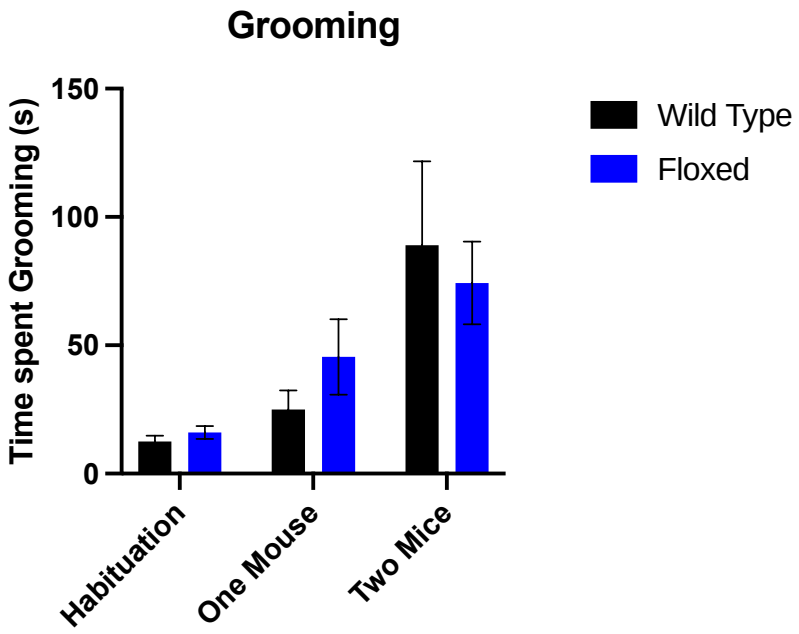

Figure 8: Floxed mice do not show signs of excessive grooming

Wild type and SOM+ PTEN KO mice spend the same amount of time grooming during the three chamber social test. Both genotypes spend more time grooming as the test goes on, with the most grooming occurring when both stranger mice are present (n=10 WT and 12 FL mice, 2 way ANOVA – Stage effect: $F(2, 63) = 9.643$, $p=0.0002$, Genotype effect: $F(2, 63) = 0.0558$, $p=0.8140$).

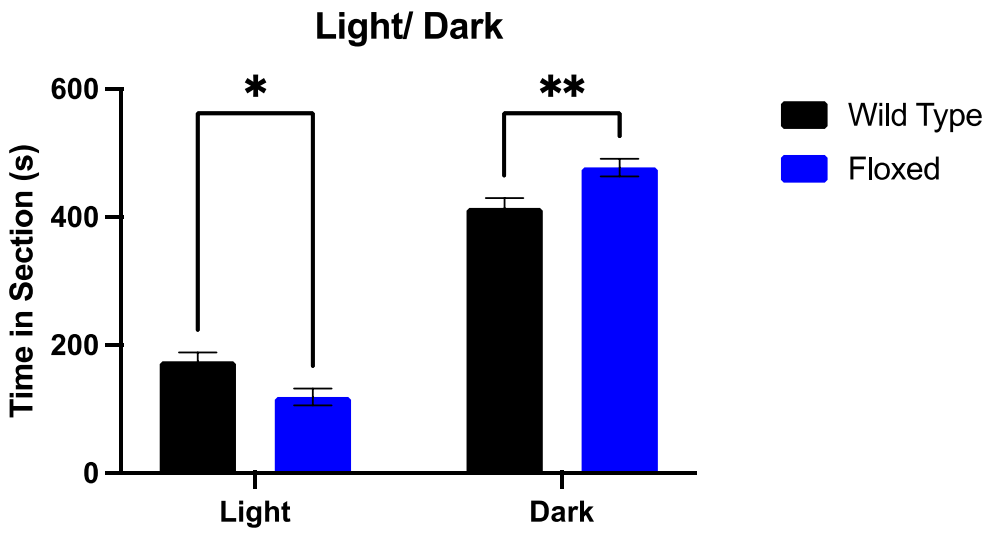

Figure 9: SOM+ PTEN KO mice show elevated levels of anxiety in the light/dark test

Both genotypes spent more time in the dark side of the light/dark test, but floxed mice spent significantly less time in the light and more in the dark compared to their wild type littermates (n=10 WT and 13 FL, 2 way ANOVA – Zone effect: $F(1,42) = 463.6$, $p<0.0001$, *** indicates Interaction: $F(1,42) = 18.29$, $p=0.0001$). Floxed mice spent less time in the light (118.9 seconds vs 174.9 seconds, Sidak's test: $p=0.0133$) and more time in the dark (477 seconds vs 414.3 seconds, Sidak's test: $p=0.0053$) compared to WT mice. All data are presented as mean +/- SEM.

A)

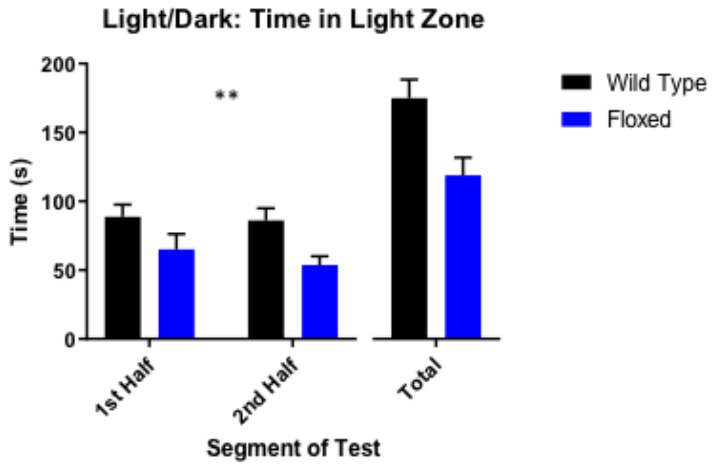

B)

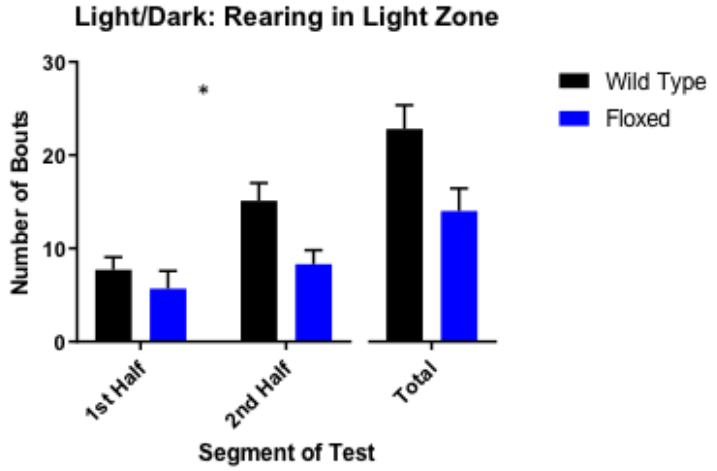

Figure 10: Floxed mice show elevated anxiety and reduced exploration in the light zone

A) Neither genotype showed a difference in light time based on the segment of the test, but floxed mice spent less time in the light than WT mice throughout (n=10 WT and 13 FL mice, 2 way ANOVA – Segment effect: F (1,42) = 0.6010, p=0.4425, ** indicates Genotype effect: F (1,42) = 9.417, p=0.0038, Total not included in ANOVA). B) Both genotypes showed an increase in exploratory rearing during the second half of the test, but floxed mice reared significantly less than WT (n=10 WT and 13 FL mice, 2 way ANOVA – Segment effect: F (1,42) = 8.405, p=0.0059, Genotype effect: F (1,42) = 6.489, p=0.0146, Total not included in ANOVA). All data are presented as mean +/- SEM.

A)

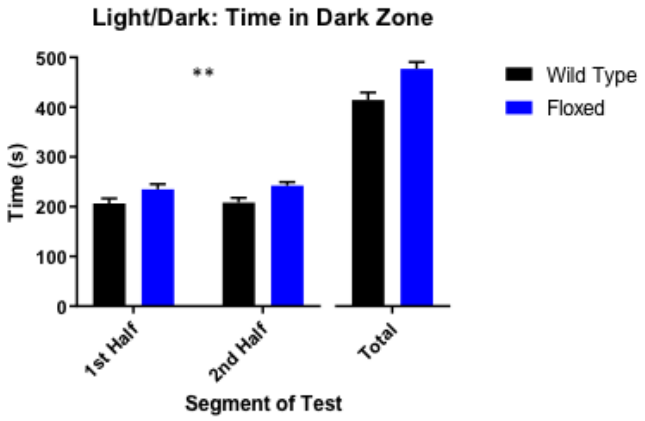

B)

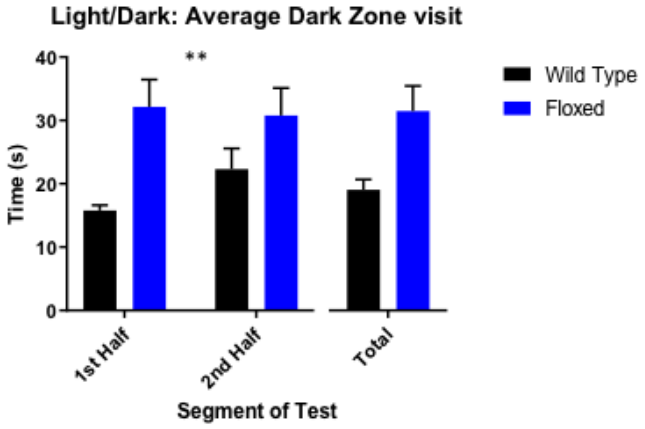

Figure 11: Floxed mice show elevated levels of anxiety in the dark zone of the light/dark test

A) Neither genotype showed a difference in dark time based on the segment of the test, but floxed mice spent more time in the dark than WT mice throughout (n=10 WT and 13 FL mice, 2 way ANOVA – Segment effect: F (1,42) = 0.2468, p=0.6220, ** indicates Genotype effect: F (1,42) = 10.84, p=0.0020, Total not included in ANOVA). B) The average visit to the dark zone was much longer for floxed mice compared to wild type mice (n=10 WT and 13 FL mice, 2 way ANOVA – Segment effect: F (1,42) = 0.4607, p=0.5010, ** indicates Genotype effect: F (1,42) = 10.70, p=0.0021, Total not included in ANOVA). All data are presented as mean +/- SEM.

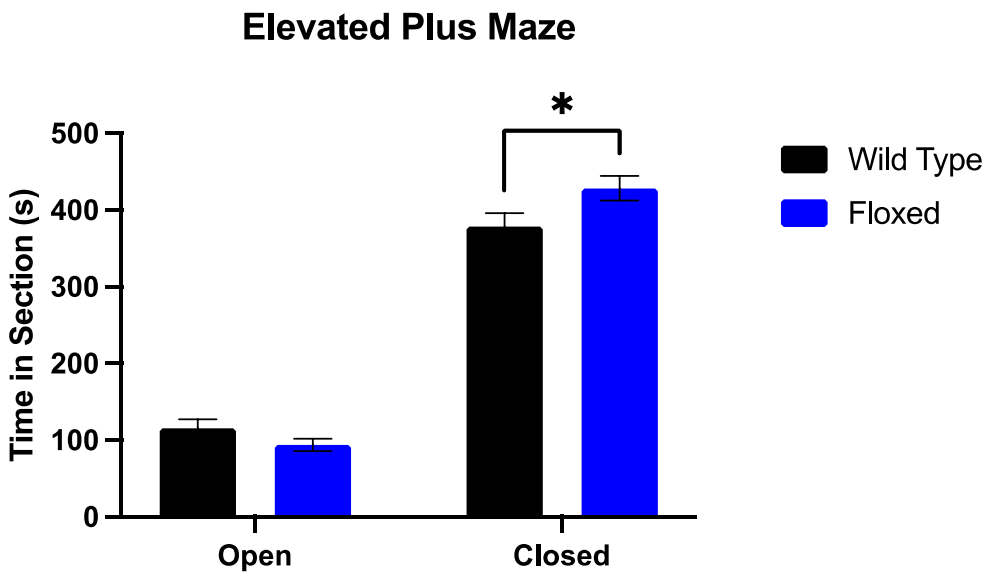

Figure 12: SOM+ PTEN KO mice show elevated levels of anxiety in the elevated plus maze

Both genotypes spent much more time in the closed arm of the EPM compared to the open arm, but the floxed mice had a more extreme preference for the closed arm (n=10 WT and 13 FL mice, 2 way ANOVA – Arm effect: $F(1,42) = 468.4$, $p<0.0001$, Interaction: $F(1,42) = 6.671$, $p=0.0134$). Floxed mice spent less time in the open arm and more time in the closed arm compared to wild type mice (Open Arm: 115.53 seconds vs 93.82 seconds, Closed Arm: 378.6 seconds vs 428.2 seconds, * indicates Sidak's test: $p=0.0295$). All data are presented as mean +/- SEM.

A)

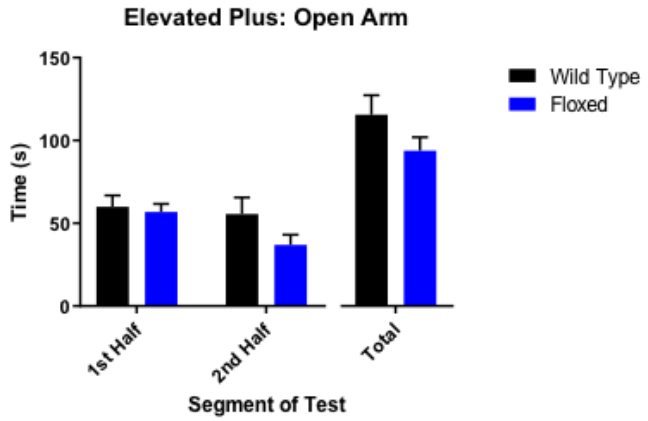

B)

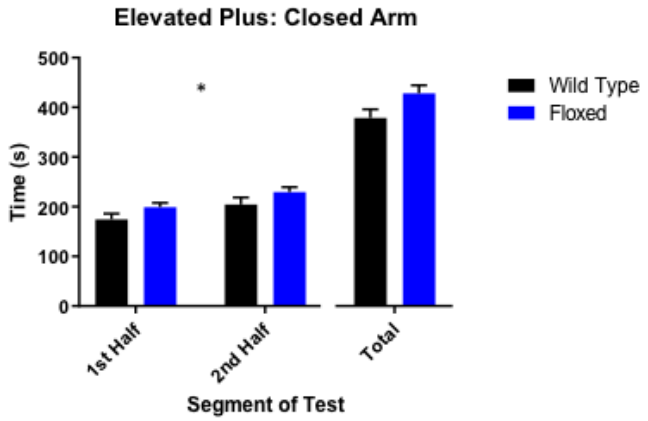

Figure 13: Floxed mice show differences in EPM activity

A) The relatively low values compared to the variability in time spent in the open arm failed to show significant differences due to the segment of the test or genotype (n=10 WT and 13 FL mice, 2 way ANOVA – Segment effect: $F(1,42) = 3.056$, $p=0.0878$, Genotype effect: $F(1,42) = 2.450$, $p=0.1251$). B) With a more representative amount of time spent in the closed arm, both genotypes showed increased time in the closed arm during the second half of the test, and the preference was stronger in floxed mice (n=10 WT and 13 FL mice, 2 way ANOVA – Segment effect: $F(1,42) = 7.540$, $p=0.0088$, Genotype effect: $F(1,42) = 4.995$, * indicates $p=0.0308$). All data are presented as mean +/- SEM.

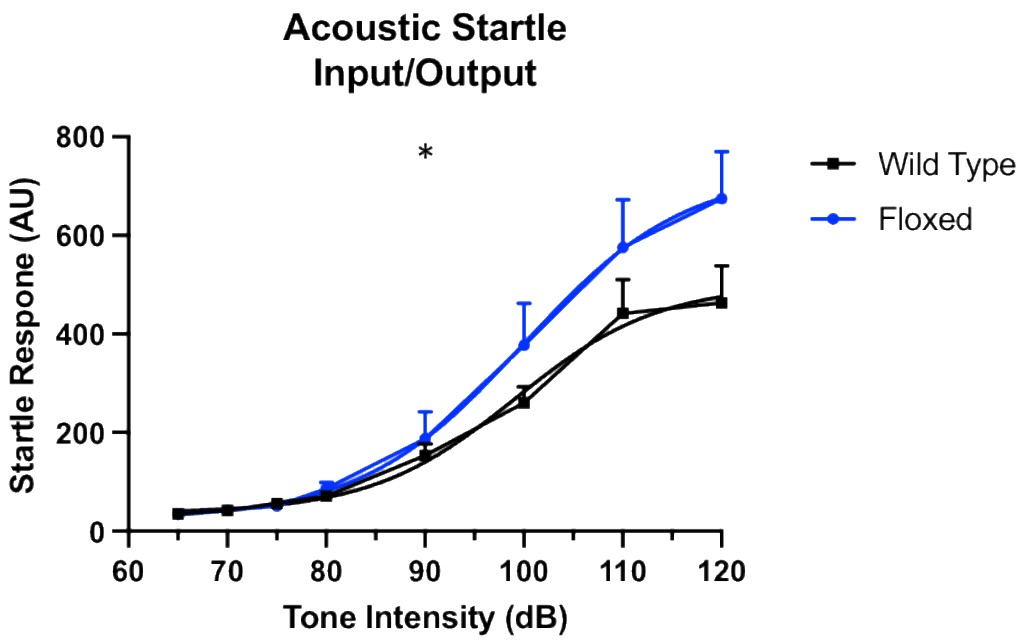

Figure 14: Floxed mice show elevated startle response to acoustic stimuli

SOM+ PTEN KO mice exhibited stronger startle responses to loud acoustic stimuli. Fitting a sigmoidal dose-response curve to the intensity of accelerometer deflection revealed an increase in the maximum startle response evoked by louder stimuli while the baseline, EC50, and slope were marginally affected (n=10 WT and 13 FL mice, EC50: 99.10 dB vs 99.91 dB, Slope: 0.060 vs 0.053, Max Response: 500.4 vs 732.3, * indicates Comparison of Fits – $F(4,176) = 3.378$, $p=0.0108$). All data are presented as mean +/- SEM.

A)

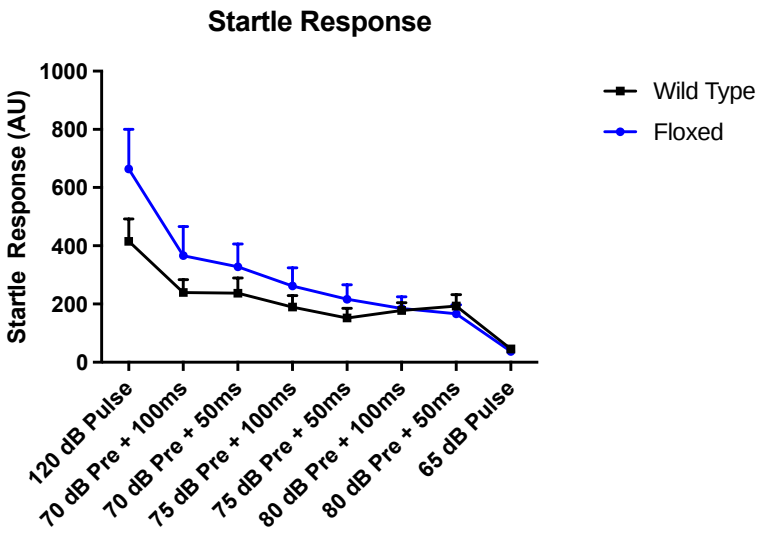

B)

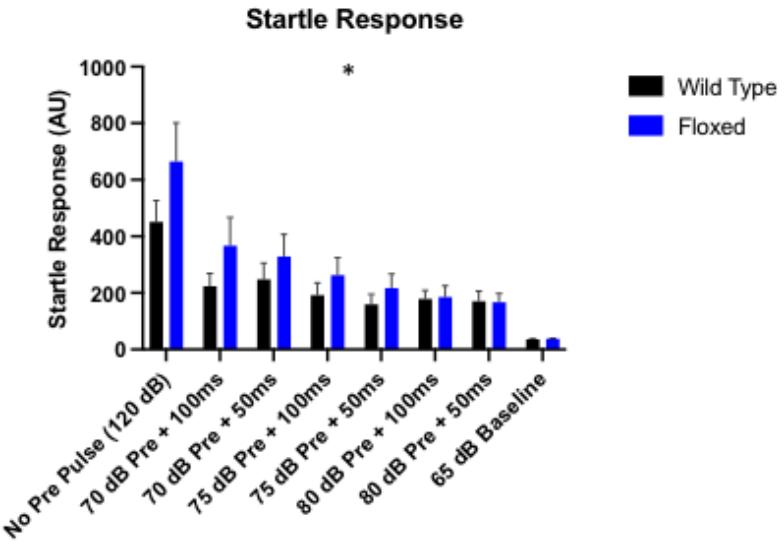

Figure 15: Startle responses to pre-pulse inhibition are still elevated in floxed mice

A) Both genotypes show reduced startle amplitude to stimuli with pre-pulses of 70, 75, and 80 dB at 100 ms and 50 ms intervals. B) Both genotypes show a strong decrease in startle amplitude to stimuli with a pre-pulse but floxed mice still startle more than their wild type littermates (n=9 WT and 13 FL mice, 2 way ANOVA – PPI effect: $F(7, 160) = 9.637$, $p<0.0001$, * indicates Genotype effect: $F(1, 160) = 4.237$, $p=0.0412$). All data are presented as mean +/- SEM.

A)

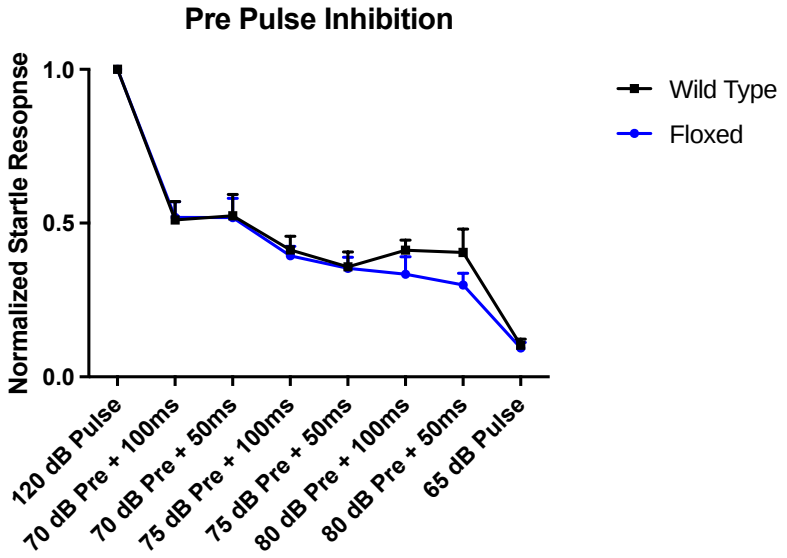

B)

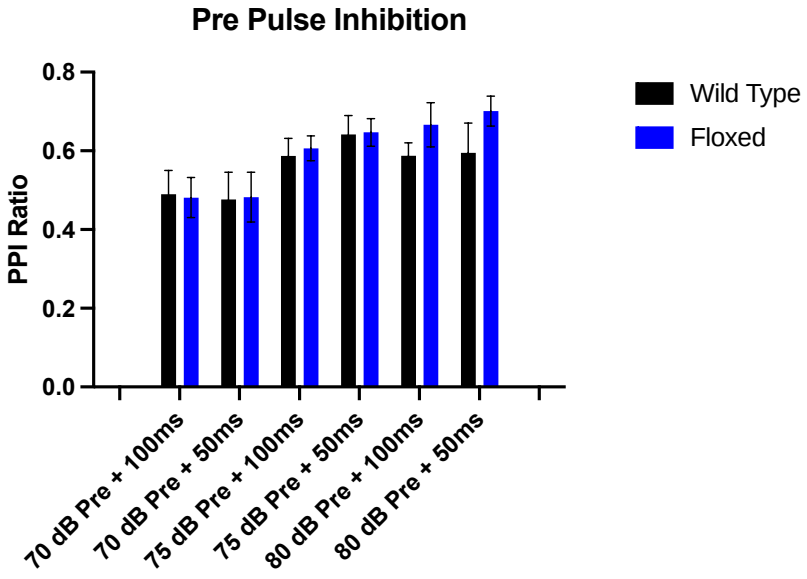

Figure 16: Pre-pulse inhibition ratio is unaffected by SOM+ PTEN KO

A) When normalized to the response of the 120 dB without a pre-pulse, both genotypes show strong PPI. B) The pre-pulse inhibition ratio is intact for floxed mice, with both genotypes showing increasing response inhibition to louder pre-pulses (n=9 WT and 13 FL mice, 2 way ANOVA – PPI effect: $F(5, 120) = 4.436$, $p=0.0010$, Genotype effect: $F(1, 120) = 1.289$, $p=0.2585$). All data are presented as mean +/- SEM.

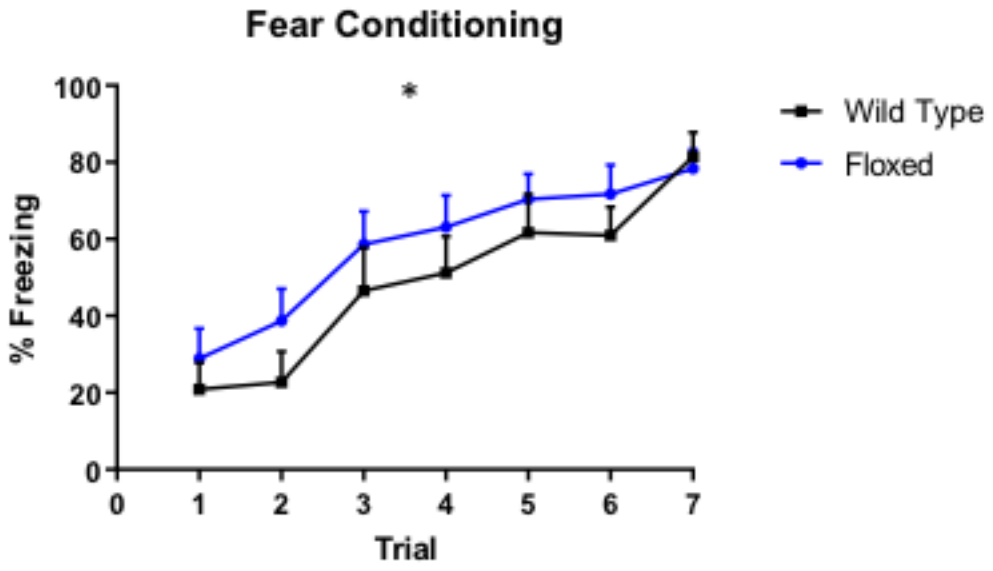

Figure 17: Floxed mice have elevated freezing during fear conditioning

Both genotypes are able to acquire fear memory, but mice with SOM+ PTEN knockouts show elevated levels of freezing to the tone paired with a mild foot shock (CS+) during conditioning compared to their wild type littermates (n=10 WT and 13 FL mice, 2 way ANOVA – Conditioning effect: $F(6,147) = 12.01$, $p<0.0001$, * indicates Genotype effect: $F(1,147) = 4.480$, $p=0.0360$). All data are presented as mean +/- SEM.

A)

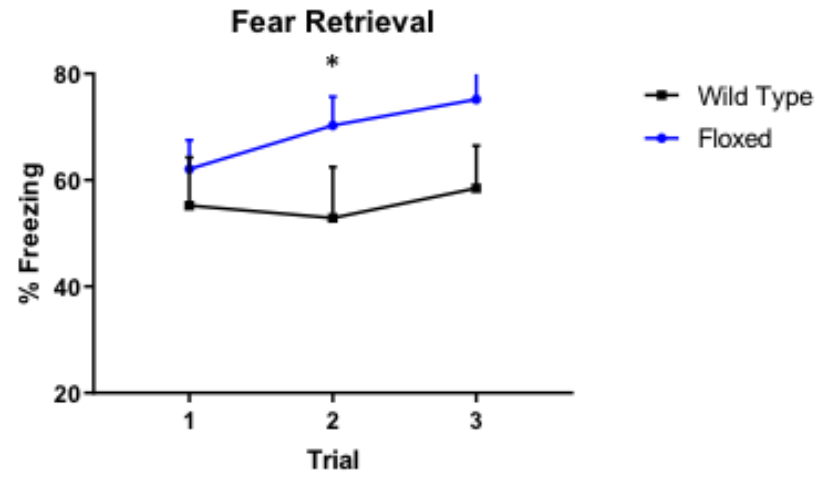

B)

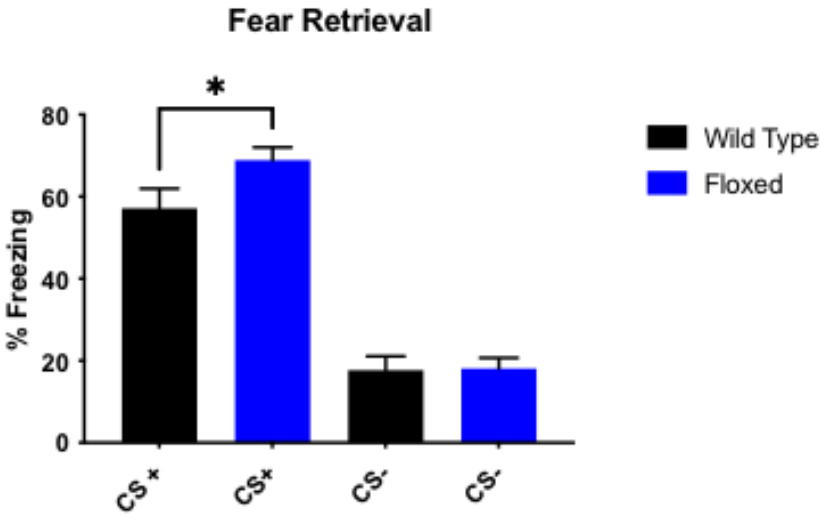

Figure 18: SOM+ PTEN KO mice show elevated levels of freezing during fear retrieval

A) Both genotypes freeze when presented with the tone previously paired with a foot shock, but the floxed mice show increased freezing behavior (n=10 WT and 13 FL mice, 2 way ANOVA – Genotype effect: $F(1, 63) = 5.683$, * indicates t-test: $p=0.0202$). B) Both genotypes are able to differentiate between the tone previously paired with a foot shock (CS+) and the tone that was not paired with a shock (CS-), while the floxed mice still froze to the CS+ tone more than WT mice (n=10 WT and 13 FL mice, CS+ Freezing: 57.17% vs 68.91%, * indicates t-test – $p=0.0364$). All data are presented as mean +/- SEM.

CHAPTER 6: CONDITIONAL KNOCKOUT OF PTEN IN SOM+ INTERNEURONS DISRUPTS LOCAL CIRCUITRY IN THE CENTRAL AMYDGDALA

Introduction

The correlation of a manifested behavioral phenotype to the underlying regional circuitry responsible is a crucial part of understanding the brain and its control of everyday action as well as its dysfunction in neurological disorders. This was especially true for us, in that further characterization of the cell-type specific effects of conditional PTEN loss provides insight into how SOM+ neuron function relates to the overall phenotype of the PTEN model of autism spectrum disorder. To this end, we wanted to investigate the corresponding morphological and physiological differences that accompanied the ASD-related behavioral deficits observed in our SOM+ PTEN KO mice.

Given the specific behavioral consequences of our conditional PTEN knockout from SOM+ neurons, we chose to focus our experiments in an area of the brain that has long been associated with the regulation of fear and anxiety, the amygdala. In humans, the amygdala has been associated with the processing and regulation of emotion (Adolphs et al., 1994; Anderson & Phelps, 2001; Phelps & LeDoux, 2005), and human patients with ASD show higher incidence of deficits in their emotional regulation (Samson et al., 2012; Simonoff et al., 2012). Additionally, given the high comorbidity of fear and anxiety related disorders that accompany

ASD in many humans (see Chapter 2), and the known role of the amygdala in regulating these behaviors, disruptions in amygdala function in ASD are probable. Accordingly, human studies have shown changes in the number of neuronal (Schumann & Amaral, 2006; Wegiel et al., 2014) and non-neuronal (Morgan et al., 2014) cells in the amygdala of post-mortem studies, as well as decreased functional connectivity within the amygdala of ASD patients using fMRI (Rausch et al., 2016).

As it is unethical and unwise to perform loss of function experiments on humans, further research into amygdala function has occurred in animal models. Early work in non-human primates and rats showed that lesions in the amygdala changed the emotional affect of the animals and resulted in increased fear and aggression (Brown & Sharpey-Schafer, 1888; LeDoux et al., 1990; Weiskrantz, 1956). Since then, many have further characterized the importance of the amygdala and its communication with other areas, such as the periaqueductal gray (PAG), bed nucleus of the stria terminalis (BNST), and medial prefrontal cortex (mPFC), in animal models of fear and anxiety (Ahrens et al., 2018; Babaev et al., 2018; De Oca et al., 1998; Ehrlich et al., 2009; Fadok et al., 2018; Fox et al., 2015; Janak & Tye, 2015; Sotres-Bayon et al., 2012; Vogel et al., 2016; Yu et al., 2017). With sufficient rationale for a prominent role of the amygdala in the behavioral disruptions we found in our SOM+ PTEN knockout mice, we decided to direct our morphological and physiological investigations there.

Since PTEN is associated so strongly with the regulation of cellular growth, and it's mutations are responsible for many types of overgrowth and tumors, as we have previously discussed (see Chapter 3), we wanted to start with a morphological

comparison of SOM+ neurons in the CeA with and without PTEN. Morphological analysis of neurons dates back to the days of Ramon y Cajal and changes in a cell's structure can have powerful implications for its ability to process and propagate information. We sought to understand the morphological effects of PTEN loss in SOM+ neurons in two ways, by measuring the size of SOM+ cell somas and by analyzing their dendritic arbors. Both of these were accomplished by a combination of confocal imaging and whole-cell filling and reconstruction with biocytin. Morphological measurements of dendritic arbors using Sholl analysis have been used for nearly 70 years and are effective for documenting the length and complexity of full dendritic arbors (Sholl, 1953). While cellular overgrowth has been shown in other animal models of PTEN mutations, it has never been demonstrated in a SOM+ specific knockout, nor have the effects of PTEN loss on the dendritic arbors of SOM+ neurons been assessed.

For our physiological characterization of the potential aberrant circuit dynamics in the amygdala as a result of the loss of PTEN from SOM+ neurons, we used a combination of patch-clamp electrophysiology, optogenetics, and two-photon (2P) imaging. We wanted to investigate the effects of PTEN mutation from both an afferent view, inputs onto CeA SOM+ neurons, and an efferent view, local outputs from SOM+ neurons within the CeA. By combining these approaches we can determine the physiological disruptions that occur as a result of our conditional knockout of PTEN.

The inputs to CeA SOM+ cells that are most relevant to the expression of fear and anxiety-related behaviors, and therefore most relevant to our experiments,

most often come from the basolateral amygdala (BLA) (Babaev et al., 2018; Duvarci & Pare, 2014; Krabbe et al., 2018; Wolff et al., 2014). In order to discover any changes in the inputs to CeA SOM+ neurons from the BLA specifically, we used a channelrhodopsin (ChR2)-assisted approach. The viral-, or genetically-, driven expression of ChR2, or one of the many subsequent versions carrying various genetically-engineered modifications, allows cells to be effectively activated by pulses of light, and therefore it is an incredibly useful tool for studying the neural circuitry and dynamics in wild type animals as well as models of neurological disorders (Boyden et al., 2005; Nagel et al., 2003, 2005; Tye & Deisseroth, 2012). We took advantage of this technology to probe the effects that SOM+ PTEN KO had on the afferent communication from BLA to CeA SOM+ neurons by injecting a viral vector for the expression of ChR2 (H134R) into the BLA of our mice. In this way, we could patch a SOM+ cell in the CeA, stimulate the opsin-expressing terminals with light, and compare the resulting EPSCs between wild type and SOM+ PTEN KO mice to probe how the proper function of PTEN affects this important fear and anxiety-related circuit.

Similarly, the local inhibitory circuitry within the central amygdala regulates the acquisition and expression of fear and anxiety through a complex, interconnected network of inhibitory cells and their projections (Ahrens et al., 2018; Babaev et al., 2018; Ciocchi et al., 2010; Ehrlich et al., 2009; Haubensak et al., 2010; H. Li et al., 2013; Penzo et al., 2014). These interneurons are electrophysiologically and molecularly heterogeneous, with some overlapping and some non-overlapping characteristics. For example, neurons classified by their spiking properties often do

not have a single molecular identity, and a single genetically-classified cell type does not have a single electrophysiological profile (Dumont et al., 2002; Duvarci & Pare, 2014; Haubensak et al., 2010; Hunt et al., 2017). In order to understand the extent to which local inhibitory communication of SOM+ neurons within the CeA is disrupted by the conditional PTEN knockouts that result in elevated fear and anxiety, we desired to perform the most sophisticated analysis of CeA inhibitory connectivity to date.

While the previously mentioned benefits of optogenetic-assisted circuit investigation are valid and important, we wanted to perform a more precise connectivity analysis that is not possible using single photon illumination and un-restricted ChR2 expression. To this end, we used a modified version of the two-photon circuit mapping technique with soma-restricted channelrhodopsin that was developed in our lab, which improves on the single-photon version in two important ways (C. A. Baker et al., 2016). First, the stimulation of opsins with single photon light does not give precise axial resolution; even if the beam can be limited to a relatively small area in the focal plane, out of focus light is still powerful enough to activate opsin-expressing cells above and below the plane of focus. On the contrary, two-photon light provides excellent optical sectioning as a result of the drastically reduced probability of out of focus light having sufficient power to produce two-photon absorption, which results in much greater axial resolution for opsin activation. Second, opsin expression in the dendrites of cells is often high enough to induce action potentials, even with off target activation; neurons with overlapping cell bodies and dendritic arbors may be activated unintentionally and reduce the

spatial resolution of the map. By restricting the expression of opsins to the soma and proximal dendrites via a piece of the Kv2.1 channel responsible for somatic targeting, we are able to limit the off-target activation of overlapping cells and dramatically increase the XY spatial resolution.

Combining all of these morphological and physiological techniques will allow us to discover the underlying circuit dysfunction in the amygdala that is associated with the elevated levels of fear and anxiety we observe in our SOM+ PTEN KO mice, and provide more insight into how the local inhibitory circuits within the amygdala contribute to animal models of ASD.

Methods

Animals – All mice were bred, housed, and maintained according to protocols approved by the IACUC at MPFI, and all surgical procedures and euthanasia were performed in line with those same protocols.

Viral Injections – Viruses were obtained from Vigene. For local circuit mapping experiments, a soma-restricted version of Chrmine was combined with GCamp6m using a P2A sequence so that infected cells expressed the opsin and Ca2+ indicator at the same time (AAV5-CAG-GCamp6m-2A-ChRmine-Kv2.1-HA). 150 uL of this construct was injected into each hemisphere of the CeA (from Bregma: -1.34 AP, +/- 3.05 ML, 4.82 DV) and allowed to express for 3 weeks prior to the experiment. Previously unsuccessful attempts at these experiments used several combinations of separate viruses for various opsins and GCamp6 in hopes of overlapping expression and optimal activation kinetics, however, sufficient activation and co-expression were not realized. In a separate set of experiments, we

injected ChR2 (AAV5-hSyn-hChR2(H134R)-EYFP) into the BLA (from Bregma: -1.75 AP, +/- 3.50 ML, 4.92 DV), waited 3 weeks for expression, and recorded photostimulated inputs onto CeA SOM+ cells.

Surgeries were performed using a semi-robotic stereotaxic system, StereoDrive (Neurostar, Tubingen, Germany). Mice were placed in a small plexiglass chamber (3"x4"x9") and anesthesia was induced using 4% Isofluorane (Patterson Veterinary Supply, Inc, Sterling, MA) in O_2 through a calibrated SurgiVet vaporizer (Smiths Medical, Minneapolis, MN). After induction, we moved the mouse to the stereotactic setup, secured them, and lowered the Isofluorane to 1.5% for the remainder of the procedure. Temperature control and all surgical tools were from Fine Science Tools (Fine Science Tools, Foster City, CA).

Electrophysiology – Mice were anesthetized using isofluorane and euthanasia was completed by cardiac perfusion of ice-cold cutting solution containing (in mM): 124 Choline Cl, 2.5 KCl, 26 NaHCO3, 1.25 NaH2PO4, 3.3 MgCl2, 10 Glucose, 0.5 CaCl2, with osmolarity adjusted to 295-305 mOsm (VAPRO Osmometer, ELITechGroup, Puteaux, France) and bubbled with 95% O2 / 5% CO2 (Airgas, Radnor, PA). The brain was then removed, placed in ice-cold cutting solution and sliced at 350 um on a Leica VT 1000 S Vibratome (Leica, Wetzlar, Germany). Slices were then placed in ACSF warmed to 37C in a hot water bath and bubbled with 95% O2 / 5% CO2. The ACSF contains (in mM): 124 NaCl, 3 KCl, 26 NaHCO3, 1.25 NaH2PO4, 1 MgCl2, 20 Glucose, 5 Na-Ascorbate, 3 Na-Pyruvate, 2 Thiourea and was adjusted to 295-305 mOsm. After 30 minutes incubation, slices

were removed from the hot water bath in the same solution and allowed to come to room temperature.

Slices were then taken to an upright Zeiss Examiner Z1 microscope (Zeiss, Oberkocken, Germany) for whole-cell patch clamp experiments. We used a combination of the following Zeiss objectives (Zeiss, Oberkocken, Germany): 10x/0.3 NA W N Achroplan, 20x/1.0 NA W Plan Apochromat, and 40x/1.0 NA W Plan Apochromat. Glass micropipettes were fabricated using a Sutter P-97 micropipette puller (Sutter, Novato, CA) with a resistance of 4-7 MOhms. We used Scientifica Microstar (Scientifica, Uckfield, UK) and Sutter MPC-200 (Sutter, Novato, CA) micromanipulators on different rigs. All data were acquired at 20kHz and low-pass filtered at 2kHz using Clampex Software (pCLAMP 10), a Multiclamp 700B amplifier, and a Digidata 1440A digitizer (Molecular Devices, San Jose, CA).

For various experiments, different internal solutions were used, including K-Gluconate (145 KGlu, 5 NaCl, 10 Hepes, 0.5 EGTA, 4 MgATP, 0.3 Na2GTP, adjusted to 290 mOsm and pH 7.25), Cs-Methanesulfonate (135 CsMeth, 6 NaCl, 10 Hepes, 0.6 EGTA, 4 MgATP, 0.3 Na2GTP, adjusted to 295 mOsm and pH 7.25), and Cs-Gluconate (135 CsGlu, 8 NaCl, 10 Hepes, 0.2 EGTA, 10 CsCl, 2 MgATP, 0.2 Na2GTP, adjusted to 295 mOsm and pH 7.25). Additional, various channel blockers were used as needed, including 20uM Bicuculine, 10uM NBQX, 50uM AP5, and 1uM TTX.

Fluorescent proteins were activated by epifluorescence from a HXP 120C halogen lamp (Zeiss, Oberkocken, Germany) in combination with Zeiss filter cubes for various fluorophores (Zeiss filter set 38 HE: 470/40 nm excitation filter, 495 nm beamsplitter, 525/50 nm emission filter for GFP and Zeiss filter set 43 HE: 545/25

nm excitation filter, 570 nm beamsplitter, 605/70 nm emission filter for TdTomato). SOM-expressing interneurons were identified for patching by their expression of TdTomato. All images were viewed by an analog DageMTI camera (Dage-MTI, Michigan City, IN).

For the stimulation of afferent, channelrhodopsin-expressing terminals from the BLA onto CeA SOM+ neurons, we used a CooLED pE-100 illumination system (CoolLED Ltd., Andover, England). The wavelength was set to 470 nm and the timing of activation was controlled through the digital outputs feature in Clampex.

Two Photon Circuit Mapping – For 2P experiments, the surgical procedures, solutions, microscope and electrophysiological equipment remained the same as above. We used one Ti:Sapph MaiTai laser (Spectra Physics-Newport, Irvine, CA) tuned to 800 nm for imaging and one Ti:Sapph MaiTai DeepSee laser (Spectra Physics-Newport, Irvine, CA) tuned to 1020 nm for stimulation. The two light paths were controlled by two galvo-galvo mirror sets in the scanhead (Bruker, Billerica, MA) and combined using a 970 shortpass dichroic (Chroma, Bellows Falls, VT). Reflected fluorescent light was deflected toward the PMTs by a 700 nm longpass dichroic (Chroma, Bellows Falls, VT) and separated using a dichroic filter cube with a 550 nm beamsplitter, 500-530 nm bandpass GFP filter and 570-620 nm TdTomato filter (Chroma, Bellows Falls, VT). Gallium-Arsenic-Palladium photomultiplier tubes (GAsP PMTs) (Model H7421, Hamamatsu, Hamamatsu City, Japan) were used to amplify fluorescent signals. 2P mapping experiments were conducted under the 20x objective with a field of view (FOV) of ~405x405 um.

To map local inhibitory circuits in the CeA, we used a combination of electrophysiology and 2P imaging. Post-synaptic cells were identified by the presence or absence of TdTomato, indicating SOM+ or SOM- cells, respectively. Such cells were patched under DIC in the whole-cell patch clamp configuration and held at 0mV with NBQX and AP-5 to block excitatory neurotransmission and isolate inhibitory post-synaptic currents. We then switch to 2-photon imaging to identify individual potential pre-synaptic partners by the expression of GCamp6 and target them for photoactivation. Spiral scanning activation (8.5 um diameter, 5 ms duration, 10 revolutions/spiral, 5 repetitions, 1020 nm stimulation laser) was used to stimulate putative pre-synaptic cells expressing ChRmine. The voltages applied to the galvo mirrors of the simulation laser corresponded to different pixel locations for the presynaptic targets and these were exported as a galvo points list (.gpl) file. Each cell was stimulated in succession with 2 frames of imaging between them such that an imaging sequence contained 3n+25 frames (where n is the number of presynaptic targets, with 25 extra frames at the end for a baseline). 512x512 pixel images were obtained at a framerate of 1.3 Hz, however, we shuttered the PMTs for 50ms around each spiral scan activation using a custom-made Arduino program. Four repetitions of each image sequence were collected for each field of view of each whole-cell patched post-synaptic cell. We controlled the 2P lasers and the imaging and activation parameters using Prairie View software (Version 5.5, Bruker, Bellerica, MA).

Data Analysis – Analysis of electrophysiological and imaging data was conducted using custom written MATLAB codes (available upon request). In brief,

for general electrophysiological experiments, the recorded traces were imported, baselined, and averaged according to the number of repetitions. Peaks were identified and exported to excel for further examination and concatenation.

For circuit mapping experiments, the analysis consisted of four parts: processing imaging sequences, processing electrophysiological signals, identifying SOM+ cells, and bringing all the data together. Imaging sequences for each FOV of each post-synaptic cell consisted of, for an example of 100 presynaptic targets, 4 repetitions of 325 images, each 512x512 pixels. Image stacks were imported into FIJI (NIH, Bethesda, MD) and separated into fluorescent channels. The green GCamp stack was saved as a TIFF to be imported into MATLAB (Mathworks, Natick, MA), while the red TdTomato stack was subjected to a median intensity projection and saved as a single image. In MATLAB, each repetition of the green GCamp fluorescence for each FOV was baselined using the last 10 frames and then averaged together and frames with the blank stimulation artifact were removed. We then used the GPL file to create a circular pixel mask 25 um in diameter for each presynaptic target for the averaged, baselined 325-frame image stack. This mask was applied to the imaging stack so that we could extract the GCamp6 fluorescence for each presynaptic target cell independently. When aligned by frame number (ie time), a successful activation of a pre-synaptic target would show quiescence up until frame 2n-1 (since the first activation occurs on the first frame and the activation frames have been removed) and then a bright spike in fluorescence immediately following the activation. A pre-synaptic target was considered to have had a spike if the corresponding region of interest (ROI) showed an increase in

fluorescence within 5 frames of activation that was greater than 3 times the standard deviation of the F/F of the ROI before being targeted for activation, according to the formula:

Equation 4 - Threshold for Confirmation of Presynaptic Spiking via GCamp6m Fluorescence

$$F_{n\ldots n+5} > 3\left(\sigma(F_{1\ldots n-1})\right)$$

where *F* is the baselined fluorescence of a particular frame, *n* is the frame corresponding to the presynaptic target, and $\sigma(F_{1\ldots n-1})$ represents computing the standard deviation of all preceding frames. If any frame in that span surpassed the threshold, that cell was considered activated. Pre synaptic targets that did not surpass this threshold for Ca2+ activity were excluded from further analysis. Threshold information, Ca2+ fluorescence traces, ROI locations, and summary data for all cells was generated and exported.

Electrophysiological signals were processed similar to other experiments. However, once the traces and peaks had been identified, we viewed each repetition separately to see responses on a trial-by-trial basis. A pre-synaptic cell was considered to be connected to the post-synaptic cell if in at least 2 of the 4 repetitions, a clear and obvious post-synaptic inhibitory current (IPSC) was observed. Summary data of peaks and latencies were exported to excel.

Next, we opened the red TdTomato image for each FOV in FIJI and, using a custom ImageJ macro, overlaid the positions of each targeted cell's ROI (generated in the same MATLAB code that translated the GPL voltages to pixel locations) and numbered them according to their order of stimulation. Then we manually

identified if the cell within each ROI was a SOM+ cell based on the expression or lack of TdTomato.

We then brought all of this data together in excel to compute various parameters such as connection probability between and within cell types as well as the relationship between post synaptic current and the distance from the pre synaptic cell body. Connection probability was computed as:

Equation 5 - Connection Probability

$$p = \frac{n_c}{n_a}$$

where n_c is the total number of presynaptic targets that showed obvious inhibitory post synaptic currents and n_a is the total number of presynaptic targets that had GCamp fluorescence that passed the threshold for time-locked activity. Connection probability was computed separately for each cell type. To determine the spatial distribution of pre synaptic cells and their relative contribution to the post synaptic currents recorded, we computed various current and distance relationships. We concatenated all the IPSC peaks, with the soma to soma distance for their corresponding pre synaptic ROI, for each stimulation pair (SOM+ to SOM+, SOM- to SOM+, etc) and sorted the peaks and distances together from lowest to highest. We then computed the cumulative current for all recordings of each class, binned by 10um of soma to soma distance as follows:

Equation 6 - Distribution of Cumulative Current by Soma to Soma Distance

$$I_d = \frac{\sum_{i=1}^{d} x_i}{\sum_{i=1}^{n} x_i}$$

where I_d is the cumulative current up until distance *d*, x_i is an individual IPSC peak, *d* is the last peak within the desired bin distance (10, 20, 30 um, etc), and *n* is the peak emanating from the pre synaptic target furthest away from the recorded cell, such that the denominator is the sum of all the total current recorded from every pre synaptic cell onto every post synaptic cell of that class. We then computed a curve for the proportion of the total IPSC current received by distance for all the post synaptic cells of each stimulation pair binned by 20 um, as follows:

Equation 7 - Distribution of Proportion of Total Current by Soma to Soma Distance

$$p_d = \frac{\sum_{i=d-20}^{d} x_i}{\sum_{i=1}^{n} x_i}$$

where p_d is the proportion of total current at *d* distance, x_i is an individual IPSC peak, *d* is the top bound of the 20 um bin for soma to soma distance, and *n* is the last IPSC in the list. Similarly, we computed a curve for the average current within each 20 um bin as follows:

Equation 8 - Distribution of Average Current by Soma to Soma Distance

$$I_c = \frac{\sum_{i=d-20}^{d} x_i}{n_c}$$

where I_c is the average current per cell for each bin, x_i is an individual IPSC peak, *d* is the top bound of the 20 um bin for soma to soma distance, and n_c is the total number of post synaptic cells recorded in that configuration (SOM+ to SOM+, SOM- to SOM+, etc). Graphs and figures were created and statistical analysis conducted using GraphPad Prism (Graphpad Software, Inc. San Diego, CA).

Confocal Imaging – We used confocal imaging for identification of SOM+ cell clusters and general SOM+ cell counts/measurements. Mice were anesthetized as

previously described, then underwent cardiac perfusion with a 4% paraformaldehyde (PFA) solution in phosphate-buffered saline (PBS) to fix the brain tissue. The brain was then extracted and post-fixed overnight in 4% PFA in PBS. We then sliced the fixed tissue in 30 um thin sections, using a separate vibratome of the same model as above, and mounted them on glass microscope slides. Clusters of red TdTomato-expressing SOM+ cells were identified in the central nucleus of the amygdala and Z-stack images were taken on a Leica TCS SP5 confocal with Leica 10x and 20x objectives (Leica Microsystems, Mannheim, Germany). For cell counts and cell body measurements, we used FIJI to produce a maximum intensity projection of the stacked images and a 200 x 200 um square was drawn around the densest area of SOM+ cells. Individual cells with red TdTomato expression were counted manually for each stack. Cell body area measurements were estimated on a subset of cells, 20 per stack, by computing the area of an ellipse. We measured the distance of orthogonal lines of each cell such that the major and minor axis distances were recorded and entered them into a simple MATLAB code to compute the area according to the formula:

Equation 9 - Area of an Ellipse

$$A = \pi \left(\frac{1}{2}a\right)\left(\frac{1}{2}b\right)$$

where a and b are the lengths of the major and minor axes, respectively.

Single cell morphological analysis – A small subset of cells were recording under conditions that would allow post hoc morphological analysis. Animals were sacrificed and slices prepared similar to other electrophysiological experiments, at a thickness of 350 um. In order to facilitate post-hoc analysis of cell morphology, we

supplemented the potassium gluconate (K-Glu) internal solution with biocytin (Sigma-Aldrich, St. Louis, MO) to a final concentration of 1.5 mg/ml. We then recorded from a SOM+ cell, identified by TdTomato fluorescence, in a whole-cell patch configuration. We maintained the seal, with access resistance below 20 mOhms, for at least 30 minutes to allow the biocytin to penetrate throughout the entire dendritic arbor. Upon removal of the patch pipette, the slice containing the filled cell was immediately transferred to a microcentrifuge tube containing 4% PFA in PBS and allowed to be fixed overnight in the fridge at 4 degrees Celsius.

The next day the slice was transferred to a microcentrifuge tube containing only PBS to await immunostaining. When a sufficient number of cells and slices had been prepared in this way, they were subjugated to an immunostaining protocol with a fluorophore-conjugated streptavidin for visualization, as streptavidin naturally binds to biocytin. Slices were washed three times for 15 minutes each with PBS containing 0.01% Triton X-100 (Sigma-Aldrich, St. Louis, MO) to facilitate membrane permeability. They were then incubated with a 1:500 dilution of Alexafluor 488-conjugated streptavidin in PBS with 0.01% Triton X-100 overnight in a cold room at 4 degrees Celsius. The following morning, slices were washed three times for 15 minutes with PBS and then mounted on microscope slides with Vectashield Antifade mounting medium (Vector Labratories, Burlingame, CA). We used plastic 300 um spacers so that we did not squish the slices and were still able to form a good seal with the coverglass.

The slices were imaged on a Zeiss LSM 880 AiryScan inverted microscope under Zeiss 10x and 20x objectives. Tiles of image stacks covering the entire

dendritic arbor were collected and stitched in Zeiss Zen software then imported in Neurolucida software for 3d-reconstruction (MBF Biosciences, Williston, VT). The image stack was rendered into 3D and we reconstructed the morphology by tracing each dendrite from the soma through all its branches. The fully traced cell was then analyzed by Neurolucida's internal algorithms for soma size, dendrite length, and Sholl analysis. For Sholl analysis, a series of concentric spheres started at the center of the soma and expanded in 10 um increments until the entire dendritic arbor was within its bounds. The total length of all dendritic segments within each concentric 10 um section was recorded, for a measure of the size of the dendritic arbor, as well as the number of times a dendrite passed the border of each sphere, as an analogue of dendritic complexity.

Results

As discussed in Chapter 5, the behavioral consequences of the conditional knockout of PTEN only in SOM+ neurons were heavily represented in tasks relating to the regulation of fear and anxiety. As such, we focused our morphological and physiological investigation of the SOM+ PTEN KO mice on the amygdala, which has long been associated with emotional regulation and the expression of fear and anxiety. We first took a simple look into the amygdala structure for SOM+ cells using confocal imaging. While SOM+ cells are relatively ubiquitous throughout the brain, pictures of unstained slices with TdTomato expressed in SOM+ cells revealed a dense cluster of SOM+ neurons in the central amygdala (Figure 19). SOM+ cells were present in the basolateral amygdala and nearby cortical regions to a much lower extent. Since so many SOM+ neurons were present in such a small and

important structure, our further experiments were directed to the central amygdala specifically.

PTEN KO leads to increased SOM+ soma size and decreased SOM+ cell count in the central amygdala – As has been well documented, a loss of PTEN function results in overgrowth of the cell body, and this was the case for the SOM+ conditional knockout of PTEN as well. In confocal images of the central amygdala, slices taken from mice lacking PTEN in SOM+ cells showed that those cells had larger cross-sectional soma areas (Figure 20A, n = 88 WT cells vs 77 FL cells, mean = 358 um^2 vs 433 um^2, t-test: $p<0.0001$). Interestingly, though the cells were larger, there were actually fewer of them. We manually counted the number of TdTomato-expressing SOM+ neurons within a 200 um by 200 um area of our maximum intensity projections of each slice. Some slices were 50 um thick and some were 100 um thick, so we extrapolated the measure for the 50 um sections by doubling the count. In slices taken from SOM+ PTEN KO mice, there were significantly fewer SOM+ cells in the densest area of the central amygdala (Figure 20B, n = 16 WT slices from 4 animals vs 14 FL slices from 4 animals, mean = 140.4 cells vs 96 cells, t-test: $p<0.0001$).

SOM+ neurons with no PTEN grow larger and more complex dendritic arbors – In order to more closely investigate the cellular overgrowth of PTEN KO SOM+ cells, a small subset of cells from acute slice electrophysiological experiments were recorded under conditions that would allow for reconstruction of the cell's entire cell body and dendritic arbor for a more complete morphological analysis. When these neurons were traced and reconstructed, the volumetric estimation of

each cell body revealed that those lacking PTEN from the conditional knockout mice were significantly larger than SOM+ neurons from wild type mice (Figure 20C, n=3 WT and 3 FL cells, 3512 um^3 vs 8255 um^3, t-test: p=0.0389).

We also analyzed the dendritic arbors of each of these filled SOM+ cells. Consistent with many previous findings that show cellular overgrowth as a result of PTEN dysfunction, the SOM+ PTEN knockout resulted in neurons with much larger dendritic structures. Representative images of biocytin-filled cells and their corresponding reconstructions with the overlaid Sholl analysis rings show that, even by eye, the PTEN KO cells are larger than the wild type SOM+ cells (Figure 21).

A more quantitative look at the structure of the dendrites showed drastically increased lengths and distal complexity for SOM+ cells lacking PTEN (Figure 22). In Sholl analysis, dendrite lengths are measured as the total amount of dendrite within each successive 10 um, concentric sphere centered at the soma. Wild type SOM+ cells have more of their dendrite length proximal to the soma, showing a higher proportion of total dendrite length between 10-60 um from the soma, with a maximum of 169.167 um of dendrite length between 30 and 40 um away. In contrast, the dendritic arbor of floxed cells is more widely distributed, with a maximum of 146.297 um of dendrite length between 80 and 90 um from the soma, and a large proportion of total dendrite length more distal than 130 um, where wild type arbors begin to taper off (Figure 22A). In addition to this, floxed cells' longest dendrites extend nearly twice as far as wild type dendrites (Figure 22B, n = 3 WT cells and 3 FL cells, Length = 190 for WT vs 360 for FL, t-test: p=0.0018).

Cells recorded from SOM+ PTEN KO mice also showed more intersections in more distal Sholl spheres compared to wild type cells, indicating more complex branching closer to the soma for wild type cells but sustained complexity further away for floxed cells (Figure 22C). Consistently, the total number of Sholl sphere crossings for floxed cells was higher than that of wild type cells (Figure 22D, n = 3 WT and 3 FL cells, # of intersections = 117 for WT and 203.667 for FL, t-test: p=0.030).

Data from the Sholl analysis were fit by lognormal Gaussian curves to compare differences in their arbors because lognormal curves more closely approximated the data compared to Gaussian (R^2 = 0.7727 vs 0.6805 for wild type and 0.7553 vs 0.6568 for floxed). Lognormal curves in GraphPad are fit according to the following equation:

Equation 10 - Curve Fitting for Lognormal Distributions

$$Y = \left(\frac{A}{x}\right) e^{-0.5\left(\frac{\ln\left(\frac{x}{GeoMean}\right)}{\ln(GeoSD)}\right)^2}$$

where *GeoMean* is the geometric mean of the distribution (not the arithmetic mean, but represents something similar to the center of mass), and *GeoSD* is the geometric standard deviation (which is related to the spread of the distribution in a multiplicative way, whereas normal standard deviation is additive). A is related to the area under the curve as follows:

Equation 11 - Relation of the Constant A to the Area Under the Curve

$$Area = A * \sqrt{2\pi} * \ln(GeoSD)$$

so a larger value for *A* and *GeoSD* give a larger area, and *A* is related to the peak amplitude of the distribution as follows:

Equation 12 - Relation of the Constant A to the Peak Amplitude

$$Amplitude = \frac{A}{GeoMean/e^{0.5*\ln(GeoSD)^2}}$$

so a larger value for *A* and a smaller value for *GeoSD* give a higher peak amplitude.

Fitting this model to our data for the length of all dendritic segments within each successive 10 um concentric Sholl sphere yields dramatically different curves for wild type SOM+ cells and SOM+ cells with no PTEN (Figure 22A, solid lines). Accordingly, the parameters for these curves are very different. For wild type cells, *A* is 10096, *GeoMean* is 75.40 um, and *GeoSD* is 1.931. For floxed cells, *A* is 14707, *GeoMean* is 149.6 um, and *GeoSD* is 2.195. A comparison of fits between wild type and floxed showed a very significant result ($F(3,158) = 41.62$, $p<0.0001$). Evaluating for area under the curve gave 16639.81 for wild type cells and 28982.59 for floxed cells, which is proportional to the simple sum of total dendritic length for segment (1512.26 um for WT and 2509.41 um for FL). Evaluating for peak amplitude according to this model gave values of 166.23 for wild type and 133.93 for floxed, which is very close to the peaks seen in the raw data (169.167 for WT and 146.297 for FL), indicating an accurate approximation.

Similarly, the curve fitting for dendrite intersections yielded close approximations of the data (Figure 22C, solid lines) and comparing the fits between wild type and floxed cells revealed large differences (*A* = 728.6 for WT vs 1134 for FL, *GeoMean* = 73.34 for WT vs 153.4 for FL, *GeoSD* = 2.031 for WT vs 2.339 for FL, Comparison of Fits: $F(3, 158) = 48.66$, $p<0.0001$). Evaluating for peak amplitude of

the number of intersections according to the model resulted in values of 12.77 for wild type and 10.61 for floxed, again very nearly approximating the raw data values of 12.67 and 10.67, suggesting an accurate fit.

Central amygdala SOM+ cells lacking PTEN have altered mEPSC and mIPSC properties – To assess the physiological effects of the conditional knockout of PTEN, and to find potential cellular correlates of the aberrant behavior seen in SOM+ PTEN KO mice (see Chapter 4), we turned to acute-slice patch clamp electrophysiology. We patched SOM+ cells in the central amygdala and recorded miniature EPSCs and IPSCs under conditions that blocked action potential generation (by adding 1uM TTX and 20 uM Bicuculine or 1 uM TTX, 10 uM NBQX, and 50 uM AP5 to the bath solution for mEPSCs and mIPSCs, respectively). Mini EPSCs and IPSCs have been demonstrated to reflect disruptions in cellular physiology connected to multiple neurological disorders. Changes in the frequency of minis is thought to be the result of changes in the number of synapses onto the recorded cell or the release probability of presynaptic vesicles, while differences in the amplitude of mini currents is associated with changes in the post synaptic strength of individual synapses.

We found that the conditional knockout of PTEN from SOM+ neurons disrupted the properties of both excitatory and inhibitory neuronal signaling (Figure 23). The frequency of excitatory miniature EPSCs onto CeA SOM+ neurons is reduced from 1.835 Hz in wild type to 0.8251 Hz in floxed cells (n = 19 WT and 15 FL cells, t-test: p=0.0028, Figure 23A). The amplitude of recorded mEPSCs onto CeA SOM+ is also significantly reduced by SOM+ PTEN KO (n=19 WT and 15 FL cells,

Amplitude = 18.32 pA vs 14.05 pA, t-test: p=0.0037, Figure 23B). While the frequency of miniature IPSCs is not affected by loss of PTEN in SOM+ neurons (n = 21 WT cells and 19 FL cells, Frequency = 0.3762 Hz vs 0.4747 Hz, t-test: p=0.2984, Figure 23C), the amplitude of recorded mIPSCs onto CeA SOM+ is reduced by SOM+ PTEN KO (n=21 WT and 19 FL cells, Amplitude = 17.35 pA vs 15.22 pA, t-test: p=0.0157, Figure 23D). Together, these data seem to indicate fewer, weaker excitatory synapses and weaker inhibitory synapses onto SOM+ neurons in SOM+ PTEN KO mice.

SOM+ PTEN KO reduces afferent NMDAR-mediated currents from BLA to CeA – The connections from BLA to CeA neurons are essential for the regulation of fear and anxiety-related behaviors. To investigate whether inputs onto CeA SOM+ neurons were disrupted by the loss of PTEN, we injected the BLA with an AAV containing ChR2 (see Chapter 6-Methods) and patched SOM+ neurons in the CeA. Using an LED under control of our Clampex software, we were able to reliably stimulate the axon terminals that synapsed onto SOM+ neurons via optogenetics and record EPSCs.

First we established an input/output curve by recording post synaptic responses to different levels of LED intensity. Overall, floxed SOM+ cells showed an increased peak current compared to wild type cells across the input/output curve (n = 18 WT and 17 FL cells, Figure 24A). We fit the input/output curves to an exponential plateau growth function in GraphPad as follows:

Equation 13 - Curve Fitting for Exponential Plateau

$$Y = Y_{max} - (Y_{max} * e^{-kx})$$

where Y_{max} is the maximum current and k is the growth rate constant. Comparing the curves for wild type and floxed input/output curves revealed significant differences (Max current – 601.3 pA vs 865.5 pA, k – 0.05119 vs 0.04985, Comparison of Fits: F (2, 382) = 8.465, p=0.0003). We found that the stimulated excitatory post synaptic currents from BLA neurons onto CeA SOM+ cells at 100% led intensity was not significantly different, most likely due to the large variability, perhaps as a result of differences in opsin expression, though there was a trend toward increased EPSCs in floxed mice (n = 17 WT and 16 FL cells, Max Current = 597.5 pA vs 882.4 pA, t-test: p=0.1805, Figure 24B).

We then sought to learn a little more about the properties of these synapses by measuring the NMDA/AMPA ratio and paired-pulse ratio to see if the conditional PTEN knockout had post synaptic or presynaptic effects, respectively. We found that the NMDA/AMPA ratio was significantly reduced in floxed SOM+ cells compared to wild type (n = 15 WT cells and 14 FL cells, Ratio = 1.001 vs 0.4609, t-test: p=0.0378, Figure 24C). On the other hand, the paired-pulse ratio of BLA inputs to CeA SOM+ neurons was not affected by loss of PTEN across any of the inter-stimulus intervals (n = 10 WT and 5 FL cells, 2 way ANOVA: Genotype effect – F (1, 98) = 0.1247, p = 0.7248, Figure 24D).

2-photon local circuit mapping in the central amygdala using GCamp6m and a soma-restricted ChRmine – After investigating inputs onto SOM+ neurons, we wanted to get a very detailed look into the effects of our conditional PTEN knockout on local inhibitory signaling within the central amygdala. As discussed previously (Chapter 3 and Chapter 6-Introduction), somatostatin-expressing

neurons exhibit their most critical role on the level of the local microcircuit. This is especially true within the amygdala. While there is evidence of long-range projections emanating from CeA SOM+ neurons, a large part of their activity affects local signaling within the central amygdala, so we endeavored to find if the presence of PTEN in SOM+ neurons was necessary for the proper function of these circuits.

To this end, we conducted dual 2-photon and electrophysiological, local circuit mapping experiments to probe single-neuron connectivity. This was enabled in part by the restriction of the high-efficiency, red-shifted opsin, Chrmine, to expression only in the soma and proximal dendrites via a targeting sequence from the potassium channel Kv2.1, as has been done with other opsins. This opsin was co-expressed with GCamp6m, by delivery on the same AAV construct, in the CeA of wild type and SOM+ PTEN KO mice. We first verified that these cells could be activated by the 2-P laser at a wavelength of 1020 nm (Figure 25). When we patched cells that expressed this opsin, we detected large excitatory currents coincident with laser activations, as well as the ability to fire action potentials reliably (Figure 25A,B). With increasing laser power, we were able to generate action potentials with more efficiency and lower latency (Figure 25C,D,E).

With the construct validated, we moved on to real mapping experiments. A typical local circuit mapping experiment would be conducted by patching a single neuron in the CeA, identifying potential presynaptic partners under 2P imaging (Figure 26), and simultaneously recording electrophysiological signals and 2P GCamp6m fluorescence as each presynaptic target was activated in turn by the stimulation laser (Figures 27, 28, and 29). We would then move the FOV to a

different Z plane (30-50 um deeper) and repeat the targeting, imaging, and recording for a separate set of presynaptic cells onto the same patched postsynaptic neuron. Imaging stacks and electrophysiological traces were collected and analyzed using a combination of MATLAB and ImageJ (see Chapter 6-Methods). This method allowed us to evaluate the presence and strength of single-cell connectivity from hundreds of presynaptic cells onto one patched neuron, an efficiency that is orders of magnitude higher than paired-patch techniques.

SOM+ PTEN KO leads to disrupted local circuit connectivity – The results of our local circuit mapping experiments were striking. Overall, the conditional knockout of PTEN drastically reduced the level of local inhibitory connectivity onto SOM+ neurons in the central amygdala by about 50% (Figure 30).

First, we looked at connections between SOM+ cells and other SOM+ cells in wild type and floxed mice. In wild type mice, SOM+ neurons showed a connection probability of 49.25% to other SOM+ neurons. Inhibitory post synaptic currents were detected from 392 out of the 796 cells that were activated by the stimulation laser and had presynaptic firing confirmed by GCamp6 fluorescence (n = 14 post synaptic cells from 5 mice, Proportion connected = 49.25 +/-1.77%, Figure 30A). Floxed mice, on the other hand, SOM+ neurons showed a reduced connection probability of just 27.05% to other SOM+ neurons. Inhibitory post synaptic currents were observed from 287 out of 1061 spike-confirmed presynaptic targets (n = 18 post synaptic cells from 6 mice, Proportion connected = 27.05 +/- 1.36%, Figure 30B).

Connection probability was also measured from SOM- neurons onto SOM+ neurons. In wild type mice, SOM- to SOM+ neurons showed a connection proportion of 52.45%. IPSCs were detected from 107 out of the 204 activated presynaptic cells (n = 14 post synaptic cells from 5 mice, Proportion connected = 52.45 +/- 3.5%, Figure 30C). Floxed mice showed SOM- to SOM+ neurons connected at a reduced probability of 21.62%. IPSCs were detected from 72 out of the 333 activated presynaptic cells (n = 18 post synaptic cells from 6 mice, Proportion connected = 21.62 +/- 2.26%, Figure 30D).

The average number of connections per cell is lower in floxed neurons compared to wild type neurons across all conditions and there was a very strong reduction in the number of connections based on the presynaptic cell type (n = 14 WT cells and 18 FL cells, 2 way ANOVA: Genotype effect – $F(1, 60) = 9.358$, $p=0.0033$, Cell type effect – $F(1, 60) = 37.79$, $p<0.0001$, Figure 30E). Importantly, the SOM+ PTEN KO does not affect the number of presynaptic cells that were able to be activated by the stimulation laser, however fewer active presynaptic SOM- cells were confirmed compared to SOM+ neurons (n = 14 WT and 18 FL post synaptic cells, 2 way ANOVA: Cell type effect – $F(1, 60) = 50.42$, $p<0.0001$, Figure 30F) as a result of the reduced number of SOM- neurons with visible GCamp6 to target (Figure 27C). So although there were fewer SOM- neurons activated than SOM+, the proportions reported in Figure 30 are only of presynaptic cells with activity confirmed by GCamp6 fluorescence, and differences in those proportions can be attributed to the lack of PTEN in SOM+ neurons.

We also mapped the local circuit connectivity onto SOM- neurons within the CeA and found it was drastically reduced as a result of the conditional knockout of PTEN in SOM+ neurons as well (Figure 31).

For wild type mice, SOM+ to SOM- neurons showed a proportion of connections of 21.78%. Inhibitory post synaptic currents were detected from 88 out of the 404 cells that had confirmed presynaptic firing by GCamp6 fluorescence (n = 4 post synaptic cells from 2 mice, Proportion connected = 21.78 +/-2.05%, Figure 31A). In contrast, floxed mice had a connection proportion of just 7.79% for SOM+ to SOM- neurons. Inhibitory post synaptic currents were observed from only 19 out of 244 spike-confirmed presynaptic targets (n = 4 post synaptic cells from 2 mice, Proportion connected = 7.79 +/- 1.70%, Figure 31B).

We also tested SOM- to SOM- connectivity. In wild type mice, SOM- to SOM- neurons showed a connection proportion of 22.94%. IPSCs were detected from 39 out of the 170 activated presynaptic cells (n = 4 post synaptic cells from 2 mice, Proportion connected = 22.94 +/- 3.22%, Figure 31C). Floxed mice, in contrast showed a proportion of connection of 6.96% for SOM- to SOM- neurons. IPSCs were detected from only 11 out of the 158 activated presynaptic cells (n = 4 post synaptic cells from 2 mice, Proportion connected = 6.96 +/- 2.02%, Figure 31D).

Again, the average number of connections per cell is lower in floxed neurons compared to wild type neurons across all conditions (n = 4 WT cells and 4 FL cells, 2 way ANOVA: Genotype effect – $F(1, 12) = 5.821$, $p=0.0328$, Figure 31E) and the SOM+ PTEN KO does not affect the number of presynaptic cells that were activated, however fewer presynaptic SOM- cells were targeted compared to SOM+ (n = 4 WT

and 4 FL post synaptic cells, 2 way ANOVA: Cell type effect – F (1, 12) = 8.866, p=0.0115, Figure 31F).

Connection probability for all cell type combinations was significantly different between wild type and floxed mice (Figure 32A). Standard deviations for each proportion were calculated as follows:

Equation 14 - Standard Deviation of a Proportion

$$\sigma_p = \sqrt{\frac{p(1-p)}{n}}$$

where *p* is the proportion of connections and *n* is the number of confirmed active presynaptic cells. The difference of proportions z tests were calculated as follows:

Equation 15 - Difference of Proportions Test

$$Z = \frac{p_1 - p_2}{\sqrt{p_t(1-p_t)\left(\frac{1}{n_1} + \frac{1}{n_2}\right)}}$$

where p_1 is the connection proportion of one set, p_2 is the connection proportion of the second set, n_1 is the number of confirmed presynaptic cells for set one, n_2 is the number of confirmed presynaptic cells for set two, and p_t is the combined proportion for both sets given by:

Equation 16 - Combined Proportion for Difference of Proportions Test

$$p_t = \frac{(c_1 + c_2)}{(n_1 + n_2)}$$

where c_1 is the number of confirmed connections of set one and c_2 is the number of confirmed connections of set two.

Every comparison between wild type mice and floxed mice for each cell type combination yielded highly significant differences of $p<0.0001$ (SOM+ to SOM+:

392/796 WT vs 287/1061 FL, Z = 9.829, SOM- to SOM+: 107/204 WT vs 72/333 FL, Z = 7.356, SOM+ to SOM-: 88/404 WT vs 19/244 FL, Z = 4.649, SOM- to SOM-: 39/170 WT vs 11/158 FL, Z = 4.023, Figure 32A) and comparisons between WT post synaptic SOM+ vs post synaptic SOM- (Z = 9.177) and between FL post synaptic SOM+ vs post synaptic SOM- (Z = 6.404) also yielded a $p<0.0001$ result.

Floxed SOM+ neurons have a lower local inhibitory connection probability than wild type SOM+ neurons when evaluated by cell as well (n = 14 WT cells and 18 FL cells, 2 way ANOVA: Genotype effect – $F(1, 60) = 5.528$, $p=0.0220$, Figure 32B). SOM- cells have lower connection probability of afferents from floxed SOM+ neurons and SOM- to SOM- connection probability is reduced as well due to conditional PTEN KO (n = 4 WT cells and 4 FL cells, 2 way ANOVA: Genotype effect – $F(1, 12) = 5.664$, $p=0.0348$, Figure 32C).

SOM+ PTEN KO leads to reduced inhibitory signaling strength within the CeA – Overall, the knockout of PTEN from SOM+ neurons also affected the strength of inhibitory connections within the central amygdala in addition to the reduced connectivity and the incoming currents onto SOM+ neurons were shifted distally in their spatial distribution.

To assess the strength and spatial distribution of incoming currents, IPSCs were binned in 20 um increments according to their corresponding presynaptic cell's soma to soma distance from the recorded post synaptic neuron and averaged (as described in Chapter 6-Methods). The resulting current distributions were fit with Gaussian curves in GraphPad according to the following formula:

Equation 17 - Curve Fitting for Gaussian Distributions

$$Y = \frac{1}{\sigma\sqrt{2\pi}} e^{-0.5\left(\frac{x-\mu}{\sigma}\right)^2}$$

where *x* is the soma to soma distance between the post synaptic and presynaptic cells, μ is the mean, and σ is the standard deviation. The resulting curves were compared for each set of cell type – cell type connections.

The data for average current onto CeA SOM+ from other SOM+ cells plotted against the distance from the stimulated presynaptic cell was fit well by a Gaussian curve (R^2 = 0.8907 for WT vs 0.9095 for FL) and reveals a significantly reduced amplitude and shift spatial distribution for SOM+ neurons lacking PTEN (n = 392 IPSCs onto 14 WT cells and 287 IPSCs onto 18 FL cells, Gaussian curves: Peak amplitude = 443.3 pA vs 228.7 pA, Mean = 102.9 um vs 121.3 um, SD = 53.88 vs 56.23, Comparison of fits: F (3, 20) = 19.49, p<0.0001, Figure 33A).

Afferent currents from CeA SOM- cells onto SOM+ cells are not affected by conditional PTEN knockout, though there was a trend toward lower current amplitude (n = 107 IPSCs onto 14 WT cells and 72 IPSCs onto 18 FL cells, Gaussian curves: Peak amplitude = 76.85 pA vs 51.34 pA, Mean = 120.0 um vs 126.4 um, SD = 82.47 vs 68.37, Comparison of fits: F (3, 20) = 3.070, p = 0.0514, Figure 33B).

We also compared all individual incoming IPSCs for each cell type combination. SOM+ to SOM+ current amplitude is reduced in SOM+ PTEN KO mice (Figure 33C). The amplitude distribution failed to pass the test for normality (Shapiro-Wilk test: 0.7988, p<0.0001 for WT and 0.7101, p<0.0001 for FL) so we compared median values (n = 392 for WT and 287 for FL, Median = 70.61 vs 57.92, Mann-Whitney Rank Sum: U=48993, p=0.0037). The strength of afferent IPSCs from

SOM- onto SOM+ neurons was unaffected by SOM+ PTEN KO (Figure 33E). The amplitude distribution failed to pass the test for normality (Shapiro-Wilk test: 0.7968, $p<0.0001$ and 0.7494, $p<0.0001$) so median values were compared (n = 107 for WT and 72 for FL, Median = 65.46 vs 63.94, Mann-Whitney Rank Sum: U=3039, p=0.8290).

Total current per cell from other SOM+ afferents was not normally distributed, but the distribution was significantly altered in floxed cells compared to wild type with a shift toward lower amplitude (n = 14 WT cells and 18 FL cells, Kolmogorov-Smirnov test: D=0.5238, p=0.0266, Figure 33D). However, SOM+ PTEN KO did not significantly affect the total inhibitory postsynaptic current per cell from SOM- onto SOM+ neurons (n = 14 WT cells and 18 FL cells, Kolmogorov-Smirnov test: D=0.3810, p=0.2032, Figure 33E).

We also assessed the strength of connections onto patched CeA SOM- cells. IPSCs were binned in 20 um increments according to their corresponding presynaptic cell's soma to soma distance from the recorded post synaptic neuron and averaged (see Chapter 6-Methods). The resulting current distributions were fit with Gaussian curves and compared to show a large shift in amplitude and distance for currents from SOM+ to SOM- cells in floxed mice (n = 88 IPSCs onto 4 WT cells and 19 IPSCs onto 4 FL cells, Gaussian curves: Peak amplitude = 293.8 pA vs 119.7 pA, Mean distance = 78.37 um vs 214.0 um, SD = 28.63 vs 6.327, Comparison of fits: F (3, 20) = 6.711, p=0.0026, Figure 34A).

Afferent currents from CeA SOM- cells onto SOM- cells are also affected by conditional PTEN knockout (n = 39 IPSCs onto 4 WT cells and 11 IPSCs onto 4 FL

cells, Gaussian curves: Peak amplitude = 97.44 pA vs 20.12 pA, Mean distance = 122.4 um vs 178.5 um, SD = 59.03 vs 44.25, Comparison of fits: $F(3, 20) = 8.362$, $p = 0.0008$, Figure 34B).

Incoming IPSCs from floxed CeA SOM+ neurons are reduced in SOM- cells. The amplitude distribution failed to pass the test for normality (Shapiro-Wilk test: 0.6991, $p<0.0001$ for WT and 0.7067, $p<0.0001$ for FL) so we compared median values (n = 88 for WT and 19 for FL, Median = 56.75 vs 37.50, Mann-Whitney Rank Sum: $U=450$, $p=0.0013$, Figure 34C). Incoming IPSCs from other CeA SOM- neurons are also reduced in SOM- cells in SOM+ PTEN KO mice. The amplitude distribution failed to pass the test for normality (Shapiro-Wilk test: 0.4109, $p<0.0001$ for WT and 0.8185, $p=0.0165$ for FL) so median values were compared (n = 39 for WT and 11 for FL, Median = 55.54 vs 40.47, Mann-Whitney Rank Sum: $U=107$, $p=0.0086$, Figure 34D).

We also confirmed that floxed SOM+ cells had higher capacitance than wild type SOM+ cells, providing further evidence of overgrowth (n = 14 WT and 18 FL cells, Capacitance = 67.43 pF vs 99.44 pF, t-test: $p=0.0122$, Figure 33H). As expected, the capacitance of recorded SOM- neurons was not significantly affected by SOM+ PTEN KO (n = 4 WT cells and 4 FL cells, Capacitance = 67.49 pF vs 82.41 pF, t-test: $p=0.5668$, Figure 34E).

SOM+ PTEN KO leads to shifts in the spatial distribution of afferent IPSCs – To further assess the spatial distribution of afferents onto SOM+, we looked at the proportion of total current that emanated from each 20 um bin of soma to soma distance and found distal shifts as a result of the conditional knockout of PTEN. The

resulting distributions were fit with Gaussian curves to investigate differences between the genotypes. The distribution for floxed SOM+ to SOM+ inputs is shifted 20 um away compared to wild type cells (n = 392 IPSCs onto 14 WT cells and 287 IPSCs onto 18 FL cells, Gaussian curves: Peak amplitude = 15.10% vs 14.40%, Mean distance = 102.9 um vs 121.4 um, SD = 53.88 vs 56.51, Comparison of fits: F (3, 20) = 3.288, p=0.0421, Figure 35A). Plots for IPSC afferents from SOM- cells to SOM+ cells, on the other hand, shows no effect to the spatial distribution on account of the conditional PTEN KO (n = 107 IPSCs onto 14 WT cells and 72 IPSCs onto 18 FL cells, Gaussian curves: Peak amplitude = 11.20% vs 12.33%, Mean distance = 120.0 um vs 126.4 um, SD = 82.47 vs 68.37, Comparison of fits: F (2, 20) = 0.2050, p = 0.8163, Figure 35C).

We also looked at the spatial distributions onto SOM- neurons. Even though SOM- neurons are not directly affected, in that their PTEN function is intact, we wanted to see if the loss of PTEN from their neighbors affected their local circuit dynamics indirectly. Plotting the soma to soma distance between the stimulated presynaptic cell and the recorded cell against the proportion of total current received from SOM+ onto SOM- neurons shows a disruption in the spatial distribution of afferents. Currents at the distal end of the distribution dominated the curve for floxed cells and pushed it much further from the soma compared to wild type cells (n = 88 IPSCs onto 4 WT cells and 19 IPSCs onto 4 FL cells, Gaussian curves: Peak amplitude = 18.87% vs 52.96%, Mean distance = 78.37 um vs 214.0 um, SD = 28.63 vs 6.327, Comparison of fits: F (3, 20) = 3.763, p=0.0272, Figure 36A). However, plots for IPSC afferents from SOM- cells to SOM- cells that were fit

with Gaussian curves did not show a significant effect to the spatial distribution on account of the conditional PTEN KO (n = 39 IPSCs onto 4 WT cells and 11 IPSCs onto 4 FL cells, Gaussian curves: Peak amplitude = 14.07% vs 16.50%, Mean distance = 122.7 um vs 180.4 um, SD = 59.65 vs 47.35, Comparison of fits: F (3, 18) = 1.296, p = 0.3063, Figure 36C).

In addition to this, we assessed the spatial distribution of inputs from a different angle to see if the cumulative proportion of current is more or less spread out in floxed mice compared to wild type cells. To this end, we binned all the incoming IPSCs in 10 um intervals and took the proportion of total current cumulatively at each 10 um step in soma to soma distance (see Chapter 6-Methods). The data were plotted and fit by sigmoidal cumulative Gaussian curves in GraphPad according to the following formula:

Equation 18 - Curve Fitting for Cumulative Gaussian Distributions

$$Y = 1 * zdist\left(\frac{x-\mu}{\sigma}\right)$$

where 1 is the top limit of the graph because currents are reported as fractions of the total incoming current, x is the soma to soma distance (in 10 um increments), μ is the mean of the distribution, σ is the standard deviation, and *zdist* refers to the value from the normal z distribution table associated with the resulting z score from each x,μ,σ combination. The resulting curve is similar to a dose-response curve, where the mean on the distribution represents the distance before which 50% of the total current has originated (akin to ED_{50}) and the standard deviation is related to the spread of the curve (akin to the Hill slope).

We plotted the cumulative proportion of current onto all the SOM+ cells we recoded, with separate curves for SOM+ to SOM+ and SOM- to SOM+ as well as wild type and floxed mice to. We found that the distribution of IPSCs from SOM+ neurons to other SOM+ neurons show distal shift of due to conditional PTEN KO. The sigmoidal curves were compared to show increased soma to soma distance for floxed IPSCs compared to wild type, while retaining the same slope (n = 392 IPSCs onto 14 WT cells and 287 IPSCs onto 18 FL cells, Sigmoidal cumulative Gaussian curves: Top and Bottom were fixed at 0 and 1, Distance at 50% (mean) = 99.12 um vs 116.2 um, SD = 53.15 um vs 54.72 um, Comparison of fits: $F(2, 52) = 94.80$, $p<0.0001$, Figure 35B). The cumulative proportion of SOM- to SOM+ current by distance, however, was not affected the removal of PTEN from SOM+ neurons (n = 107 IPSCs onto 14 WT cells and 72 IPSCs onto 18 FL cells, Sigmoidal cumulative Gaussian curves: Top and Bottom were fixed at 0 and 1, Distance at 50% (mean) = 115.9 um vs 114.9 um, SD = 66.18 um vs 63.05 um, Comparison of fits: $F(2, 48) = 0.5105$, $p=0.6034$, Figure 35D).

In the same way, we also looked at the cumulative proportion of currents for all SOM- cells we recorded. Plotting the cumulative proportion of current by 10 um-binned distances reveals a distal shift of SOM+ to SOM- IPSCs due to conditional PTEN KO. The data fit by sigmoidal curves and compared showed increased soma to soma distance for floxed IPSCs and an increase in the SD, indicating a gentler slope and greater spread (n = 88 IPSCs onto 4 WT cells and 19 IPSCs onto 4 FL cells, Sigmoidal cumulative Gaussian curves: Top and Bottom were fixed at 0 and 1, Distance at 50% (mean) = 98.49 um vs 136.8 um, SD = 59.74 um vs 87.51 um,

Comparison of fits: F (2, 46) = 31.93, p<0.0001, Figure 36B). Additionally, the cumulative proportion of SOM- to SOM- current by distance was shifted significantly by the removal of PTEN from SOM+ neurons (n = 39 IPSCs onto 4 WT cells and 11 IPSCs onto 4 FL cells, Sigmoidal cumulative Gaussian curves: Top and Bottom were fixed at 0 and 1, Distance at 50% (mean) = 116.8 um vs 157.8 um, SD = 57.25 um vs 50.25, Comparison of fits: F (2, 46) = 59.12, p<0.0001, Figure 36D).

Discussion and Conclusions

The conditional knockout of PTEN from SOM+ neurons results in major dysfunction in SOM+ cells as well as central amygdala circuitry. The implications of our experiments are numerous and apply to the understanding of PTEN's role in morphology, synaptic signaling, and local circuit dynamics.

Morphology **–** PTEN mutations in other mouse models has confirmed the macroencephaly seen in human patients (Clipperton-Allen & Page, 2014) as well as individual cellular overgrowth (Fraser et al., 2004; Kwon et al., 2001, 2006; Vogt et al., 2015), but not in a cell type specific manner. Here, we clearly show that SOM+ neurons lacking PTEN are overgrown compared to wild type cells, though we did not observe changes in gross morphology, most likely due to the restricted nature of the PTEN knockout. This cellular overgrowth was seen in multiple measures, including cross-sectional soma area, soma volume, and the length of dendritic arbors. Interestingly, we found that within the central amygdala, the number of SOM+ neurons was reduced as a result of PTEN loss. Though it may seem counter-intuitive that the loss of a tumor-suppressing gene results in fewer cells, it has been shown before that the increased cellular proliferation observed in PTEN mutations

in various cancers may be cell type specific, since a previous study revealed the loss of PTEN in astrocytes and neurons resulted in higher astrocyte density, but lower neuronal density, even as those neurons were enlarged (Fraser et al., 2004).

We also demonstrated, for the first time, a detailed analysis of dendritic morphology of SOM+ neurons without PTEN. Sholl analysis of dendritic length and complexity had not previously been applied to SOM+ neurons in PTEN mutation models. Our findings that the entire dendritic arbor seems to be stretched out compared to wild type neurons has never been shown directly. Importantly, our data show that the accelerated growth of cells due to the lack of PTEN does not result in a large increase in the number of dendritic branches, as the peak number of dendritic intersections was not larger in the SOM+ PTEN KO cells, but rather it extends the existing dendrites further than they would have reached if the cellular signaling were unaltered. The peaks of dendritic length and complexity of SOM+ PTEN KO neurons were shifted away from the soma, in addition to showing greater total dendrite length and much longer individual dendrites. This implies that the cellular mechanisms for creating dendritic branch points, which are not directly affected by the loss of PTEN signaling in SOM+ neurons, are distinct from those that elongate existing branches, which are dependent on proper PTEN function for arresting growth. Interestingly, this growth is consistent with, and may be related to, the phenomenon of enhanced axon regeneration via disruption of PTEN signaling observed in models of spinal cord injury as well (Liu et al., 2010; Park et al., 2008; Singh et al., 2014; Sun et al., 2011; Zukor et al., 2013).

These longer dendritic branches observed in our PTEN KO cells could play a role in the physiological responses of SOM+ neurons as well. If nothing else in a post synaptic cell were changed, longer dendrites and an extended dendritic arbor could result in a dampening of afferent currents since the changes in voltage have to travel further to be integrated together and eventually reach the soma. If, on the other hand, the volume of the dendrites was also increased, this would lead to lower internal resistance and a longer length constant, as the voltage along a dendrite decreases in an exponential decay with distance from the synaptic input, and this could make up for some of the changes in the length of the dendrites. While the confocal images we used for Sholl analysis did not have the spatial resolution to accurately assess any changes in dendritic volume, we suspect that the increased length may play a larger role in physiological changes to SOM+ PTEN KO cells.

Miniature Post Synaptic Currents and Afferents from the BLA – The physiological implications of our conditional PTEN knockouts were also of great interest to us, and we observed that the lack of PTEN in SOM+ neurons resulted in aberrant inputs onto the post synaptic SOM+ cells.

Recording miniature post synaptic currents has been a common measure of synaptic properties since it was first reported in the 1950s (Fatt & Katz, 1952). It is commonly accepted that changes in the amplitude of mini PSPs/PSCs represent changes in the post synaptic properties, such as the expression or concentration of receptors and ion channels, while changes in the frequency represent increases or decreases in presynaptic features, such as the number of synapses or the probability of vesicle release. In addition to recording mEPSCs and mIPSCs, we used

channelrhodopsin to stimulate the afferents from the basolateral amygdala onto SOM+ neurons in the central amygdala as a way to investigate whether or not the conditional loss of PTEN had an effect on the inputs onto SOM+ neurons.

We found a decrease in both the amplitude and frequency of miniature excitatory post synaptic currents onto SOM+ neurons that did not have PTEN. This seems to indicate that there are changes at excitatory synapses in both the pre and post synaptic cells as a result of PTEN knockout. It has been shown that PTEN loss results in disruptions to synaptic structure observed through an electron microscope (Fraser et al., 2008), and this could potentially lead to the pruning of synapses that are presumed to be defective, which would lead to a reduced mini frequency. However, some have shown that PTEN loss in other circuits can increase the number of dendritic protrusions of affected neurons (Williams et al., 2015). Additionally, in our optical stimulation of opsin-expressing BLA afferents, the paired pulse ration was not changed as a result of PTEN loss, indicating that the presynaptic probability of release was not affected. Together, these data seem to indicate that there are fewer excitatory connections onto SOM+ neurons in the CeA that do not have a functional PTEN protein.

Conversely, the decrease in the amplitude of mEPSCs onto SOM+ PTEN KO cells may be harder to understand. Though the classical interpretation of decreased miniature EPSC amplitude would suggest decreased synaptic efficiency, perhaps as a result of receptor concentration, previous research has shown that PTEN loss can result in increased excitability (Luikart et al., 2011; Sperow et al., 2012; Williams et al., 2015). Indeed, PTEN mutations in PV+ cells in the cortex have also shown an

increase in the current from pyramidal cells onto PV+ cells in paired-patch experiments (Baohan et al., 2016). In addition to this, PIP3, the molecule that is dephosphorylated by PTEN and is therefore increased in PTEN knockouts, has been shown to stabilize post synaptic AMPA receptors, which would theoretically increase the efficiency of post synaptic currents (Arendt et al., 2010). The results from our opsin-mediated afferent stimulation are consistent with this line of previous research, as the input/output curve was significant increased in SOM+ PTEN KO cells in the CeA. Additionally, though the maximum evoked current was largely increased in SOM+ PTEN KO cells, it was not significantly different, but this may be due to the extreme variability in responses as a result of differential expression of channelrhodopsin in different cells. Though this may appear contradictory to the lower mEPSC amplitude, it has been shown that evoked EPSCs and miniature EPSCs do not always follow the same trends, and that perhaps synapse-specific changes in post synaptic receptor density or diversity could be a contributing factor. For example, inhibiting metabotropic glutamate receptors in SOM+ neurons of the anterior cingulate cortex increased the amplitude of evoked EPSCs, but did not change the amplitude of mEPSCs (Guo et al., 2020). Additionally, it is plausible that, given the large overgrowth of the dendritic arbors in SOM+ neurons and the relatively small amplitudes of mEPSCs in general, the currents were more attenuated by the passive filtering before they got to the soma. Conversely, the it may be the case that the increases in evoked responses represent a non-linear summation from different dendritic compartments or some kind of compensatory active conductance to the soma.

Interestingly, we also observed a large reduction in the NMDA/AMPA ratio from basolateral amygdala afferents onto SOM+ neurons that did not have PTEN. The relative contribution of NMDA currents, recorded at a +40mV holding potential, compared to AMPA currents, recorded at -70mV, was significantly decreased. Such a drastic decrease in NMDA current has implications for the synaptic plasticity of SOM+ neurons. Indeed, PTEN has been shown to associate with NMDA receptor subunits, and losing PTEN results in an inhibition of NMDAR activity via the lack of its protein phosphatase function, independent of its lipid phosphatase action on PIP3 (Ning et al., 2004). Accordingly, disruptions in LTP and LTD have been reported in other models of PTEN knockouts in hippocampal circuits (Fraser et al., 2008; Sperow et al., 2012).

Local Circuit Mapping in the Central Amygdala – The most novel and impactful aspect of our experiments has to do with the results from the local circuit mapping within the central amygdala. This type of large scale, single-cell connectivity mapping has never been done before, and our findings provide new and important insight into the way that PTEN affects local circuitry in models of ASD as well as the everyday function of the central amygdala.

While a few researchers have demonstrated the effects of PTEN loss on excitatory neurontransmission, even fewer have experimented with inhibitory populations. The handful of experiments that looked into the disruption of PTEN in inhibitory neurons focused more on the behavioral and morphological effects, however one group knocked out PTEN from interneuron progenitors and reported an increase in mIPSC frequency, with no change in the amplitude, in recordings onto

neocortical pyramidal neurons as well as a decrease in gamma-band EEG activity (Vogt et al., 2015). On the other hand, we saw no significant change in mIPSC frequency, but a reduction in mIPSC amplitude in post synaptic SOM+. It is conceivable that this is a cell-type specific effect, or that it has to do with different wiring patterns in the CeA compared to the neocortex. Also, the PTEN knockout in MGE progenitor cells resulted in a loss of PTEN from PV+ and SOM+ neurons and a marked increase in PV+ expressing neurons and the PV+/SOM+ ratio, such that increases in mIPSC frequency could have depended more on PV+ cell function than on SOM+ neurons.

The only previous attempt at local circuit mapping that we know of investigated how PTEN mutations in PV+ neurons can affect the physiology of inhibitory circuits in the visual cortex. This group patched layer 2/3 pyramidal cells and optically stimulated PV+ neurons around the cell using a single-photon blue laser across multiple cortical layers. They found that the total inhibitory current from PV+ neurons onto layer 2/3 pyramidal cells was reduced in mice with PTEN mutations in PV+ cells (Baohan et al., 2016). The greatest reduction was found within layer 2/3, but reduced currents from other layers were also observed.

While those experiments are impressive and important for understanding some of the ways PTEN can affect local signaling in the cortex, they did not explore SOM+ neuron function or circuitry in the amygdala. Using the improved techniques afforded to us via 2P circuit mapping, we have provided the most comprehensive local circuit mapping in the central amygdala to date. We were able to record the post synaptic currents onto SOM+ neurons that originated from hundreds of

individual presynaptic target cells with single cell resolution. The dramatic effect of PTEN loss on the connectivity of SOM+ neurons, seen in the greatly reduced connection probability and total recorded post synaptic current, has never been shown before.

Previous attempts at probing the connectivity of neurons in the central amygdala has been limited to either the use of single-photon activation, the inadequacies of which we have just discussed, or paired-patch electrophysiology. While paired-patch experiments are respectable in regards to their internal validity, they are limited by inefficiency and low throughput. Indeed there has been one attempt at characterizing the connection probability among different cell types in the CeA using paired-patch electrophysiology that showed relatively similar trends to the connectivity in our wild type mice (Hunt et al., 2017). They showed ~60% connectivity between SOM+ and SOM+ neurons (5 out of 8 had at least a unidirectional connection) and ~25% connectivity between SOM- and SOM- neurons (3 out of 7 had bi-directional connections). We have shown similar connectivity patterns in the central amygdala of our wild type mice, with 392 out of 796 SOM+ neurons connected to a SOM+ neuron (49.2%) and 39 out of 170 SOM- connected to SOM- (22.9%). We also were able to investigate connectivity between neuron classes, showing 107 out of 204 SOM- neurons synapsing onto a SOM+ neuron (52.5%) and 88 out of 404 SOM+ cells connecting to a SOM- neuron (21.8%). The drastic improvement in the scale of our experiments is immediately apparent. We are able to probe hundreds of presynaptic cells instead of one at a time to create the highest possible detection of synaptic connections, however, this method does

not allow for the detection of reciprocal connections and for that information, we rely on estimates from paired-patching experiments.

Nonetheless, the power of two-photon circuit mapping is exhibited when comparing physiology in different brain areas, cell types, or models of neurological disorders. Here we are able to clearly see the massive disruption of CeA connectivity as a result of PTEN loss from SOM+ neurons as it reduced synaptic detection among every combination of cell types by 50% while still maintaining a very large sample of presynaptic neurons. SOM+ to SOM+ connections were reduced to 267 out of 1061 (27%), SOM- to SOM+ declined to 72 out of 333 (21.6%), SOM+ to SOM- fell to just 19 out of 244 (7.78%) and SOM- to SOM- was also reduced to 11 out of 158 (6.96%). Even with a lower sample size of SOM- neurons to target, due to differences in the expression of the ChRmine/GCamp6, clear deficits in local circuitry were observed. The impact of proper PTEN function on the inhibitory communication within the CeA is profound and had never before been demonstrated.

Furthermore, we retain the benefit of the excellent quantitative analysis of the afferent currents onto our post synaptic recorded cells, via patch clamp electrophysiology, that would not be available with an all-optical approach. In this way, we were able to observe the consequences of reduced currents within the CeA as a result of the conditional SOM+ PTEN knockout. Previous paired-patch recordings have shown that PTEN loss from PV+ interneurons decreases their efferent communication in the cortex, both onto pyramidal cells and onto each other (Baohan et al., 2016). We also observed smaller individual currents onto SOM+ and

from SOM+ to other interneurons in the CeA. However, we were also able to show, for the first time, the combined effect of smaller individual currents and lower connection probability, as the total afferent current onto SOM+ neurons from other SOM+ neurons was drastically reduced, limiting the CeA's ability to perform proper local inhibition.

An additional benefit of the spatial resolution afforded by our 2P local circuit mapping technique is that of probing the effect of PTEN mutations on the spatial distribution of local connections, something that has never even been attempted on this scale. We are able to show the total strength of all detected synaptic connections as a result of their distance from the recorded cell in a brand new way. We have shown that the loss of PTEN in SOM+ neurons results, not just in a reduction of afferent IPSCs, but also a broadened spatial distribution of those afferents. The currents recorded onto SOM+ from which PTEN had been knocked out were more dispersed by an average of about 20 um, consistent with the well-documented overgrowth of PTEN mutant cells, and SOM- to SOM- IPSCs were also affected. Our measurements were for the soma-to-soma distance of connected neurons, not precisely the distance of the synapse, however, they still indicate that the loss of PTEN in SOM+ neurons spreads the distribution of local connectivity in the CeA.

Implications for a working model of CeA activity in fear and anxiety – Altogether, our for data provide important insights for the way PTEN mutations in SOM+ neurons disrupt lateral inhibition and affect CeA activity and the associated behaviors. We suggest that this disordered inhibition among SOM+ neurons in the

CeA is what gives rise to the elevated fear and anxiety we observed in our SOM+ PTEN KO mice.

The central amygdala is commonly accepted to play an essential role in gating the output of the amygdala complex, and as such, it is a major regulator of the expression of fear and anxiety. While it was outside the scope of this project to do pre- and post-fear conditioning experiments, we clearly show that the removal of PTEN from SOM+ interneurons affects the circuitry of the CeA by disrupting both their inputs and their outputs in a way that leads to increased fear and anxiety (Figure 37).

The increased input from BLA principal neurons could result in the potentiation of fear-related information traveling into the CeA, as greater BLA principal cell activity increases freezing during fear recall and LA inputs to CeA SOM+ neurons undergo plasticity during fear conditioning (Krabbe et al., 2018; H. Li et al., 2013). In addition to the increased evoked inputs from BLA to CeA SOM+ neurons, SOM+ cells in the BLA have been shown to synapse on the dendrites of BLA principle cells to perform feed-forward inhibition (Muller et al., 2007; Unal et al., 2014) and form a disinhibitory circuit with PV+ cells to inhibit fear output in wild type mice (Wolff et al., 2014). Though we did not test it directly, if the SOM+ neurons in the BLA fail to form the proper number of strong synapses, as they fail to do in the CeA, this would conceivably reduce the inhibition onto BLA principle cells and thereby further increase fear output. Such a disruption of inhibition in the BLA could also contribute to elevated anxiety levels through the over-activation of the

BLA neurons that project to the medial prefrontal cortex (Felix-Ortiz et al., 2013, 2016; Vogel et al., 2016).

Meanwhile, the decreased inhibition within the CeA by SOM+ neurons limits their effects on other interneurons and contributes to increased fear and anxiety via their disrupted outputs. Lateral inhibition is the process by which activated neurons inhibit those around them, and it can produce more distinct responses to excitatory inputs as well as protect from overstimulation. Since, various populations of inhibitory neurons within the CeA have been shown to contributed differentially to fear and anxiety, as well as other defensive and survival related behaviors (Asok et al., 2018; Cai et al., 2014; Ciocchi et al., 2010; Haubensak et al., 2010; H. Li et al., 2013; Penzo et al., 2014), disruptions in lateral inhibition of inputs into the CeA may indirectly contribute to increased fear outputs. Additionally, higher activity onto SOM+ neurons in the CeA can directly contribute to fear and anxiety in multiple ways, by disinhibiting central medial amygdala (CeM) neurons that project to the freezing centers in the periaqueductal grey (PAG) and by direct long-range projections to the PAG (De Oca et al., 1998; Haubensak et al., 2010; LeDoux et al., 1988; Penzo et al., 2014) as well as the anxiety-associated BNST (Ahrens et al., 2018; Davis et al., 1997).

Taken together, the physiological effects of the conditional knockout of PTEN from SOM+ neurons that we observe in our circuit mapping experiments are a very probable source of the behavioral deficits we found in our mice. The over-stimulation of inputs combined with an improper amount of lateral inhibition conceivably gives rise to a greater output from the CeA to influence downstream

fear and anxiety. This not only provides insight into the mechanisms of PTEN dysfunction in models of ASD and human pathology, but also into the proper function of the amygdala circuitry in the absence of any neurological disorder-related mutations, and our experiments open the door for further directed investigation into the local circuit dynamics of other brain areas and other models of neurological conditions.

A) **B)**

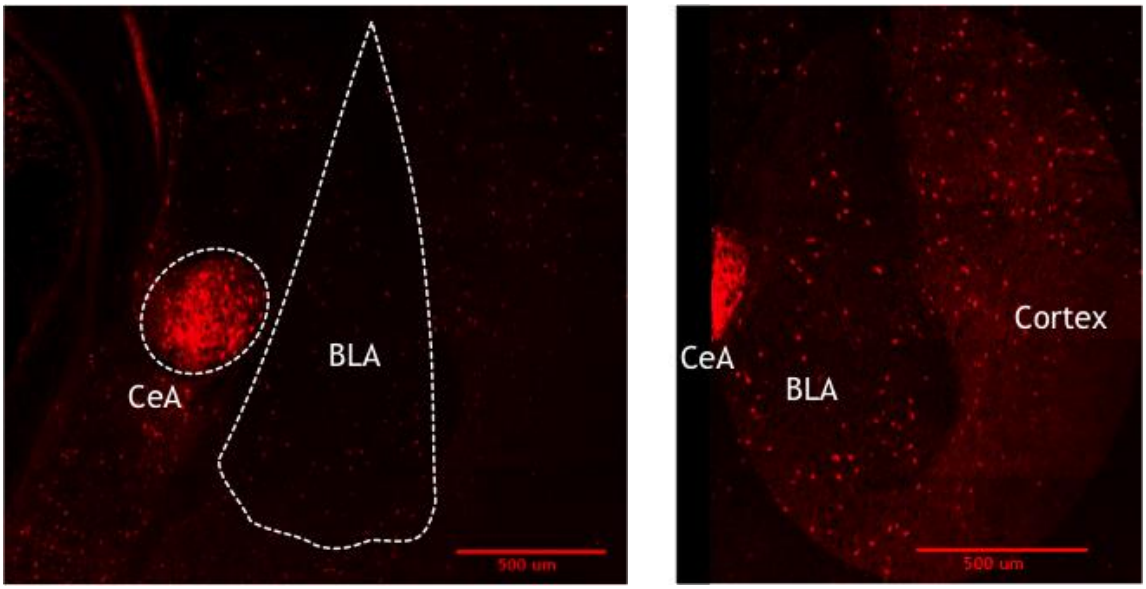

Figure 19: A dense population of SOM+ neurons exists in the central amygdala

A) A representative confocal image of an unstained slice showing the dense cluster of red TdTomato-expressing SOM+ cells visible in the central amygdala, just medial to the basolateral amygdala.

B) The same image, zoomed in with the contrast adjusted to reveal that SOM+ cells are still present in the adjacent basolateral amygdala, as well as the cortex, but not nearly at the same concentration.

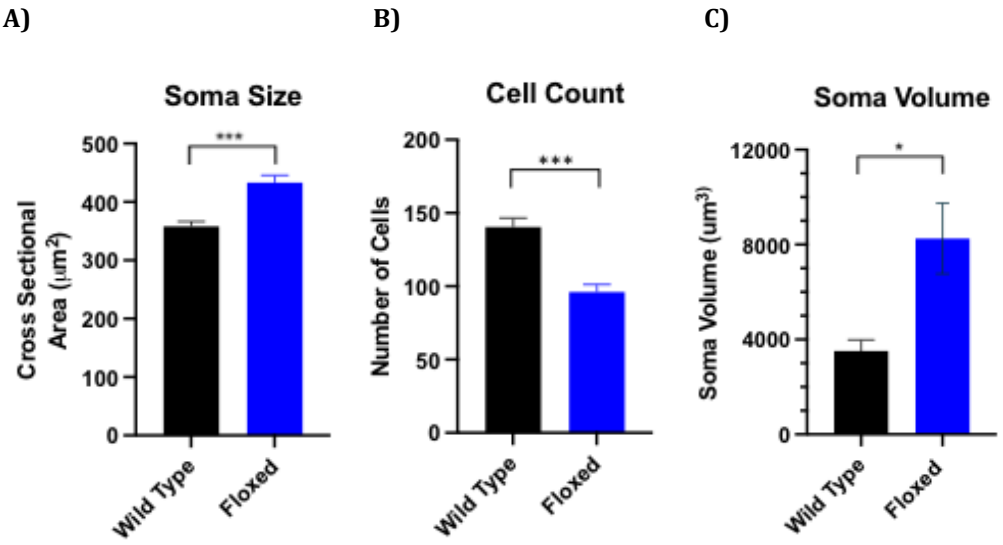

Figure 20: The CeA of floxed mice has fewer, but larger, neurons

A) CeA SOM+ cells from floxed mice have a larger cross-sectional area than CeA SOM+ cells of wild type mice (n = 88 WT cells vs 77 FL cells, = 358 um^2 vs 433 um^2, *** indicates t-test: $p<0.0001$). B) Though the cells are smaller in floxed mice, there are fewer SOM+ cells in a 200x200x100 voxel of the central amygdala in conditional PTEN knockout mice (n = 16 WT slices from 4 animals vs 14 FL slices from 4 animals, mean = 140.4 cells vs 96 cells, *** indicates t-test: $p<0.0001$). C) In a separate set of experiments, SOM+ cells were filled with biocytin, immunostained with fluorophore-conjugated streptavidin (which binds to biocytin) and reconstructed. Volumetric analysis of SOM+ cells shows that wild type cells are significantly smaller than SOM+ cells lacking PTEN (n = 3 WT cells and 3 FL cells, Volume = 3512 um^3 vs 8255 um^3, * indicates t-test: $p=0.0389$). All data are presented as mean +/- SEM.

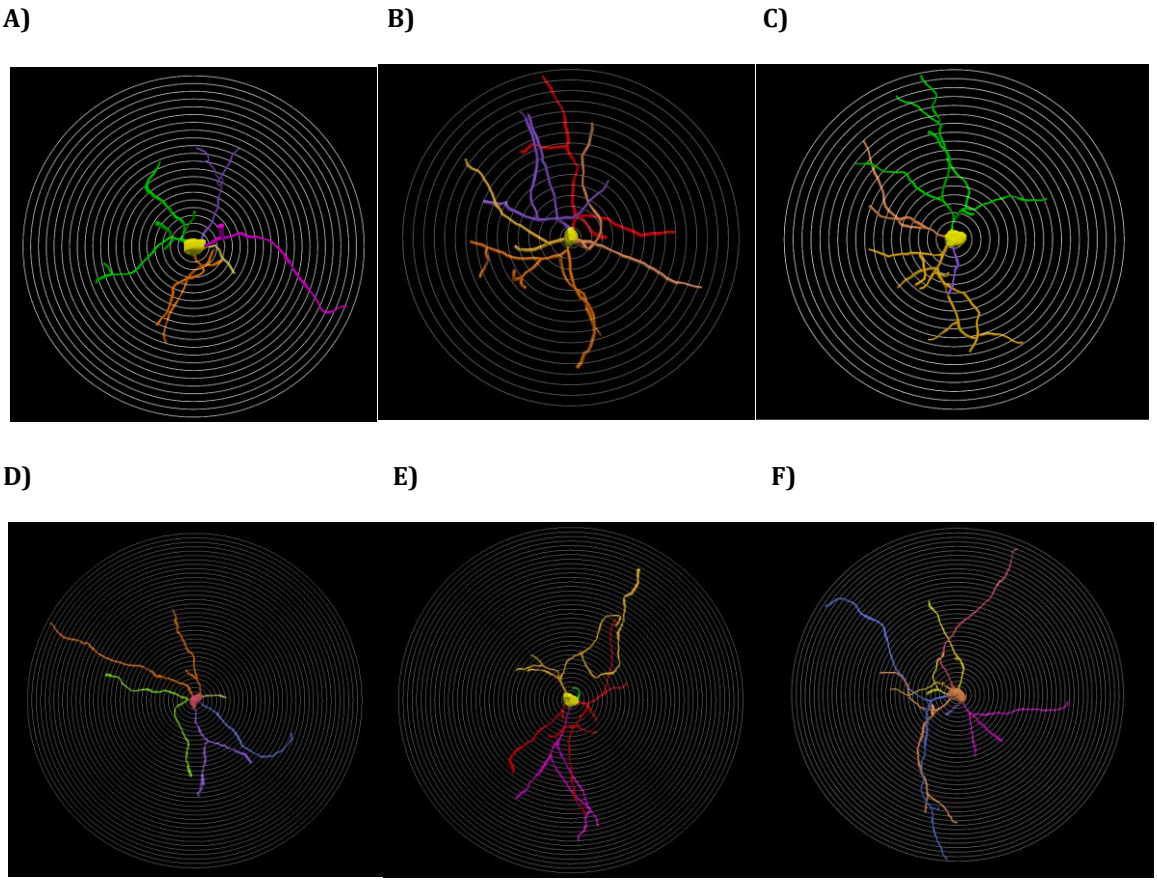

Figure 21: SOM+ PTEN KO cells have overgrown dendritic arbors

A) – F) Sholl analysis of reconstructed wild type cells showing traces of the dendrites and somas. Each concentric circle has a radius 10 um larger than the previous circle. D) – F) Sholl analysis of the floxed cells showing traces of the dendrites and soma. The scale of the rings is the same as wild type cells, showing how many more rings are required to fit the floxed cell compared to the wild type cell.

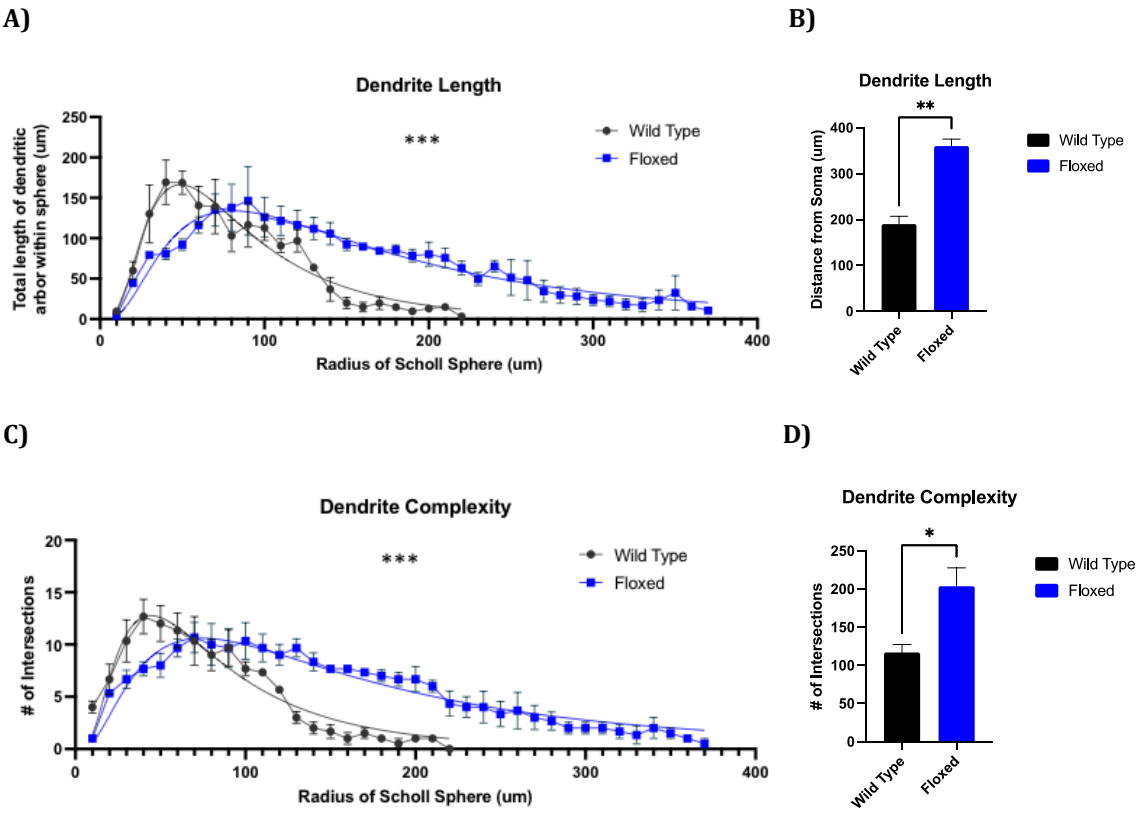

Figure 22: SOM+ PTEN KO cells have longer dendritic processes with more distal complexity

A) The dendrites of SOM+ cells in floxed mice extend nearly twice as far as those from wild type mice. (n = 3 WT cells and 3 FL cells, Lognormal Gaussian curve: A (related to area under curve) = 10096 vs 14707, Geometric Mean = 75.40 um vs 149.6 um, Geometric SD = 1.931 vs 2.195, *** indicates Comparison of Fits: $F(3, 158) = 41.62$, $p<0.0001$). B) SOM+ cells lacking PTEN extend their dendrites further than wild type cells (n = 3 WT cells and 3 FL cells, Length = 190 for WT vs 360 for FL, ** indicates t-test: $p=0.0018$). C) Similar to (A), the number of dendritic intersections with each concentric sphere is significantly higher for SOM+ cells lacking PTEN as you move further from the soma (n = 3 WT cells and 3 FL cells, Lognormal Gaussian curve: A = 728.6 vs 1134, Geometric Mean = 73.34 um vs 153.4 um, Geometric SD = 2.031 vs 2.339, *** indicates Comparison of Fits: $F(3, 158) = 48.66$, $p<0.0001$). D) The dendritic arbors of SOM+ cells from floxed mice are more complex (n = 3 WT and 3 FL cells, # of intersections = 117 for WT and 203.667 for FL, * indicates t-test: $p=0.030$). Data in B and D are presented as mean+/- SEM.

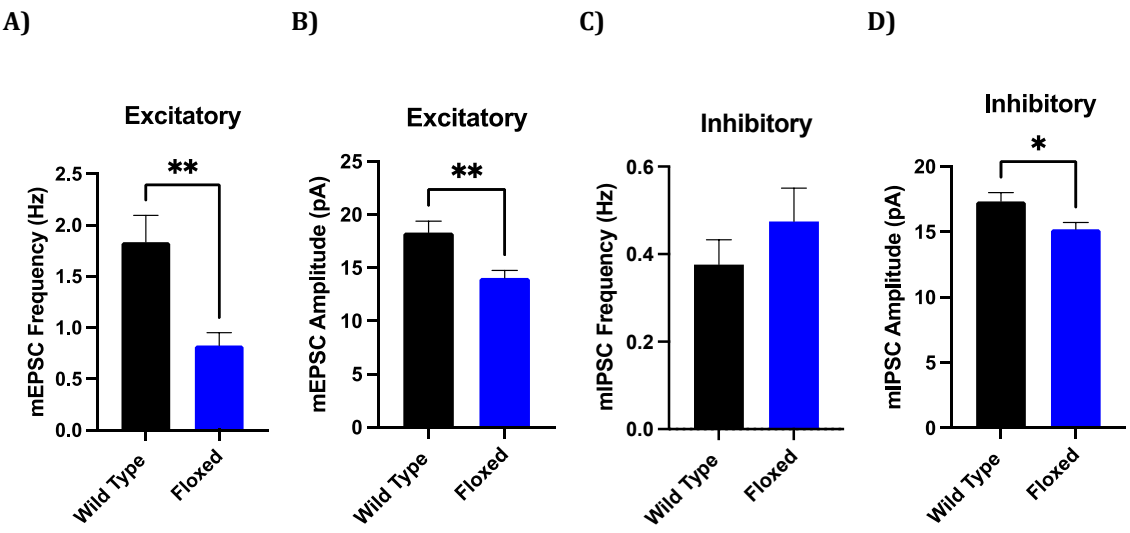

Figure 23: The properties of mEPSCs and mIPSCs are disrupted by SOM+ PTEN KO

A) The frequency of excitatory miniature EPSCs onto CeA SOM+ is reduced in floxed cells compared to wild type (n = 19 WT and 15 FL cells, Frequency = 1.835 Hz vs 0.8251 Hz, ** indicates t-test: p=0.0028). B) The amplitude of recorded mEPSCs onto CeA SOM+ is reduced by SOM+ PTEN KO (n=19 WT and 15 FL cells, Amplitude = 18.32 pA vs 14.05 pA, ** indicates t-test: p=0.0037). C) The frequency of miniature IPSCs is not affected by loss of PTEN in SOM+ neurons (n = 21 WT cells and 19 FL cells, Frequency = 0.3762 Hz vs 0.4747 Hz, t-test: p=0.2984). D) The amplitude of recorded mIPSCs onto CeA SOM+ is reduced by SOM+ PTEN KO (n=21 WT and 19 FL cells, Amplitude = 17.35 pA vs 15.22 pA, * indicates t-test: p=0.0157).

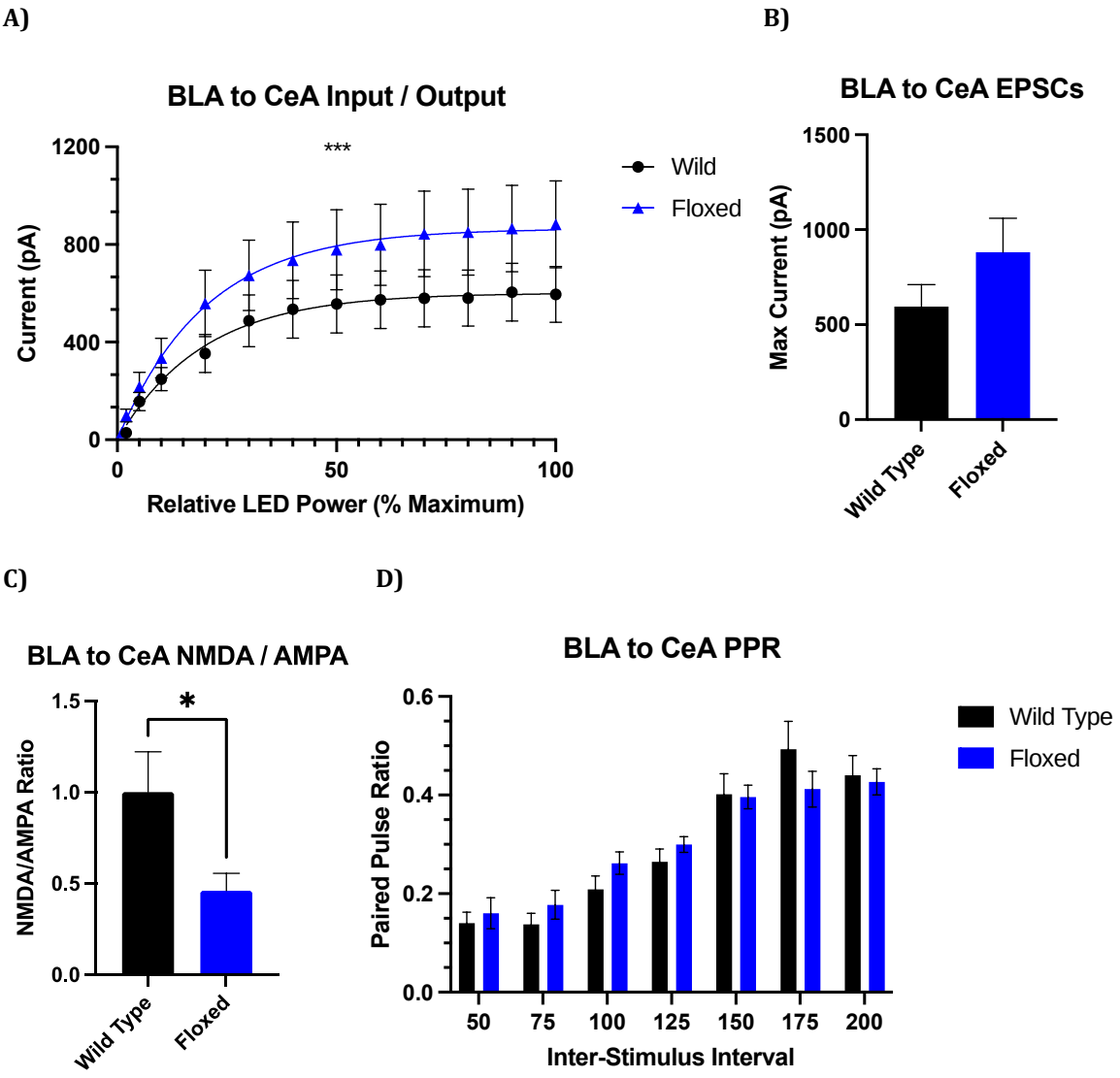

Figure 24: SOM+ PTEN KO results in increased excitatory inputs, but greatly reduces NMDA/AMPA ratio from BLA to CeA

A) Optogenetic stimulation of axon terminal inputs from the basolateral amygdala to central amygdala SOM+ neurons results in reliable EPSCs. Floxed SOM+ cells show increased peak current compared to wild type across the input/output curve (n = 18 WT and 17 FL cells, Exponential plateau curves: Max Current – 601.3 pA vs 865.5 pA, Growth Contstant – 0.05119 vs 0.04985, *** indicates Comparison of Fits: F (2, 382) = 8.465, p=0.0003). B) Maximum currents for EPSCs from BLA to CeA SOM+ neurons at 100% power are increased, but fail to a significant difference (n = 17 WT and 16 FL cells, Max Current = 597.5 pA vs 882.4 pA, t-test: p=0.1805). C) The NMDA/AMPA ratio was

significantly reduced in floxed SOM+ cells compared to wild type (n = 15 WT cells and 14 FL cells, Ratio = 1.001 vs 0.4609, * indicates t-test: p=0.0378). D) The paired-pulse ratio of BLA inputs to CeA SOM+ neurons was not affected by loss of PTEN across all inter-stimulus intervals (n = 10 WT and 5 FL cells, 2 way ANOVA: Genotype effect – $F(1, 98) = 0.1247$, $p = 0.7248$). All data are reported as mean +/- SEM.

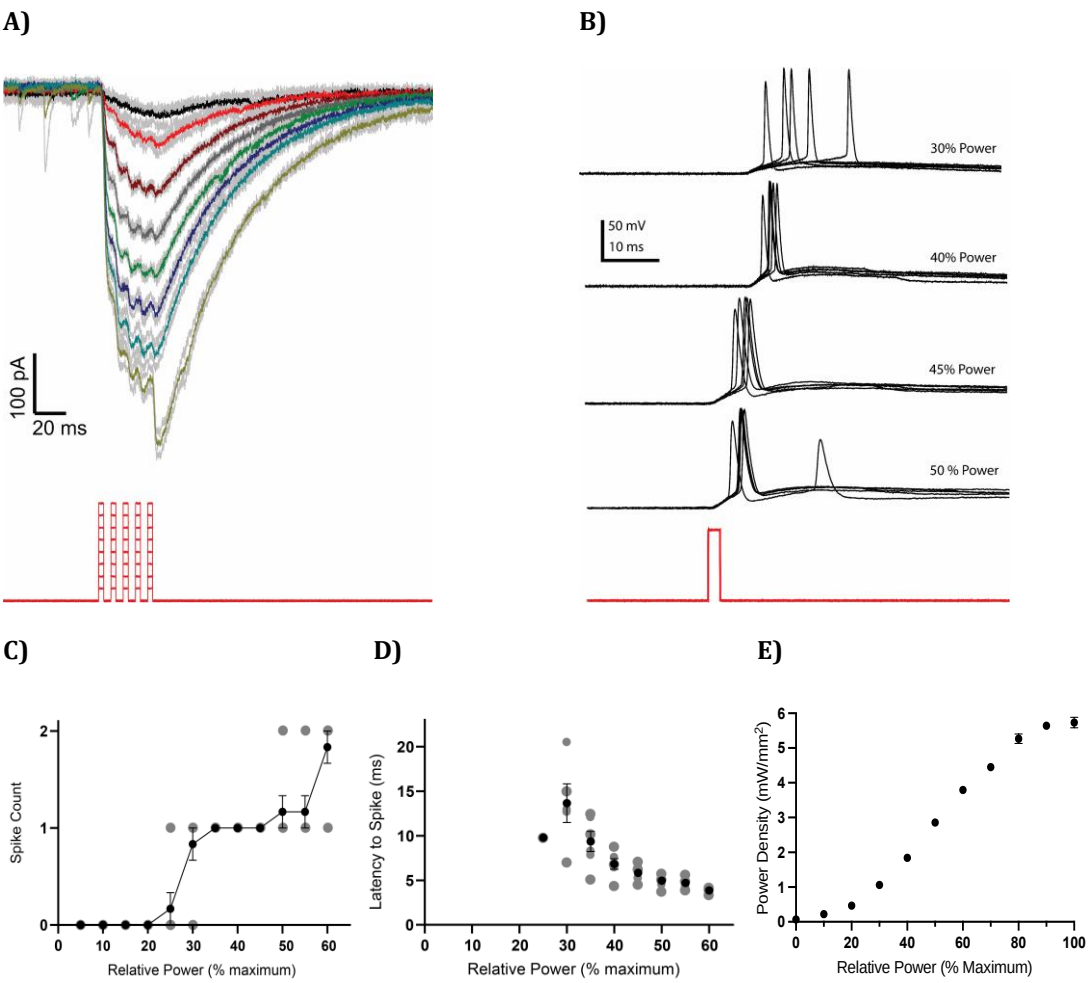

Figure 25: Chrmine-expressing SOM+ neurons can be reliably activated by 1020 nm laser

A) Representative traces from a CeA SOM+ neuron patched in whole-cell voltage clamp mode show that increasing the power of the laser from 10% to 80% power increases direct current from the opsin. B) In a separate cell in current clamp mode, 5 ms laser pulses are sufficient to elicit an action potential. C) Quantification of spikes at different power levels. D) Latency to spike reduces as laser power is increased. E) The measured power density through the 20x objective (mW/mm^2).

A) B)

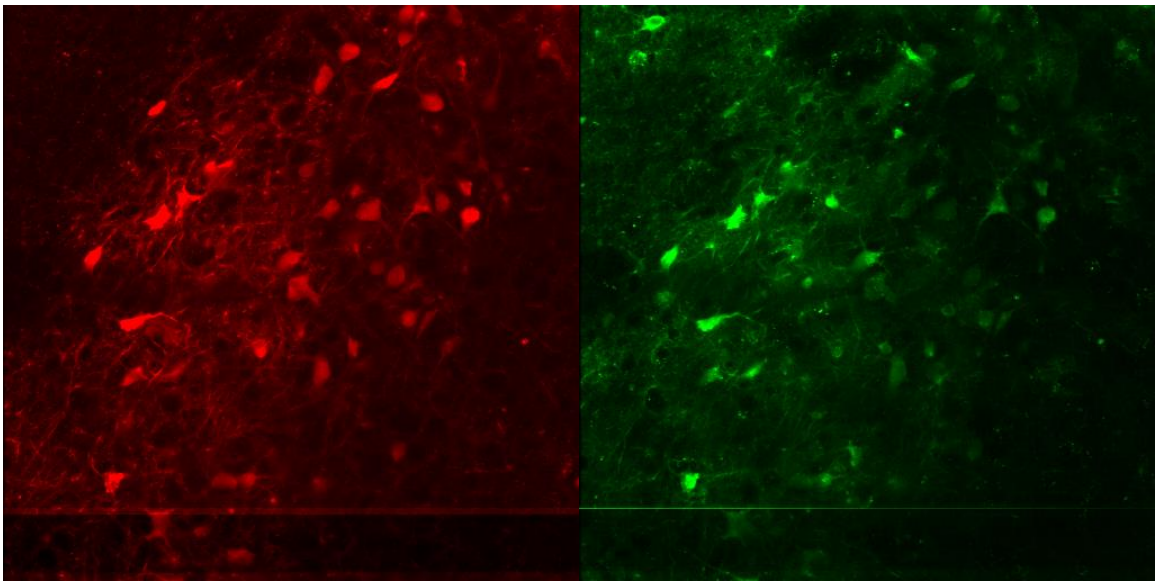

C) D)

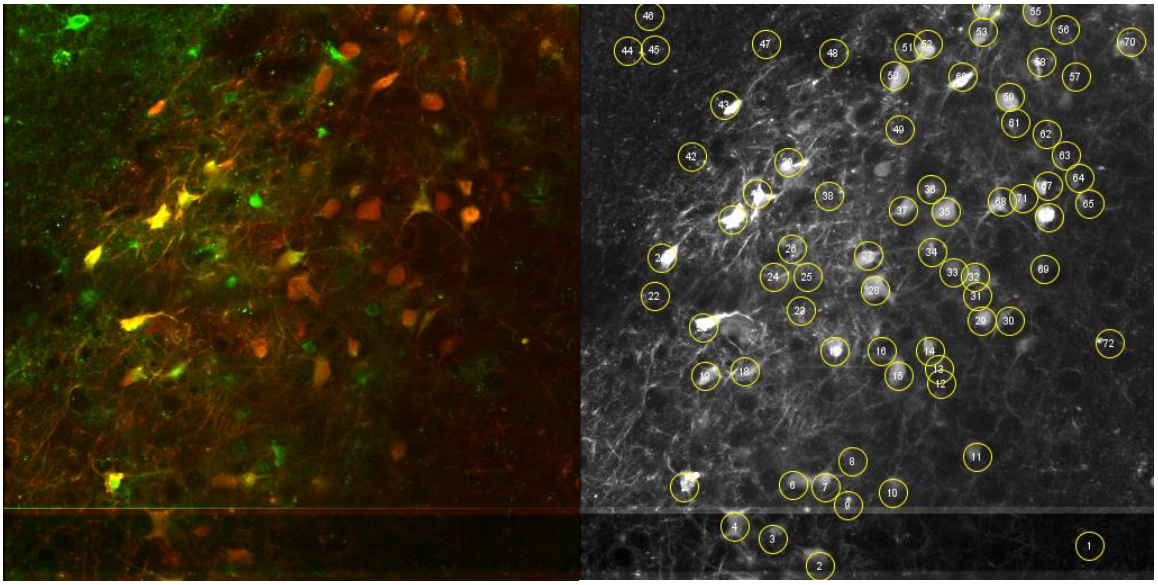

Figure 26: TdTomato-expressing SOM+ cells and GCamp6m-expressing cells in the CeA can be identified for photostimulation via 2-photon microscopy

A) TdTomato labeled SOM+ neurons in the central amygdala; the shadow of the patch pipette can be seen touching the centermost SOM+ cell. B) GCamp6m is used to identify cells for photostimulation as it necessarily indicates the co-expression of Chrmine. C) The merged image shows overlap between SOM+ and GCamp6m-expressing neurons. Note that there is a high degree of overlap

between SOM+ and GCamp6m. Since fewer SOM- neurons had visible GCamp fluorescence, it limited the number of presynaptic target cells that were SOM- compared to those that were SOM+. D) The 72 ROIs targeted in this experiment are circled and numbered. Yellow circles and numbers come from the analysis pipeline, and do not represent the diameter of spiral scan activation, which was much smaller. All images are of the same 400x400um FOV.

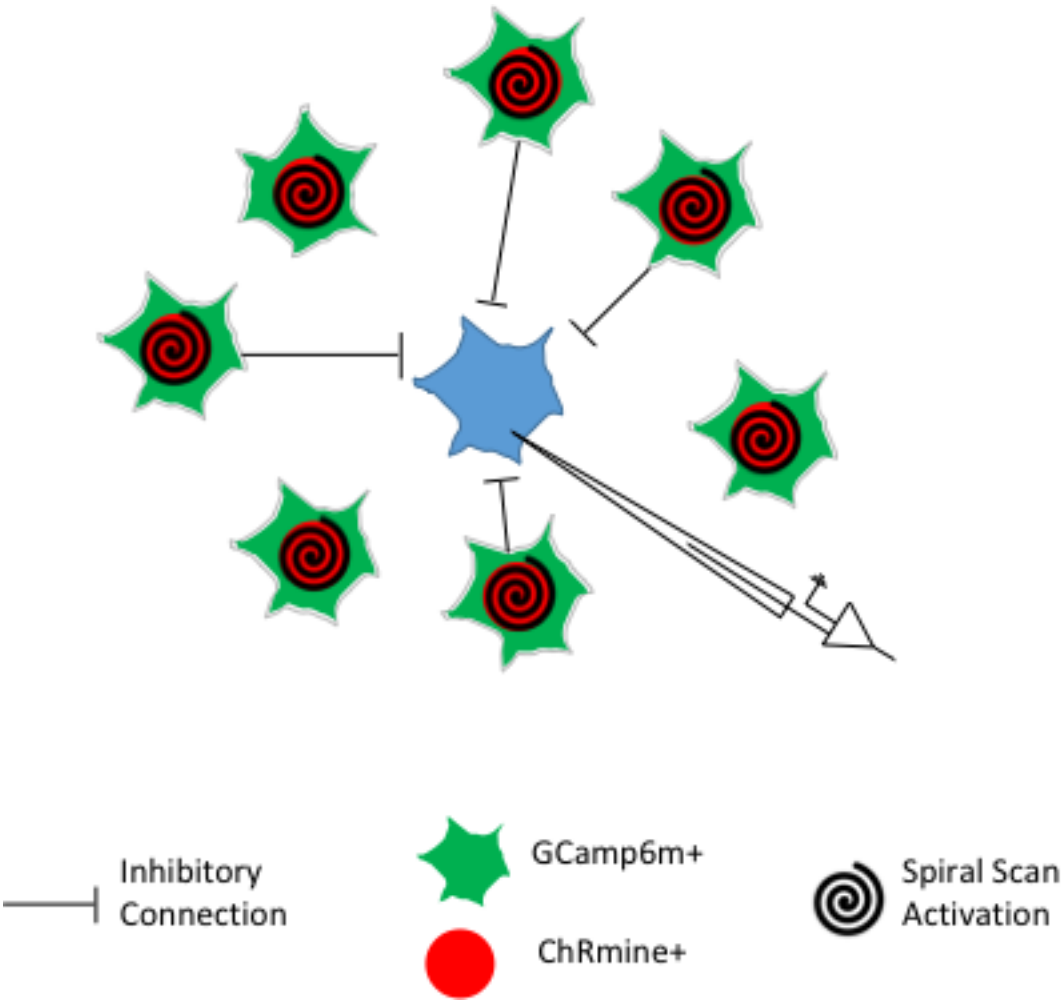

Figure 27: Schematic of circuit mapping experiment

This is a cartoon representation of the circuit mapping procedure. GCamp6m and ChRmine positive cells are targeted one at a time for spiral scan activation with the 1020 nm laser while a cell in the center of the field of view is recorded in a whole-cell patch clamp configuration. Presynaptic action potentials are verified by changes in GCamp6m fluorescence and inhibitory connections are detected as post synaptic currents onto the recorded cell.

A) **B)**

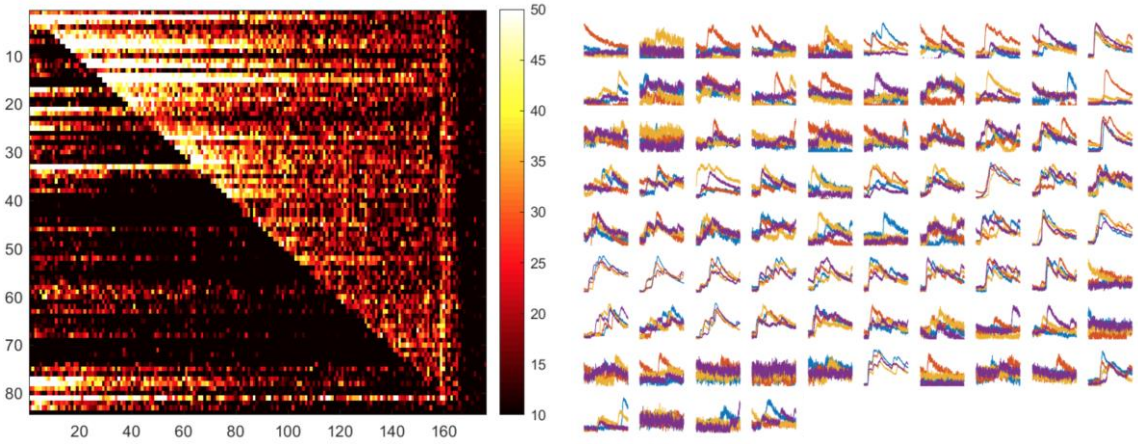

Figure 28: Circuit mapping heatmap and post synaptic currents for a wild type SOM+ neuron in the CeA show numerous connections

A) Representative heatmap of Ca^{2+} signals (dF/F GCamp6m fluorescence) for a wild type SOM+ neuron. Each row represents different ROI that was targeted for photoactivation and each column represents one frame from the calcium imaging stack. The diagonal shows successful activation of each ROI as you progress through the imaging sequence. Some cells (18, 22, 33, 81) show significant activity before being targeted by the stimulating laser, and thus did not pass the 3σ threshold for time-locked fluorescence change. Color map is 10% to 50% dF/F. B) The corresponding post synaptic currents recorded from the same cell. Each graph represents the recorded current from a single ROI, with different colored traces for each repetition. A post synaptic current was confirmed by having at least two sweeps with obvious time-locked post synaptic currents above 10 pA. The Y-axis is variable, since each graph is scaled to the peak current for that ROI, but each X-axis is 75 ms.

A) B)

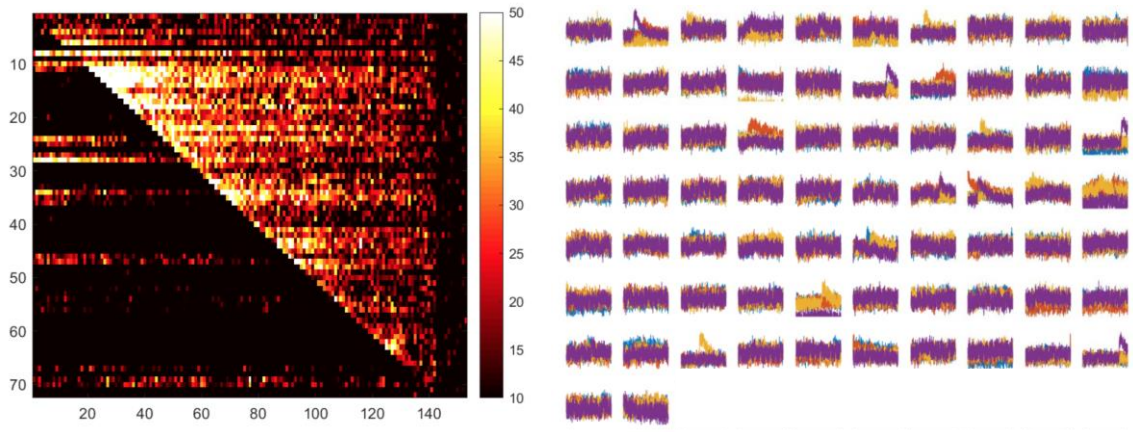

Figure 29: Circuit mapping in CeA SOM+ cells lacking PTEN showed fewer post synaptic currents

A) Representative heatmap of Ca^{2+} signals (dF/F GCamp6m fluorescence) for a floxed SOM+ neuron. Each row represents a different ROI and each column represents one frame from the calcium imaging stack. Activity along the diagonal indicates time-locked photoactivation of each ROI in turn, while activity to the left is spontaneous fluorescence prior to laser stimulation. Color map is 10% to 50% dF/F. B) The corresponding post synaptic currents recorded from the same cell. Again, each graph represents time-locked currents recorded during photostimulaiton of each ROI. Different colored traces represent each of the 4 repetitions. Note that very few traces show any post synaptic currents even with a similar number of activated potential presynaptic partners. The Y-axis is variable, since each graph is scaled to the peak current for that ROI, but each X-axis is 75 ms.

A)

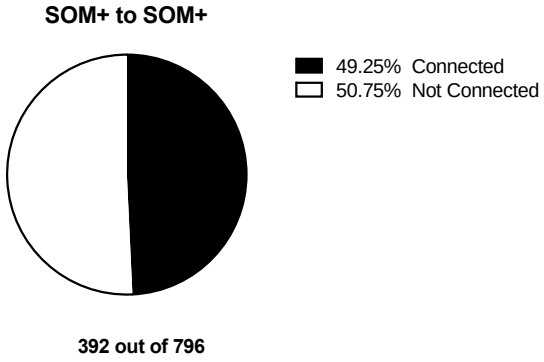

392 out of 796

B)

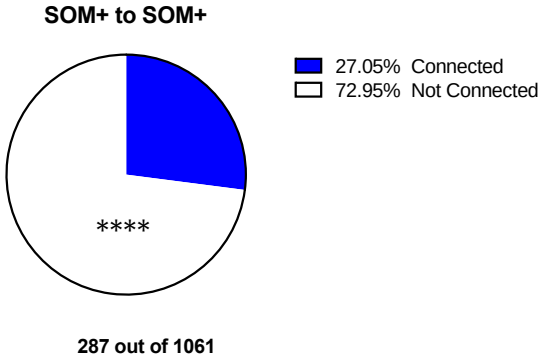

287 out of 1061

C)

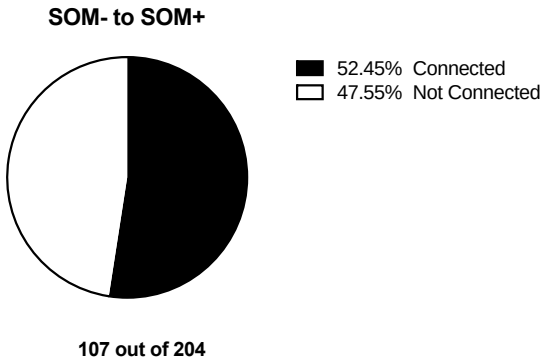

107 out of 204

D)

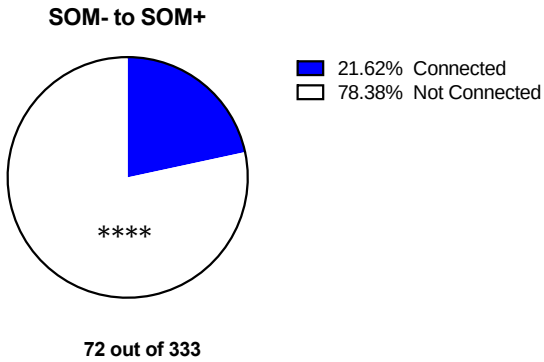

72 out of 333

E)

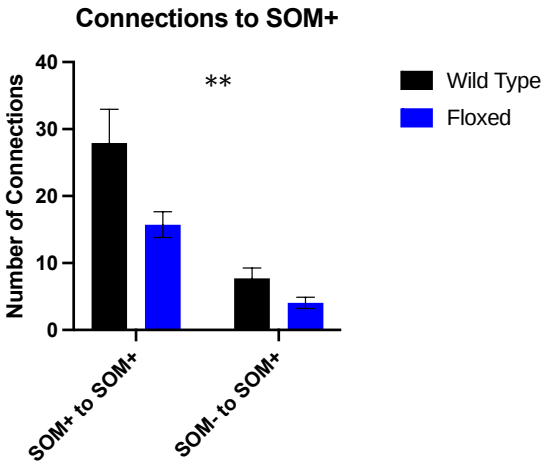

F)

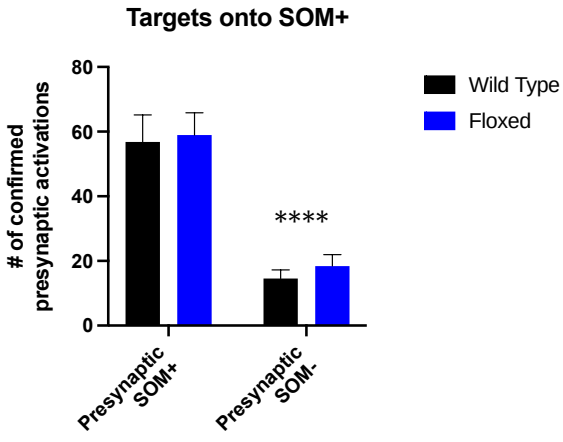

Figure 30: Central amygdala SOM+ neurons lacking PTEN receive drastically fewer synaptic connections from their local neighbors than wild type SOM+ cells

A) Wild type SOM+ to SOM+ neurons showed a connection proportion of 49.25%. Inhibitory post synaptic currents were detected from 392 out of the 796 cells that had confirmed presynaptic firing by GCamp6 fluorescence (n = 14 post synaptic cells from 5 mice, Proportion connected = 49.25 +/- 1.77%). B) Floxed SOM+ to SOM+ neurons showed a connection proportion of 27.05%. Inhibitory post synaptic currents were observed from 287 out of 1061 spike-confirmed presynaptic targets (n = 18 post synaptic cells from 6 mice, Proportion connected = 27.05 +/- 1.36%, **** indicates $p<0.0001$ difference of proportions test vs WT SOM+ to SOM+). C) Wild type SOM- to SOM+ neurons showed a connection proportion of 52.45%. IPSCs were detected from 107 out of the 204 activated presynaptic cells (n = 14 post synaptic cells from 5 mice, Proportion connected = 52.45 +/- 3.5%). D) Floxed SOM- to SOM+ neurons showed a connection proportion of 21.62%. IPSCs were detected from 72 out of the 333 activated presynaptic cells (n = 18 post synaptic cells from 6 mice, Proportion connected = 21.62 +/- 2.26%, **** indicates $p<0.0001$ difference of proportions test vs WT SOM- to SOM+). E) The average number of connections per cell is lower in floxed neurons compared to wild type neurons (n = 14 WT cells and 18 FL cells, ** indicates 2 way ANOVA: Genotype effect – $F(1, 60) = 9.358$, $p=0.0033$, note that there was also a very strong reduction of inputs due to presynaptic cell type – Cell type effect – $F(1, 60) = 37.79$, $p<0.0001$). F) SOM+ PTEN KO does not affect the number of presynaptic cells that were activated, however fewer presynaptic SOM- cells were targeted compared to SOM+ (n = 14 WT and 18 FL post synaptic cells, **** indicates 2 way ANOVA: Cell type effect – $F(1, 60) = 50.42$, $p<0.0001$). Data in E and F are presented as mean +/- SEM.

A)

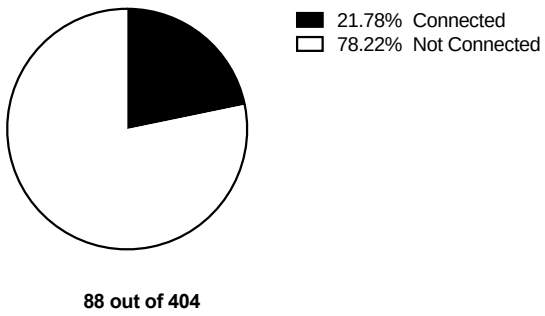

88 out of 404

B)

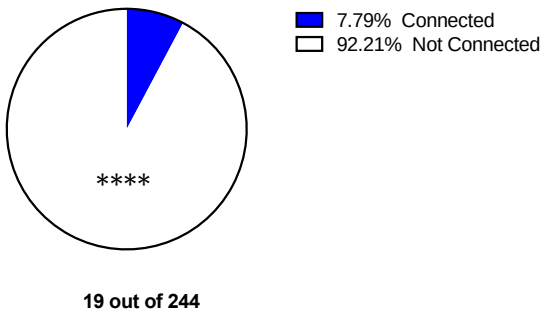

19 out of 244

C)

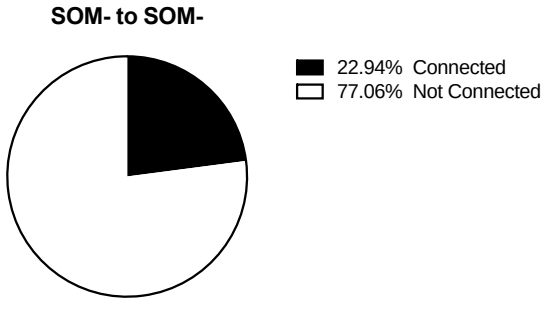

39 out of 170

D)

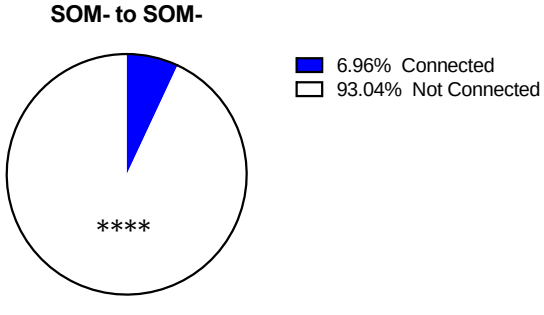

11 out of 158

E)

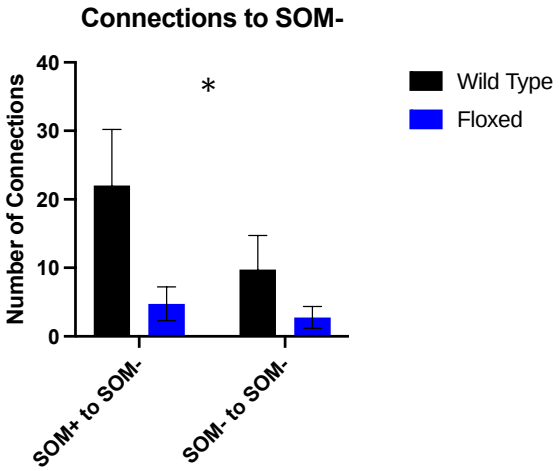

F)

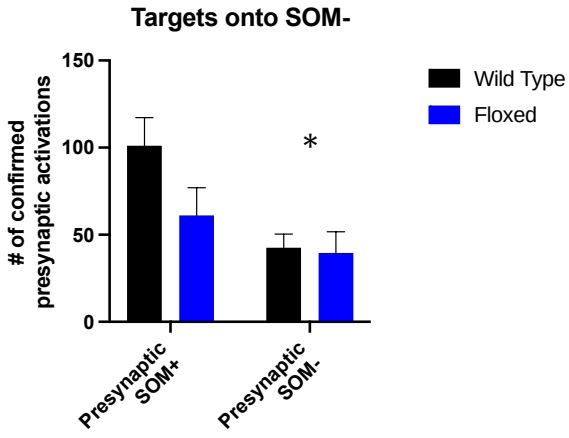

Figure 31: SOM- neurons in the central amygdala receive fewer connections from local SOM+ cells as a result of conditional PTEN KO

A) Wild type SOM+ to SOM- neurons showed a connection proportion of 21.78%. Inhibitory post synaptic currents were detected from 88 out of the 404 cells that had confirmed presynaptic firing by GCamp6 fluorescence (n = 4 post synaptic cells from 2 mice, Proportion connected = 21.78 +/- 2.05%). B) Floxed SOM+ to SOM- neurons showed a connection proportion of 7.79%. Inhibitory post synaptic currents were observed from 19 out of 244 spike-confirmed presynaptic targets (n = 4 post synaptic cells from 2 mice, Proportion connected = 7.79 +/- 1.70%, **** indicates $p<0.0001$ difference of proportions test vs WT SOM+ to SOM-). C) Wild type SOM- to SOM- neurons showed a connection proportion of 22.94%. IPSCs were detected from 39 out of the 170 activated presynaptic cells (n = 4 post synaptic cells from 2 mice, Proportion connected = 22.94 +/- 3.22%).
D) Floxed SOM- to SOM- neurons showed a connection proportion of 6.96%. IPSCs were detected from 11 out of the 158 activated presynaptic cells (n = 4 post synaptic cells from 2 mice, Proportion connected = 6.96 +/- 2.02%, **** indicates $p<0.0001$ difference of proportions test vs WT SOM- to SOM-). E) The average number of connections per cell is lower in floxed neurons compared to wild type neurons (n = 4 WT cells and 4 FL cells, * indicates 2 way ANOVA: Genotype effect – $F(1, 12) = 5.821$, $p=0.0328$). F) SOM+ PTEN KO does not affect the number of presynaptic cells that were activated, however fewer presynaptic SOM- cells were targeted compared to SOM+ (n = 4 WT and 4 FL post synaptic cells, * indicates 2 way ANOVA: Cell type effect – $F(1, 12) = 8.866$, $p=0.0115$). Data in E and F are presented as mean +/- SEM.

A)

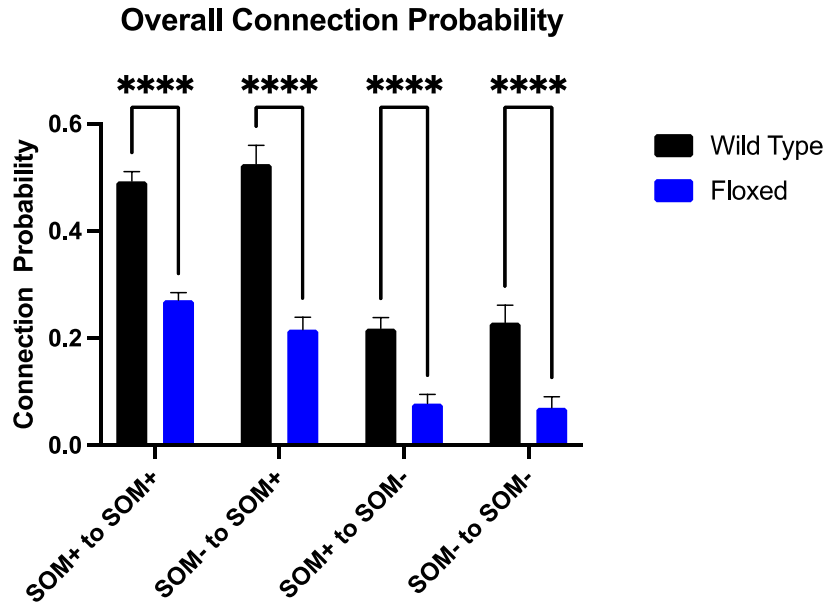

B)

C)

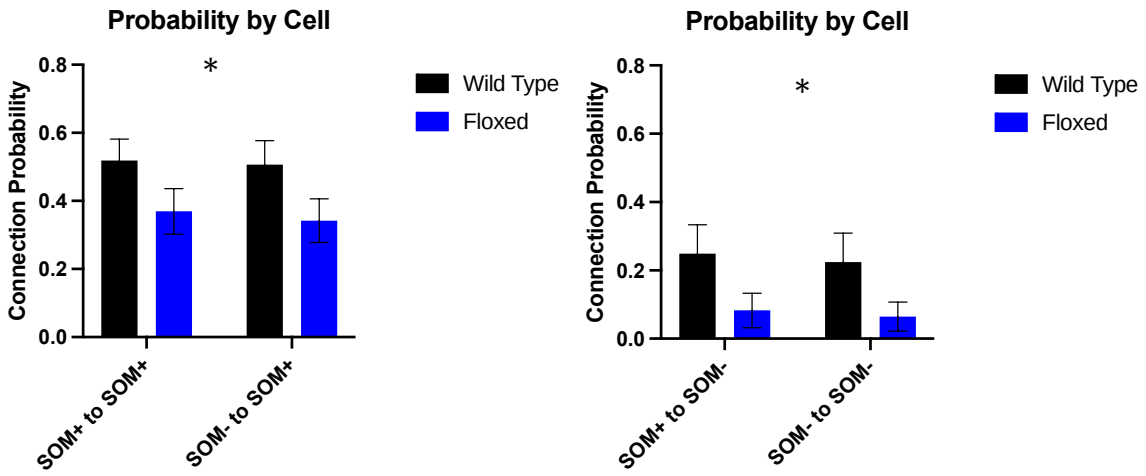

Figure 32: Floxed SOM+ neurons send and receive fewer local inhibitory connections within the central amygdala

A) Summary of overall connection probability (total connected cells/total number of confirmed presynaptic cells activated) shows roughly 50% fewer connections onto SOM+ neurons as a result of conditional PTEN knockout. Every comparison between wild type and floxed mice for each cell type combination yeilded highly significant results (SOM+ to SOM+: 392/796 WT vs 287/1061 FL, Z = 9.829, SOM- to SOM+: 107/204 WT vs 72/333 FL, Z = 7.356, SOM+ to SOM-: 88/404 WT vs 19/244

FL, Z = 4.649, SOM- to SOM-: 39/170 WT vs 11/158 FL, Z = 4.023, **** indicates p<0.0001 difference of proportions test, note that comparisons between WT post synaptic SOM+ vs post synaptic SOM- (Z = 9.177) and between FL post synaptic SOM+ vs post synaptic SOM- (Z = 6.404) also yeilded p<0.0001 results). B) Floxed SOM+ neurons have a lower local inhibitory connection probability than wild type SOM+ neurons when evaluated by cell (n = 14 WT cells and 18 FL cells, * indicates 2 way ANOVA: Genotype effect – F (1, 60) = 5.528, p=0.0220). C) SOM- cells have lower connection probability from floxed SOM+ neurons and SOM- to SOM- connection probability is reduced as well due to conditional PTEN KO (n = 4 WT cells and 4 FL cells, * indicates 2 way ANOVA: Genotype effect – F (1, 12) = 5.664, p=0.0348).

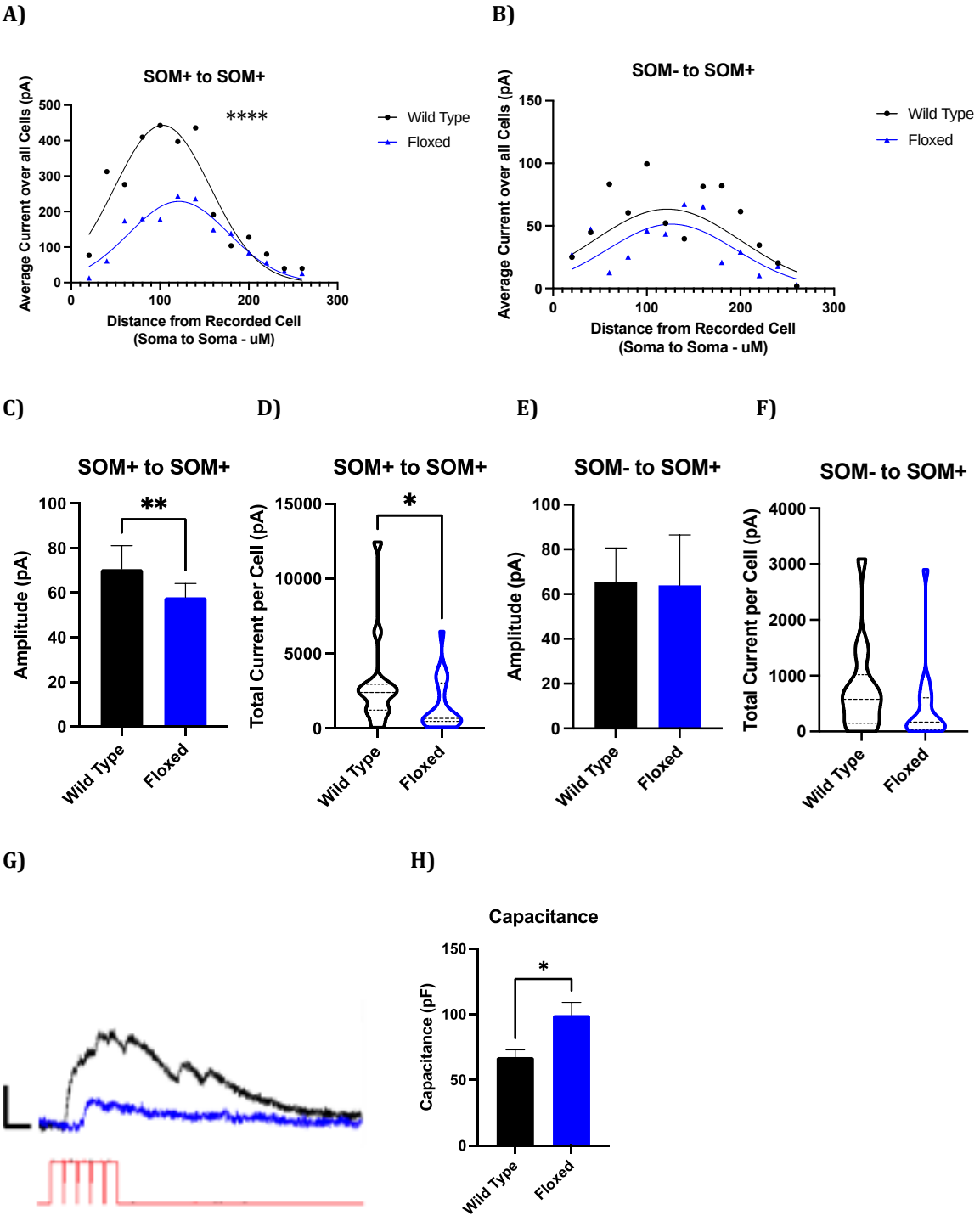

Figure 33: Currents from SOM+ to SOM+ neurons in the CeA are reduced, but those from SOM- to SOM+ are unaffected

A) Average current onto CeA SOM+ cells plotted against the distance from the stimulated presynaptic cell reveals a reduced amplitude and shift in distance for SOM+ neurons lacking PTEN. IPSCs were

binned in 20 um increments according to their corresponding presynaptic cell's soma to soma distance from the recorded post synaptic neuron and averaged. The resulting current distributions were fit with Gaussian curves and compared (n = 392 IPSCs onto 14 WT cells and 287 IPSCs onto 18 FL cells, Gaussian curves: Peak amplitude = 443.3 pA vs 228.7 pA, Mean = 102.9 um vs 121.3 um, SD = 53.88 vs 56.23, **** indicates Comparison of fits: $F(3, 20) = 19.49$, $p<0.0001$). B) Afferent currents from CeA SOM- cells onto SOM+ cells are not affected by conditional PTEN knockout (n = 107 IPSCs onto 14 WT cells and 72 IPSCs onto 18 FL cells, Gaussian curves: Peak amplitude = 76.85 pA vs 51.34 pA, Mean = 120.0 um vs 126.4 um, SD = 82.47 vs 68.37, Comparison of fits: $F(3, 20) = 3.070$, $p = 0.0514$). C) Incoming IPSCs from other CeA SOM+ neurons are reduced in SOM+ PTEN KO mice. The amplitude distribution failed to pass the test for normality (Shapiro-Wilk test: 0.7988, $p<0.0001$ for WT and 0.7101, $p<0.0001$ for FL) so median values are presented (n = 392 for WT and 287 for FL, Median = 70.61 vs 57.92, Mann-Whitney Rank Sum: $U=48993$, $p=0.0037$). Bars indicate 95% confidence interval for the median. D) Total current per cell from other SOM+ afferents was not normally distributed, but the distribution was significantly altered in floxed cells compared to wild type (n = 14 WT cells and 18 FL cells, * indicates Kolmogorov-Smirnov test: $D=0.5238$, $p=0.0266$). E) The strength of afferent IPSCs from SOM- onto SOM+ neurons was unaffected by SOM+ PTEN KO. The amplitude distribution failed to pass the test for normality (Shapiro-Wilk test: 0.7968, $p<0.0001$ and 0.7494, $p<0.0001$) so median values are presented (n = 107 for WT and 72 for FL, Median = 65.46 vs 63.94, Mann-Whitney Rank Sum: $U=3039$, $p=0.8290$). Bars indicate 95% confidence interval for the median. F) SOM+ PTEN KO did not affect the total inhibitory postsynaptic current per cell from SOM- onto SOM+ neurons (n = 14 WT cells and 18 FL cells, Kolmogorov-Smirnov test: $D=0.3810$, $p=0.2032$). G) An example trace of SOM+ to SOM+ IPSCs show reduced amplitude for the floxed cell (blue) compared to the wild type cell (black) in response to the laser stimulation of a presynaptic cell (red). Scale bars indicate 100 pA and 10 ms. H) Floxed SOM+ cells had higher capacitance than wild type SOM+ cells, providing further evidence of overgrowth (n = 14 WT and 18 FL cells, Capacitance = 67.43 pF vs 99.44 pF, * indicates t-test: $p=0.0122$, Data are mean +/- SEM).

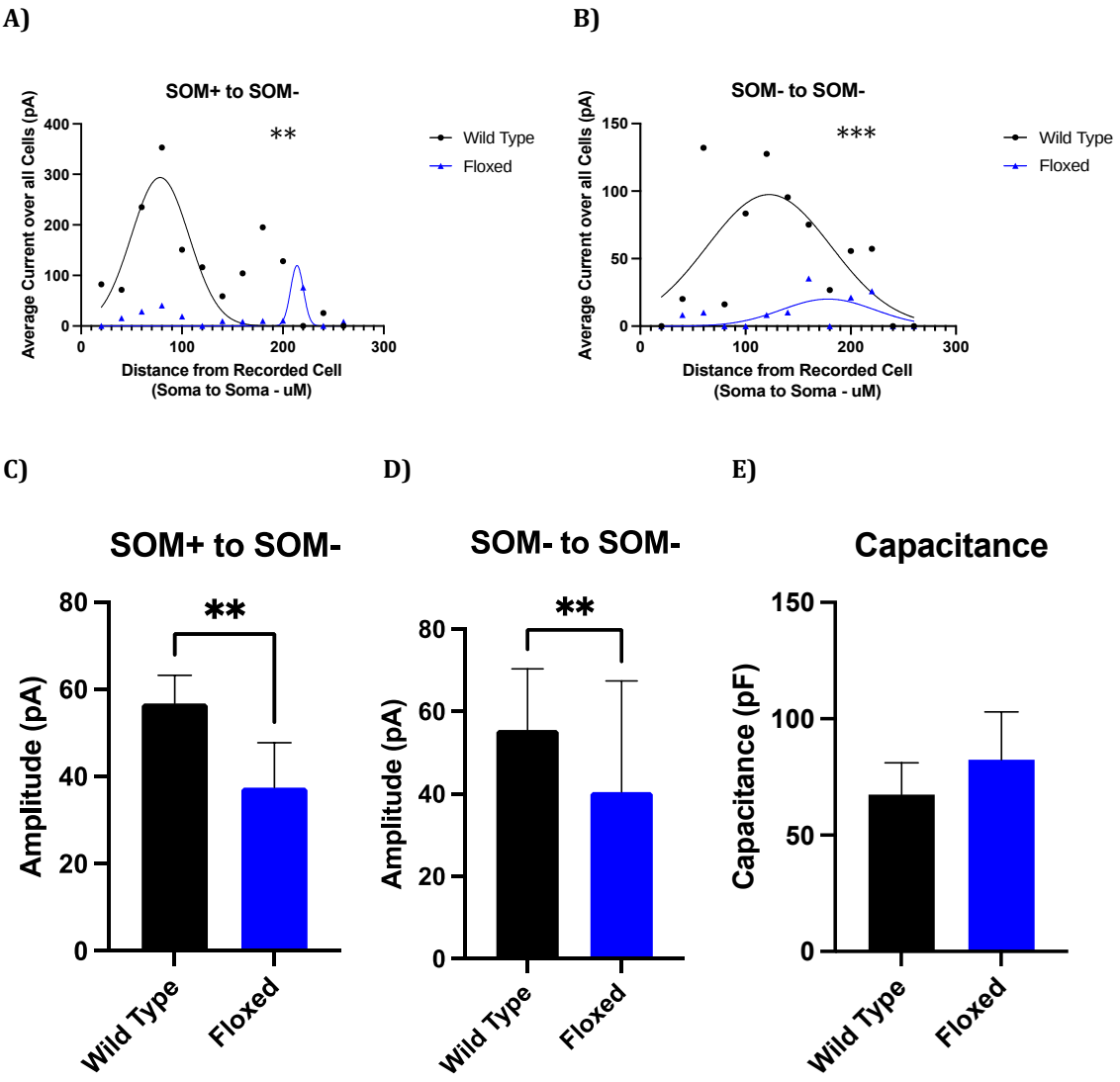

Figure 34: Currents from floxed SOM+ neurons onto SOM- cells are reduced, and SOM+ PTEN KO affects SOM- to SOM- IPSCs as well

A) Average current onto CeA SOM- cells plotted against the distance from the stimulated presynaptic cell reveals a reduced amplitude and shift in distance for IPSCs coming from SOM+ neurons lacking PTEN. IPSCs were binned in 20 um increments according to their corresponding presynaptic cell's soma to soma distance from the recorded post synaptic neuron and averaged. The resulting current distributions were fit with Gaussian curves and compared (n = 88 IPSCs onto 4 WT cells and 19 IPSCs onto 4 FL cells, Gaussian curves: Peak amplitude = 293.8 pA vs 119.7 pA, Mean distance = 78.37 um vs 214.0 um, SD = 28.63 vs 6.327, ** indicates Comparison of fits: F (3, 20) = 6.711, p=0.0026). B) Afferent currents from CeA SOM- cells onto SOM- cells are also affected by conditional PTEN

knockout (n = 39 IPSCs onto 4 WT cells and 11 IPSCs onto 4 FL cells, Gaussian curves: Peak amplitude = 97.44 pA vs 20.12 pA, Mean distance = 122.4 um vs 178.5 um, SD = 59.03 vs 44.25, *** indicates Comparison of fits: F (3, 20) = 8.362, p = 0.0008). C) Incoming IPSCs from floxed CeA SOM+ neurons are reduced in SOM- cells. The amplitude distribution failed to pass the test for normality (Shapiro-Wilk test: 0.6991, p<0.0001 for WT and 0.7067, p<0.0001 for FL) so median values are presented (n = 88 for WT and 19 for FL, Median = 56.75 vs 37.50, ** indicates Mann-Whitney Rank Sum: U=450, p=0.0013). Bars show 95% confidence interval for the median. D) Incoming IPSCs from other CeA SOM- neurons are also reduced in SOM- cells in SOM+ PTEN KO mice. The amplitude distribution failed to pass the test for normality (Shapiro-Wilk test: 0.4109, p<0.0001 for WT and 0.8185, p=0.0165 for FL) so median values are presented (n = 39 for WT and 11 for FL, Median = 55.54 vs 40.47, ** indicates Mann-Whitney Rank Sum: U=107, p=0.0086). Bars show 95% confidence interval for the median. E) The capacitance of recorded SOM- neurons was unaffected by SOM+ PTEN KO (n = 4 WT cells and 4 FL cells, Capacitance = 67.49 pF vs 82.41 pF, t-test: p=0.5668). Data in E are presented as mean +/- SEM.

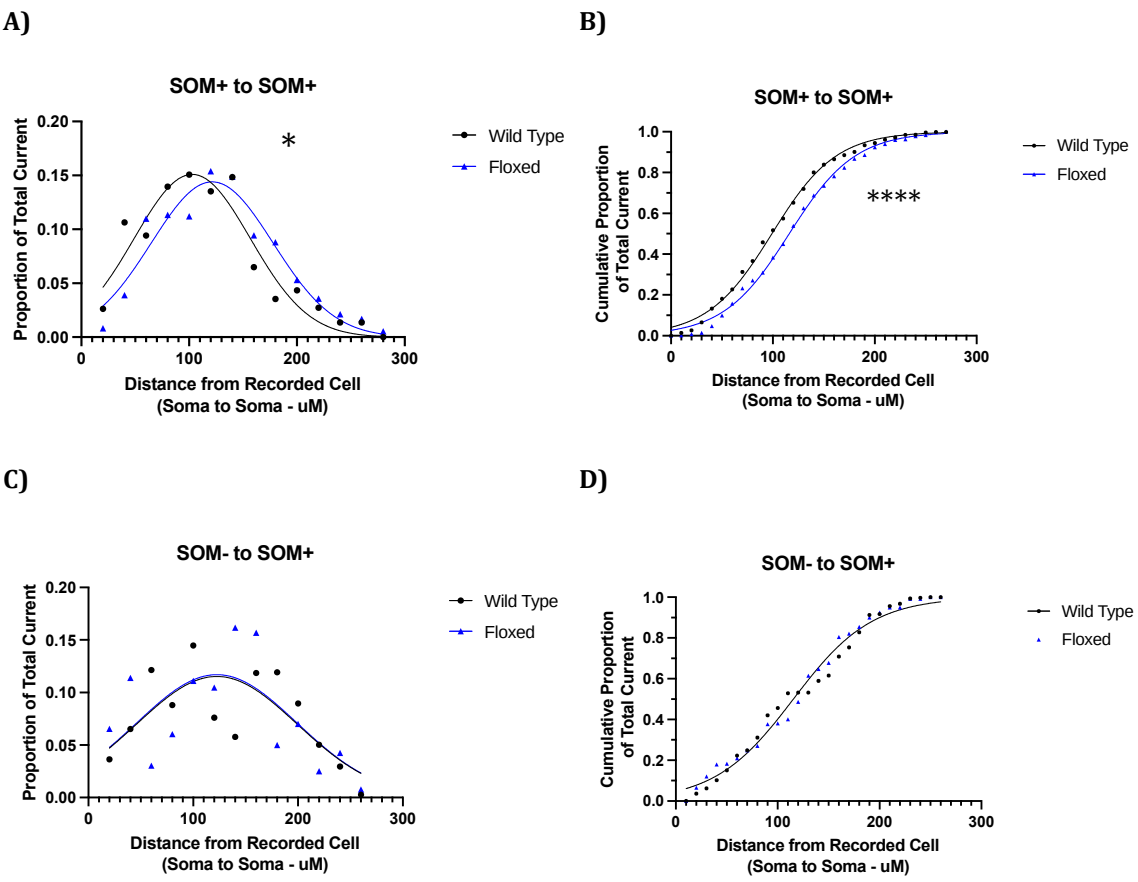

Figure 35: The distribution of IPSCs from SOM+ onto SOM+ neurons is shifted away from the soma

A) Plotting the soma to soma distance between the stimulated presynaptic cell and the recorded cell against the proportion of total current received from SOM+ onto SOM+ neurons shows a shift in the curve toward more distal afferents. All IPSCs were binned in 20 um intervals, to represent the proportion of all the incoming current that originated from that distance, and fit with a Gaussian curve. The distribution for floxed SOM+ is shifted 20 um away compared to wild type cells (n = 392 IPSCs onto 14 WT cells and 287 IPSCs onto 18 FL cells, Gaussian curves: Peak amplitude = 15.10% vs 14.40%, Mean distance = 102.9 um vs 121.4 um, SD = 53.88 vs 56.51, * indicates Comparison of fits: F (3, 20) = 3.288, p=0.0421). B) Plotting the cumulative proportion of current by 10 um-binned distances shows the distal shift of SOM+ to SOM+ IPSCs due to conditional PTEN KO. These data were fit by sigmoidal cumulative Gaussian curves and compared to show increased soma to soma distance for floxed IPSCs while retaining the same slope (n = 392 IPSCs onto 14 WT cells and 287

IPSCs onto 18 FL cells, Sigmoidal curves: Top and Bottom were fixed at 0 and 1, Distance at 50% (mean) = 99.12 um vs 116.2 um, Slope = 53.15 vs 54.72, **** indicates Comparison of fits: F (2, 52) = 82.24, p<0.0001). C) Plots for IPSC afferents from SOM- cells to SOM+ cells shows no effect to the spatial distribution on account of the conditional PTEN KO (n = 107 IPSCs onto 14 WT cells and 72 IPSCs onto 18 FL cells, Gaussian curves: Peak amplitude = 11.20% vs 12.33%, Mean distance = 120.0 um vs 126.4 um, SD = 82.47 vs 68.37, Comparison of fits: F (2, 20) = 0.2050, p = 0.8163). D) The cumulative proportion of SOM- to SOM+ current by distance was not affected the removal of PTEN from SOM+ neurons (n = 107 IPSCs onto 14 WT cells and 72 IPSCs onto 18 FL cells, Sigmoidal curves: Top and Bottom were fixed at 0 and 1, Distance at 50% (mean) = 115.9 um vs 114.9 um, Slope = 66.18 vs 63.05, Comparison of fits: F (2, 48) = 05105, p=0.6034).

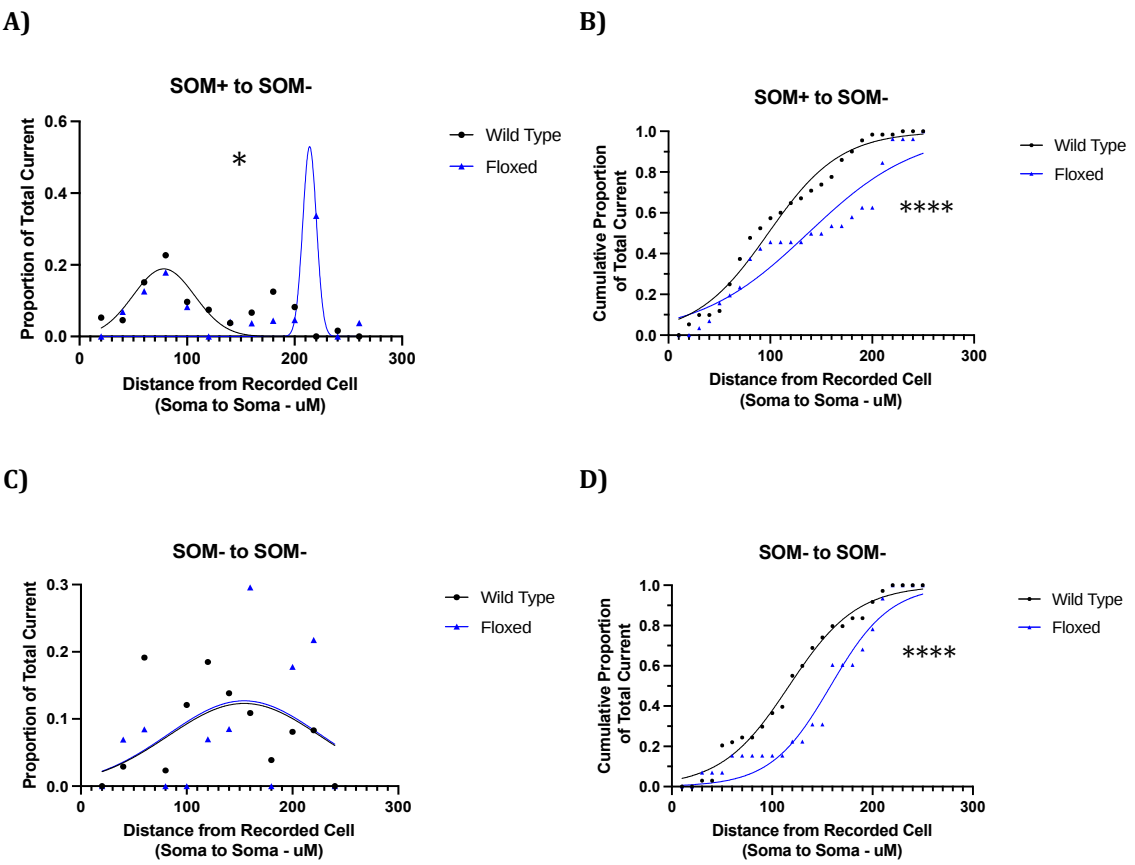

Figure 36: SOM+ knockout of PTEN affects the spatial distribution of IPSCs onto SOM- cells

A) Plotting the soma to soma distance between the stimulated presynaptic cell and the recorded cell against the proportion of total current received from SOM+ onto SOM- neurons shows a disruption in the spatial distribution of afferents. All IPSCs were binned in 20 um intervals, to represent the proportion of all the incoming current that originated from that distance, and fit with a Gaussian curve. Currents at the distal end of the distribution dominated the curve for floxed cells and pushed it much further from the soma compared to wild type cells (n = 88 IPSCs onto 4 WT cells and 19 IPSCs onto 4 FL cells, Gaussian curves: Peak amplitude = 18.87% vs 52.96%, Mean distance = 78.37 um vs 214.0 um, SD = 28.63 vs 6.327, * indicates Comparison of fits: F (3, 20) = 3.763, p=0.0272). B) Plotting the cumulative proportion of current by 10 um-binned distances shows the distal shift of SOM+ to SOM- IPSCs due to conditional PTEN KO. These data were fit by sigmoidal cumulative Gaussian curves and compared to show increased soma to soma distance for floxed IPSCs and a decrease in the slope (n = 88 IPSCs onto 4 WT cells and 19 IPSCs onto 4 FL cells, Sigmoidal curves:

Top and Bottom were fixed at 0 and 1, Distance at 50% (mean) = 98.46 um vs 136.8 um, Slope = 59.74 vs 87.51 **** indicates Comparison of fits: F (2, 46) = 29.41, p<0.0001). C) Plots for IPSC afferents from SOM- cells to SOM- cells shows no significant effect to the spatial distribution on account of the conditional PTEN KO (n = 39 IPSCs onto 4 WT cells and 11 IPSCs onto 4 FL cells, Gaussian curves: Peak amplitude = 14.07% vs 16.50%, Mean distance = 122.7 um vs 180.4 um, SD = 59.65 vs 47.35, Comparison of fits: F (3, 18) = 1.296, p = 0.3063). D) The cumulative proportion of SOM- to SOM- current by distance was shifted significantly by the removal of PTEN from SOM+ neurons (n = 39 IPSCs onto 4 WT cells and 11 IPSCs onto 4 FL cells, Sigmoidal curves: Top and Bottom were fixed at 0 and 1, Distance at 50% (mean) = 116.8 um vs 157.8 um, SD = 57.25 vs 50.25, **** indicates Comparison of fits: F (2, 46) = 59.12, p<0.0001).

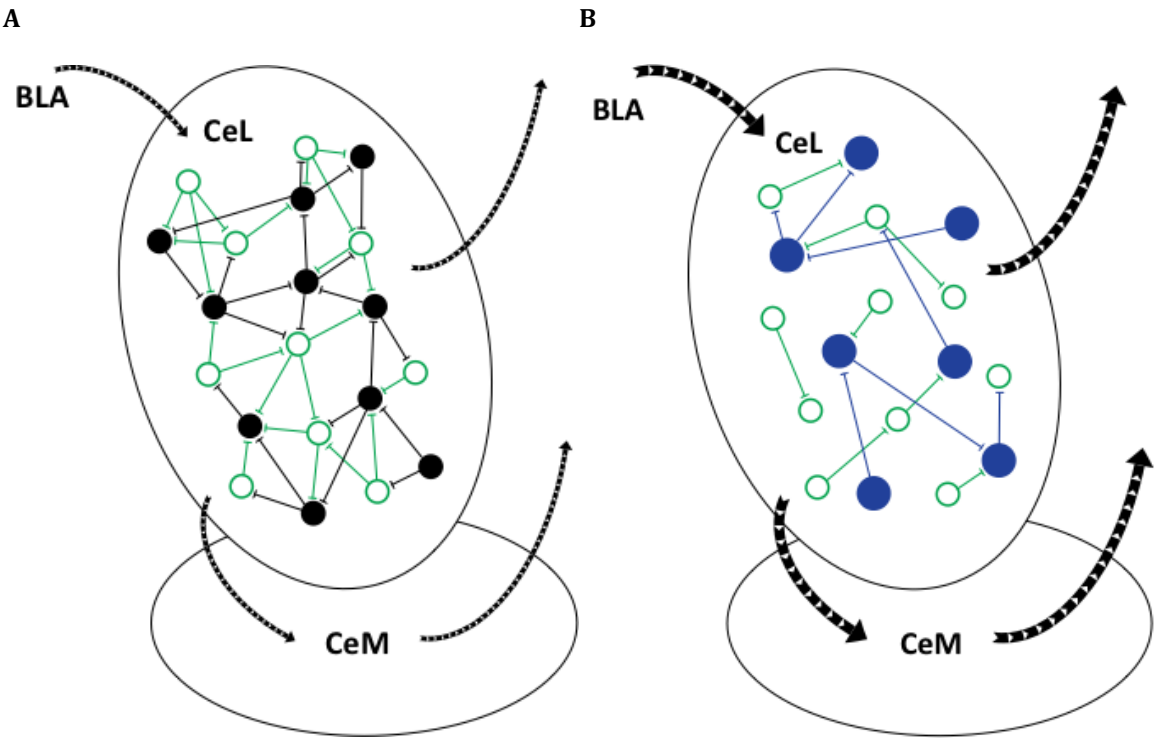

Figure 37: Summary Model of CeA Circuitry

A) In the wild type condition, inputs from the BLA synapse onto a highly interconnected network of inhibitory neurons in the central-lateral amygdala, including SOM+ neurons. These interneurons make local inhibitory connections among one another to regulate the output to downstream fear and anxiety related brain regions, including the PAG and BNST. The output from CeL SOM+ neurons is sufficiently inhibited by the local connections to maintain reasonable levels of fear outputs. B) When SOM+ neurons are lacking PTEN, they grow larger and less populated neurons in the CeL that form less connected local inhibitory networks. Therefore, when they receive stronger inputs from the BLA, the signals are not sufficiently inhibited within the CeL, which results in stronger outputs to downstream fear-inducing brain regions.

CHAPTER 7: CONCLUSIONS AND FUTURE RESEARCH

Conclusions

As we have shown, the lack of proper PTEN function in somatostatin-expressing interneurons results in elevated fear and anxiety in mice that is associated with decreased lateral inhibition in the central amygdala and an increased excitatory drive onto SOM+ neurons. Our experiments highlight the importance of determining the roles of specific cell types in various models of neurological disorders, to enable further characterization of the circuits responsible for specific behavioral deficits. These results have implications for our understanding of autism spectrum disorder, the PTEN gene, SOM+ interneurons, and local circuitry.

Autism spectrum disorder research has come a long way in a relatively short time, and has benefited from the rapid advancement of genetic and scientific technology. We joined the ongoing efforts to better understand the development and progression of ASD, and along with all other researchers of neurological disorders, hope for the emergence of better and more specific therapeutic interventions. ASD is a specifically difficult group of disorders to treat from a medical point of view, in part because there are many who feel that there is nothing "wrong" with the individuals affected. As the number of people diagnosed with ASD has risen and the issues surrounding ASD have become a topic of public opinion, it

has become increasingly important to discuss intervention options with sensitivity. Since the degree to which ASD affects an individual's life, and the lives of those around them, is so variable, treatments for ASD have to be adjusted accordingly. Our research helps to provide evidence for the possibility of treating some of the less desirable symptoms of the ASD phenotype while potentially not disrupting other aspects of the patient's personality. By identifying specific cell types and circuits responsible for some parts of behavioral dysfunction but not others, as we have seen, it may be possible to develop treatments that can target fear and anxiety without attempting to force the need to "fix" any and all idiosyncrasies that a patient or family member view as part of their personality. As should always be the goal with medical treatment, we hope that our research will go on to enable more compassionate care for the people affected by ASD.

Additionally, research into the function of PTEN has accelerated and expanded in scope since its discovery as a cancer suppressor, and our results provide important considerations for PTEN's function in the brain. While it has been shown before that PTEN mutations affect behaviors related to ASD, we have demonstrated that specific cell types contribute differentially to the behavioral phenotype associated with PTEN dysfunction. Additionally, we have provided evidence for the role of PTEN in regulating local circuit connectivity and synaptic strength in important brain regions related to ASD-related behaviors. Most research into PTEN has been focused on its role in intracellular signaling and cell growth, and though some have shown that PTEN mutations can affect synaptic signaling, our research reveals a powerful new aspect of PTEN's function in SOM+

cells, namely the organization of local inhibitory networks necessary for proper amygdala function.

Our results also provide for richer understanding of the role of SOM+ neurons in general, and especially in their contribution to the computations within the central amygdala. As we discussed in the previous chapter, our findings bring novel insights into these connectivity patterns of the local networks within the central amygdala as it relates to the fear and anxiety circuitry. However, they have broader implications for other amygdala-related behaviors outside of just PTEN and ASD. While other researchers have investigated local synaptic partnerships, we are the first to do so on this scale and our local circuit mapping technique may open the door for further experiments into local inhibition or excitation patterns in other brain areas or other cell types.

If the accurate integration of information within a local circuit is indeed necessary for the proper functional output of a specific brain region, as is presumed by computational neuroscientists and accepted by most, then our technique will allow researchers to probe the functional mesoscale connectivity patterns that have previously been confined to anatomical mapping or broad, regional inputs or outputs. As it is improbable that every cell in a certain brain region is activated simultaneously during a given behavior, discovering the interplay between individual neurons, or, more likely, neuronal ensembles, will be of utmost importance for understanding how local circuit computation gives rise to an intelligible behavioral output.

Future Research

Our experiments have clearly shown the value of investigating single cell-type manipulations of candidate genes for neurological disorders, the implications of which we have discussed at length. However, progression in science is achieved, in part, by not settling for great experiments and always pushing forward to try new things. This is certainly the case for our lab and our future plans. We will expand upon the results obtained here in several ways, implementing both in-vivo and in-silico approaches, some of which are already underway.

One area of future research we are interested in is that of in-vivo manipulation of specific local circuitry during ASD-related behaviors. To do so, we aim to employ the technologies of in-vivo optogenetics and DREADDs. Both of these methods allow for researchers to increase or decrease the activity of genetically and spatially specific neural populations in awake, behaving animals, although there are advantages and disadvantages to each. Optogenetics affords the advantage of great temporal control since it activates or deactivates neurons via pulses of light delivered through fiber optic cables, and newer opsins can operate with millisecond-precision. However, the activation created by illumination of opsin channels may not be physiologically relevant to their spiking patterns in-vivo. Conversely, DREADDs offer the advantage of a seemingly more physiologically relevant mechanism, that of potentiating or inhibiting the intrinsic inputs and activity that already occurring in-vivo. However, the temporal precision of cellular activation or inactivation by DREADDs is very poor, as the channel agonist activity peaks ~30 minutes after systemic injection into a mouse, and the effects can last up

to two hours. Overall, optogenetics provides a better tool for the investigation of circuit elements, while DREADDs may give a more accurate model of potential therapeutic intervention.

While optogenetics and DREADDs are designed for manipulating cellular activity, another direction for future research in our lab focuses on visualizing the actual activity of neural circuits in-vivo with miniature head-mounted microscopes. This is accomplished by the implantation of very small GRIN lenses that can reach down even to ventral targets such as the amygdala. Small, LED-driven fluorescent microscopes can then be securely attached a mouse's skull and enable imaging of cellular activity, reported as changes in GCamp fluorescence in freely behaving animals. We have been able to perform these experiments and can reliably record the activity of hundreds of cells at a time, all with single cell resolution. The observed changes in circuit activity are then correlated to behavioral activity to better understand the in-vivo circuit dynamics that underlie patterns of mouse behavior in wild type and neurological disorder models. Additionally, the miniature microscope system can be paired with optogenetic or DREADD manipulations to control and visualize circuit dynamics simultaneously in-vivo, allowing for unprecedented insight into how specific circuitry is responsible for important mouse behaviors.

Finally, given the implications of our research regarding the power of disruptions in local circuit connectivity, we will investigate how different patterns and strengths of local circuits affect neuronal output using computational modeling. This in-silico approach will allow us to tweak many different parameters to model

the implications of the various activity patterns we observe in-vivo. Of particular interest will be the associations between connection probability and synaptic strength differences of separate cell types, as we observed in our SOM+ PTEN knockout mice, and the output characteristics of the circuits they constitute. We will be able to determine the effects of multiple different connectivity patterns in attempts to more accurately model the influences of different cell types to the output of important behavior-related circuitry.

REFERENCES

Abate-Shen, C., Banach-Petrosky, W. A., Sun, X., Economides, K. D., Desai, N., Gregg, J. P., Borowsky, A. D., Cardiff, R. D., & Shen, M. M. (2003). Nkx3.1; Pten Mutant Mice Develop Invasive Prostate Adenocarcinoma and Lymph Node Metastases. *Cancer Research*, *63*(14), 3886–3890.

Abrahams, B. S., & Geschwind, D. H. (2008). Advances in autism genetics: On the threshold of a new neurobiology. *Nature Reviews Genetics*, *9*(5), 341–355. https://doi.org/10.1038/nrg2346

Adolphs, R., Tranel, D., Damasio, H., & Damasio, A. (1994). Impaired recognition of emotion in facial expressions following bilateral damage to the human amygdala. *Nature*, *372*(6507), 669–672. https://doi.org/10.1038/372669a0

Ahrens, S., Wu, M. V., Furlan, A., Hwang, G.-R., Paik, R., Li, H., Penzo, M. A., Tollkuhn, J., & Li, B. (2018). A Central Extended Amygdala Circuit That Modulates Anxiety. *The Journal of Neuroscience*, *38*(24), 5567–5583. https://doi.org/10.1523/JNEUROSCI.0705-18.2018

Alarcón, M., Abrahams, B. S., Stone, J. L., Duvall, J. A., Perederiy, J. V., Bomar, J. M., Sebat, J., Wigler, M., Martin, C. L., Ledbetter, D. H., Nelson, S. F., Cantor, R. M., & Geschwind, D. H. (2008). Linkage, Association, and Gene-Expression Analyses Identify CNTNAP2 as an Autism-Susceptibility Gene. *The American Journal of*

Human Genetics, *82*(1), 150–159. https://doi.org/10.1016/j.ajhg.2007.09.005

Alvarez-Nuñez, F., Bussaglia, E., Mauricio, D., Ybarra, J., Vilar, M., Lerma, E., Leiva, A. de, & Matias-Guiu, X. (2006). PTEN Promoter Methylation in Sporadic Thyroid Carcinomas. *Thyroid*, *16*(1), 17–23. https://doi.org/10.1089/thy.2006.16.17

Anderson, A. K., & Phelps, E. A. (2001). Lesions of the human amygdala impair enhanced perception of emotionally salient events. *Nature*, *411*(6835), 305–309. https://doi.org/10.1038/35077083

Arendt, K. L., Royo, M., Fernández-Monreal, M., Knafo, S., Petrok, C. N., Martens, J. R., & Esteban, J. A. (2010). PIP3 controls synaptic function by maintaining AMPA receptor clustering at the postsynaptic membrane. *Nature Neuroscience*, *13*(1), 36–44. https://doi.org/10.1038/nn.2462

Arking, D. E., Cutler, D. J., Brune, C. W., Teslovich, T. M., West, K., Ikeda, M., Rea, A., Guy, M., Lin, S., Cook, E. H., & Chakravarti, A. (2008). A Common Genetic Variant in the Neurexin Superfamily Member CNTNAP2 Increases Familial Risk of Autism. *American Journal of Human Genetics*, *82*(1), 160–164. https://doi.org/10.1016/j.ajhg.2007.09.015

Asok, A., Draper, A., Hoffman, A. F., Schulkin, J., Lupica, C. R., & Rosen, J. B. (2018). Optogenetic silencing of a corticotropin-releasing factor pathway from the central amygdala to the bed nucleus of the stria terminalis disrupts sustained fear. *Molecular Psychiatry*, *23*(4), 914–922. https://doi.org/10.1038/mp.2017.79

Babaev, O., Piletti Chatain, C., & Krueger-Burg, D. (2018). Inhibition in the amygdala anxiety circuitry. *Experimental & Molecular Medicine*, *50*(4), 1–16. https://doi.org/10.1038/s12276-018-0063-8

Backman, S. A., Stambolic, V., Suzuki, A., Haight, J., Elia, A., Pretorius, J., Tsao, M.-S., Shannon, P., Bolon, B., Ivy, G. O., & Mak, T. W. (2001). Deletion of Pten in mouse brain causes seizures, ataxia and defects in soma size resembling Lhermitte-Duclos disease. *Nature Genetics*, *29*(4), 396–403. https://doi.org/10.1038/ng782

Bai, Z., Ye, Y., Chen, D., Shen, D., Xu, F., Cui, Z., & Wang, S. (2007). Homeoprotein Cdx2 and nuclear PTEN expression profiles are related to gastric cancer prognosis. *APMIS*, *115*(12), 1383–1390. https://doi.org/10.1111/j.1600-0463.2007.00654.x

Bailey, A., Le Couteur, A., Gottesman, I., Bolton, P., Simonoff, E., Yuzda, E., & Rutter, M. (1995). Autism as a strongly genetic disorder: Evidence from a British twin study. *Psychological Medicine*, *25*(1), 63–77. https://doi.org/10.1017/s0033291700028099

Baker, C. A., Elyada, Y. M., Parra, A., & Bolton, M. M. (2016). Cellular resolution circuit mapping with temporal-focused excitation of soma-targeted channelrhodopsin. *ELife*, *5*, e14193. https://doi.org/10.7554/eLife.14193

Baker, P., Piven, J., & Sato, Y. (1998). Autism and tuberous sclerosis complex: Prevalence and clinical features. *Journal of Autism and Developmental Disorders*, *28*(4), 279–285. https://doi.org/10.1023/a:1026004501631

Baohan, A., Ikrar, T., Tring, E., Xu, X., & Trachtenberg, J. T. (2016). Pten and EphB4 regulate the establishment of perisomatic inhibition in mouse visual cortex. *Nature Communications*, *7*. https://doi.org/10.1038/ncomms12829

Bartak, L., Rutter, M., & Cox, A. (1977). A comparative study of infantile autism and specific developmental receptive language disorders. III. Discriminant function analysis. *Journal of Autism and Childhood Schizophrenia*, *7*(4), 383–396. https://doi.org/10.1007/BF01540396

Belmonte, M. K., Cook, E. H., Anderson, G. M., Rubenstein, J. L. R., Greenough, W. T., Beckel-Mitchener, A., Courchesne, E., Boulanger, L. M., Powell, S. B., Levitt, P. R., Perry, E. K., Jiang, Y. H., DeLorey, T. M., & Tierney, E. (2004). Autism as a disorder of neural information processing: Directions for research and targets for therapy*. *Molecular Psychiatry*, *9*(7), 646–663. https://doi.org/10.1038/sj.mp.4001499

Betancur, C. (2011). Etiological heterogeneity in autism spectrum disorders: More than 100 genetic and genomic disorders and still counting. *Brain Research*, *1380*, 42–77. https://doi.org/10.1016/j.brainres.2010.11.078

Boeckers, T. M., Bockmann, J., Kreutz, M. R., & Gundelfinger, E. D. (2002). ProSAP/Shank proteins – a family of higher order organizing molecules of the postsynaptic density with an emerging role in human neurological disease. *Journal of Neurochemistry*, *81*(5), 903–910. https://doi.org/10.1046/j.1471-4159.2002.00931.x

Bowers, M. E., & Ressler, K. J. (2015). Interaction between the Cholecystokinin and Endogenous Cannabinoid Systems in Cued Fear Expression and Extinction

Retention. *Neuropsychopharmacology*, *40*(3), 688–700. https://doi.org/10.1038/npp.2014.225

Boyden, E. S., Zhang, F., Bamberg, E., Nagel, G., & Deisseroth, K. (2005). Millisecond-timescale, genetically targeted optical control of neural activity. *Nature Neuroscience*, *8*(9), 1263–1268. https://doi.org/10.1038/nn1525

Braff, D., Stone, C., Callaway, E., Geyer, M., Glick, I., & Bali, L. (1978). Prestimulus Effects on Human Startle Reflex in Normals and Schizophrenics. *Psychophysiology*, *15*(4), 339–343. https://doi.org/10.1111/j.1469-8986.1978.tb01390.x

Bronisz, A., Godlewski, J., Wallace, J. A., Merchant, A. S., Nowicki, M. O., Mathsyaraja, H., Srinivasan, R., Trimboli, A. J., Martin, C. K., Li, F., Yu, L., Fernandez, S. A., Pécot, T., Rosol, T. J., Cory, S., Hallett, M., Park, M., Piper, M. G., Marsh, C. B., … Ostrowski, M. C. (2012). Reprogramming of the tumour microenvironment by stromal PTEN-regulated miR-320. *Nature Cell Biology*, *14*(2), 159–167. https://doi.org/10.1038/ncb2396

Brown, S., & Sharpey-Schafer, E. A. (1888). XI. An investigation into the functions of the occipital and temporal lobes of the monkey's brain. *Philosophical Transactions of the Royal Society of London. (B.)*, *179*, 303–327. https://doi.org/10.1098/rstb.1888.0011

Butler, M. G., Dasouki, M. J., Zhou, X.-P., Talebizadeh, Z., Brown, M., Takahashi, T. N., Miles, J. H., Wang, C. H., Stratton, R., Pilarski, R., & Eng, C. (2005). Subset of individuals with autism spectrum disorders and extreme macrocephaly associated with germline PTEN tumour suppressor gene mutations. *Journal*

of Medical Genetics, *42*(4), 318–321. https://doi.org/10.1136/jmg.2004.024646

Cai, H., Haubensak, W., Anthony, T. E., & Anderson, D. J. (2014). Central amygdala PKC-δ + neurons mediate the influence of multiple anorexigenic signals. *Nature Neuroscience*, *17*(9), 1240–1248. https://doi.org/10.1038/nn.3767

Cairns, P., Okami, K., Halachmi, S., Halachmi, N., Esteller, M., Herman, J. G., Jen, J., Isaacs, W. B., Bova, G. S., & Sidransky, D. (1997). Frequent Inactivation of PTEN/MMAC1 in Primary Prostate Cancer. *Cancer Research*, *57*(22), 4997–5000.

Careaga, M., Murai, T., & Bauman, M. D. (2017). Maternal immune activation and autism spectrum disorder: From rodents to nonhuman and human primates. *Biological Psychiatry*, *81*(5), 391–401. https://doi.org/10.1016/j.biopsych.2016.10.020

Carracedo, A., Ma, L., Teruya-Feldstein, J., Rojo, F., Salmena, L., Alimonti, A., Egia, A., Sasaki, A. T., Thomas, G., Kozma, S. C., Papa, A., Nardella, C., Cantley, L. C., Baselga, J., & Pandolfi, P. P. (2008). Inhibition of mTORC1 leads to MAPK pathway activation through a PI3K-dependent feedback loop in human cancer. *The Journal of Clinical Investigation*, *118*(9), 3065–3074. https://doi.org/10.1172/JCI34739

Chen, L., & Toth, M. (2001). Fragile X mice develop sensory hyperreactivity to auditory stimuli. *Neuroscience*, *103*(4), 1043–1050. https://doi.org/10.1016/S0306-4522(01)00036-7

Ciocchi, S., Herry, C., Grenier, F., Wolff, S. B. E., Letzkus, J. J., Vlachos, I., Ehrlich, I., Sprengel, R., Deisseroth, K., Stadler, M. B., Müller, C., & Lüthi, A. (2010). Encoding of conditioned fear in central amygdala inhibitory circuits. *Nature*, *468*(7321), 277–282. https://doi.org/10.1038/nature09559

Clipperton-Allen, A. E., & Page, D. T. (2014). Pten haploinsufficient mice show broad brain overgrowth but selective impairments in autism-relevant behavioral tests. *Human Molecular Genetics*, *23*(13), 3490–3505. https://doi.org/10.1093/hmg/ddu057

Crawley, J. N. (2007). Mouse Behavioral Assays Relevant to the Symptoms of Autism*. *Brain Pathology*, *17*(4), 448–459. https://doi.org/10.1111/j.1750-3639.2007.00096.x

Dahia, P. L. M., Marsh, D. J., Zheng, Z., Zedenius, J., Komminoth, P., Frisk, T., Wallin, G., Parsons, R., Longy, M., Larsson, C., & Eng, C. (1997). Somatic Deletions and Mutations in the Cowden Disease Gene, PTEN, in Sporadic Thyroid Tumors. *Cancer Research*, *57*(21), 4710–4713.

Davis, M., Walker, D. L., & Lee, Y. (1997). Amygdala and bed nucleus of the stria terminalis: Differential roles in fear and anxiety measured with the acoustic startle reflex. *Philosophical Transactions of the Royal Society B: Biological Sciences*, *352*(1362), 1675–1687.

De Oca, B. M., DeCola, J. P., Maren, S., & Fanselow, M. S. (1998). Distinct Regions of the Periaqueductal Gray Are Involved in the Acquisition and Expression of Defensive Responses. *The Journal of Neuroscience*, *18*(9), 3426–3432. https://doi.org/10.1523/JNEUROSCI.18-09-03426.1998

De Rubeis, S., He, X., Goldberg, A. P., Poultney, C. S., Samocha, K., Ercument Cicek, A., Kou, Y., Liu, L., Fromer, M., Walker, S., Singh, T., Klei, L., Kosmicki, J., Fu, S.-C., Aleksic, B., Biscaldi, M., Bolton, P. F., Brownfeld, J. M., Cai, J., … Buxbaum, J. D. (2014). Synaptic, transcriptional and chromatin genes disrupted in autism. *Nature*, *515*(7526), 209–215. https://doi.org/10.1038/nature13772

Di Cristofano, A., De Acetis, M., Koff, A., Cordon-Cardo, C., & Pandolfi, P. P. (2001). Pten and p27 KIP1 cooperate in prostate cancer tumor suppression in the mouse. *Nature Genetics*, *27*(2), 222–224. https://doi.org/10.1038/84879

Di Cristofano, A., Pesce, B., Cordon-Cardo, C., & Pandolfi, P. P. (1998). Pten is essential for embryonic development and tumour suppression. *Nature Genetics*, *19*(4), 348–355. https://doi.org/10.1038/1235

Dong-Dong, L., Xi-Ran, Z., & Xiang-Rong, C. (2003). Expression and significance of new tumor suppressor gene PTEN in primary liver cancer. *Journal of Cellular and Molecular Medicine*, *7*(1), 67–71. https://doi.org/10.1111/j.1582-4934.2003.tb00204.x

Dumont, É. C., Martina, M., Samson, R. D., Drolet, G., & Paré, D. (2002). Physiological properties of central amygdala neurons: Species differences. *European Journal of Neuroscience*, *15*(3), 545–552. https://doi.org/10.1046/j.0953-816x.2001.01879.x

Duvarci, S., & Pare, D. (2014). Amygdala Microcircuits Controlling Learned Fear. *Neuron*, *82*(5), 966–980. https://doi.org/10.1016/j.neuron.2014.04.042

Ehrlich, I., Humeau, Y., Grenier, F., Ciocchi, S., Herry, C., & Lüthi, A. (2009). Amygdala Inhibitory Circuits and the Control of Fear Memory. *Neuron*, *62*(6), 757–771. https://doi.org/10.1016/j.neuron.2009.05.026

Fadok, J. P., Markovic, M., Tovote, P., & Lüthi, A. (2018). New perspectives on central amygdala function. *Current Opinion in Neurobiology*, *49*, 141–147. https://doi.org/10.1016/j.conb.2018.02.009

Fang, M., Shen, Z., Huang, S., Zhao, L., Chen, S., Mak, T. W., & Wang, X. (2010). The ER UDPase ENTPD5 Promotes Protein N-Glycosylation, the Warburg Effect, and Proliferation in the PTEN Pathway. *Cell*, *143*(5), 711–724. https://doi.org/10.1016/j.cell.2010.10.010

Fatt, P., & Katz, B. (1952). Spontaneous subthreshold activity at motor nerve endings. *The Journal of Physiology*, *117*(1), 109–128.

Felix-Ortiz, A. C., Beyeler, A., Seo, C., Leppla, C. A., Wildes, C. P., & Tye, K. M. (2013). BLA to vHPC Inputs Modulate Anxiety-Related Behaviors. *Neuron*, *79*(4), 658–664. https://doi.org/10.1016/j.neuron.2013.06.016

Felix-Ortiz, A. C., Burgos-Robles, A., Bhagat, N. D., Leppla, C. A., & Tye, K. M. (2016). Bidirectional modulation of anxiety-related and social behaviors by amygdala projections to the medial prefrontal cortex. *Neuroscience*, *321*, 197–209. https://doi.org/10.1016/j.neuroscience.2015.07.041

Fombonne, E., Quirke, S., & Hagen, A. (2009). Prevalence and Interpretation of Recent Trends in Rates of Pervasive Developmental Disorders. *McGill Journal of Medicine : MJM*, *12*(2). https://www.ncbi.nlm.nih.gov/pmc/articles/PMC2997266/

Fombonne, E., Rogé, B., Claverie, J., Courty, S., & Frémolle, J. (1999). Microcephaly and macrocephaly in autism. *Journal of Autism and Developmental Disorders*, *29*(2), 113–119. https://doi.org/10.1023/a:1023036509476

Fox, A. S., Oler, J. A., Tromp, D. P. M., Fudge, J. L., & Kalin, N. H. (2015). Extending the amygdala in theories of threat processing. *Trends in Neurosciences*, *38*(5), 319–329. https://doi.org/10.1016/j.tins.2015.03.002

Fraser, M. M., Bayazitov, I. T., Zakharenko, S. S., & Baker, S. J. (2008). Pten deficiency in brain causes defects in synaptic structure, transmission and plasticity, and myelination abnormalities. *Neuroscience*, *151*(2), 476–488. https://doi.org/10.1016/j.neuroscience.2007.10.048

Fraser, M. M., Zhu, X., Kwon, C.-H., Uhlmann, E. J., Gutmann, D. H., & Baker, S. J. (2004). Pten Loss Causes Hypertrophy and Increased Proliferation of Astrocytes In vivo. *Cancer Research*, *64*(21), 7773–7779.

Freund, T. F., & Katona, I. (2007). Perisomatic Inhibition. *Neuron*, *56*(1), 33–42. https://doi.org/10.1016/j.neuron.2007.09.012

Gillberg and, C., & Billstedt, E. (2000). Autism and Asperger syndrome: Coexistence with other clinical disorders. *Acta Psychiatrica Scandinavica*, *102*(5), 321–330. https://doi.org/10.1034/j.1600-0447.2000.102005321.x

Gillberg, C., & Billstedt, E. (2000). Autism and Asperger syndrome: Coexistence with other clinical disorders. *Acta Psychiatrica Scandinavica*, *102*(5), 321–330. https://doi.org/10.1034/j.1600-0447.2000.102005321.x

Gillott, A., Furniss, F., & Walter, A. (2001). Anxiety in High-Functioning Children with Autism. *Autism*, *5*(3), 277–286. https://doi.org/10.1177/1362361301005003005

Goffin, A., Hoefsloot, L. H., Bosgoed, E., Swillen, A., & Fryns, J.-P. (2001). PTEN mutation in a family with Cowden syndrome and autism. *American Journal of Medical Genetics*, *105*(6), 521–524. https://doi.org/10.1002/ajmg.1477

Gonchar, Y., Turney, S., Price, J. L., & Burkhalter, A. (2002). Axo-axonic synapses formed by somatostatin-expressing GABAergic neurons in rat and monkey visual cortex. *Journal of Comparative Neurology*, *443*(1), 1–14. https://doi.org/10.1002/cne.1425

Goorden, S. M. I., Woerden, G. M. van, Weerd, L. van der, Cheadle, J. P., & Elgersma, Y. (2007). Cognitive deficits in Tsc1+/−mice in the absence of cerebral lesions and seizures. *Annals of Neurology*, *62*(6), 648–655. https://doi.org/10.1002/ana.21317

Grønbæk, K. (1998). Alterations of the MMAC1/PTEN Gene in Lymphoid Malignancies. *Blood*, *91*(11), 4388–4390. https://doi.org/10.1182/blood.V91.11.4388

Guigon, C., Zhao, L., Willingham, M., & Cheng, S.-Y. (2009). PTEN deficiency accelerates tumour progression in a mouse model of thyroid cancer. *Oncogene*, *28*(4), 509–517. https://doi.org/10.1038/onc.2008.407

Guo, C., Wang, C., He, T., Yu, B., Li, M., Zhao, C., Yuan, Y., & Chen, H. (2020). The effect of mGlu2/3 receptors on synaptic activities to different types of GABAergic

interneurons in the anterior cingulate cortex. *Neuropharmacology*, *175*, 108180. https://doi.org/10.1016/j.neuropharm.2020.108180

Gutierrez, A., Sanda, T., Grebliunaite, R., Carracedo, A., Salmena, L., Ahn, Y., Dahlberg, S., Neuberg, D., Moreau, L. A., Winter, S. S., Larson, R., Zhang, J., Protopopov, A., Chin, L., Pandolfi, P. P., Silverman, L. B., Hunger, S. P., Sallan, S. E., & Look, A. T. (2009). High frequency of PTEN, PI3K, and AKT abnormalities in T-cell acute lymphoblastic leukemia. *Blood*, *114*(3), 647–650. https://doi.org/10.1182/blood-2009-02-206722

Gutilla, E. A., Buyukozturk, M. M., & Steward, O. (2016). Long-term consequences of conditional genetic deletion of PTEN in the sensorimotor cortex of neonatal mice. *Experimental Neurology*, *279*, 27–39. https://doi.org/10.1016/j.expneurol.2016.02.013

Halabisky, B., Shen, F., Huguenard, J. R., & Prince, D. A. (2006). Electrophysiological Classification of Somatostatin-Positive Interneurons in Mouse Sensorimotor Cortex. *Journal of Neurophysiology*, *96*(2), 834–845. https://doi.org/10.1152/jn.01079.2005

Hatton, D. D., Sideris, J., Skinner, M., Mankowski, J., Bailey, D. B., Roberts, J., & Mirrett, P. (2006). Autistic behavior in children with fragile X syndrome: Prevalence, stability, and the impact of FMRP. *American Journal of Medical Genetics Part A*, *140A*(17), 1804–1813. https://doi.org/10.1002/ajmg.a.31286

Haubensak, W., Kunwar, P. S., Cai, H., Ciocchi, S., Wall, N. R., Ponnusamy, R., Biag, J., Dong, H.-W., Deisseroth, K., Callaway, E. M., Fanselow, M. S., Lüthi, A., & Anderson, D. J. (2010). Genetic dissection of an amygdala microcircuit that

gates conditioned fear. *Nature*, *468*(7321), 270–276. https://doi.org/10.1038/nature09553

Hioki, H., Okamoto, S., Konno, M., Kameda, H., Sohn, J., Kuramoto, E., Fujiyama, F., & Kaneko, T. (2013). Cell Type-Specific Inhibitory Inputs to Dendritic and Somatic Compartments of Parvalbumin-Expressing Neocortical Interneuron. *Journal of Neuroscience*, *33*(2), 544–555. https://doi.org/10.1523/JNEUROSCI.2255-12.2013

Hollander, E., King, A., Delaney, K., Smith, C. J., & Silverman, J. M. (2003). Obsessive–compulsive behaviors in parents of multiplex autism families. *Psychiatry Research*, *117*(1), 11–16. https://doi.org/10.1016/S0165-1781(02)00304-9

Hunt, S., Sun, Y., Kucukdereli, H., Klein, R., & Sah, P. (2017). Intrinsic Circuits in the Lateral Central Amygdala. *ENeuro*, *4*(1). https://doi.org/10.1523/ENEURO.0367-16.2017

Huse, J. T., Brennan, C., Hambardzumyan, D., Wee, B., Pena, J., Rouhanifard, S. H., Sohn-Lee, C., Sage, C. le, Agami, R., Tuschl, T., & Holland, E. C. (2009). The PTEN-regulating microRNA miR-26a is amplified in high-grade glioma and facilitates gliomagenesis in vivo. *Genes & Development*, *23*(11), 1327–1337. https://doi.org/10.1101/gad.1777409

Inoki, K., Li, Y., Zhu, T., Wu, J., & Guan, K.-L. (2002). TSC2 is phosphorylated and inhibited by Akt and suppresses mTOR signalling. *Nature Cell Biology*, *4*(9), 648–657. https://doi.org/10.1038/ncb839

Isoardi, N. A., Bertotto, M. E., Martijena, I. D., Molina, V. A., & Carrer, H. F. (2007). Lack of feedback inhibition on rat basolateral amygdala following stress or

withdrawal from sedative-hypnotic drugs. *European Journal of Neuroscience*, *26*(4), 1036–1044. https://doi.org/10.1111/j.1460-9568.2007.05714.x

Janak, P. H., & Tye, K. M. (2015). From circuits to behaviour in the amygdala. *Nature*, *517*(7534), 284–292. https://doi.org/10.1038/nature14188

Kawaguchi, Y., & Kubota, Y. (1996). Physiological and morphological identification of somatostatin- or vasoactive intestinal polypeptide-containing cells among GABAergic cell subtypes in rat frontal cortex. *Journal of Neuroscience*, *16*(8), 2701–2715. https://doi.org/10.1523/JNEUROSCI.16-08-02701.1996

Kepecs, A., & Fishell, G. (2014). Interneuron cell types are fit to function. *Nature*, *505*(7483), 318–326. https://doi.org/10.1038/nature12983

Kinkade, C. W., Castillo-Martin, M., Puzio-Kuter, A., Yan, J., Foster, T. H., Gao, H., Sun, Y., Ouyang, X., Gerald, W. L., Cordon-Cardo, C., & Abate-Shen, C. (2008). Targeting AKT/mTOR and ERK MAPK signaling inhibits hormone-refractory prostate cancer in a preclinical mouse model. *The Journal of Clinical Investigation*, *118*(9), 3051–3064. https://doi.org/10.1172/JCI34764

Kondrakiewicz, K., Kostecki, M., Szadzińska, W., & Knapska, E. (2019). Ecological validity of social interaction tests in rats and mice. *Genes, Brain and Behavior*, *18*(1), e12525. https://doi.org/10.1111/gbb.12525

Krabbe, S., Gründemann, J., & Lüthi, A. (2018). Amygdala Inhibitory Circuits Regulate Associative Fear Conditioning. *Biological Psychiatry*, *83*(10), 800–809. https://doi.org/10.1016/j.biopsych.2017.10.006

Kvitsiani, D., Ranade, S., Hangya, B., Taniguchi, H., Huang, J. Z., & Kepecs, A. (2013). Distinct behavioural and network correlates of two interneuron types in

prefrontal cortex. *Nature*, *498*(7454), 363–366. https://doi.org/10.1038/nature12176

Kwon, C.-H., Luikart, B. W., Powell, C. M., Zhou, J., Matheny, S. A., Zhang, W., Li, Y., Baker, S. J., & Parada, L. F. (2006). Pten Regulates Neuronal Arborization and Social Interaction in Mice. *Neuron*, *50*(3), 377–388. https://doi.org/10.1016/j.neuron.2006.03.023

Kwon, C.-H., Zhu, X., Zhang, J., Knoop, L. L., Tharp, R., Smeyne, R. J., Eberhart, C. G., Burger, P. C., & Baker, S. J. (2001). Pten regulates neuronal soma size: A mouse model of Lhermitte-Duclos disease. *Nature Genetics*, *29*(4), 404–411. https://doi.org/10.1038/ng781

Lainhart, J. E., Piven, J., Wzorek, M., Landa, R., Santangelo, S. L., Coon, H., & Folstein, S. E. (1997). Macrocephaly in Children and Adults With Autism. *Journal of the American Academy of Child & Adolescent Psychiatry*, *36*(2), 282–290. https://doi.org/10.1097/00004583-199702000-00019

Lakunina, A. A., Nardoci, M. B., Ahmadian, Y., & Jaramillo, S. (2020). Somatostatin-Expressing Interneurons in the Auditory Cortex Mediate Sustained Suppression by Spectral Surround. *The Journal of Neuroscience*, *40*(18), 3564–3575. https://doi.org/10.1523/JNEUROSCI.1735-19.2020

LeDoux, J., Cicchetti, P., Xagoraris, A., & Romanski, L. (1990). The lateral amygdaloid nucleus: Sensory interface of the amygdala in fear conditioning. *The Journal of Neuroscience*, *10*(4), 1062–1069. https://doi.org/10.1523/JNEUROSCI.10-04-01062.1990

LeDoux, J., Iwata, J., Cicchetti, P., & Reis, D. (1988). Different projections of the central amygdaloid nucleus mediate autonomic and behavioral correlates of conditioned fear. *The Journal of Neuroscience*, *8*(7), 2517–2529. https://doi.org/10.1523/JNEUROSCI.08-07-02517.1988

Lee, J.-O., Yang, H., Georgescu, M.-M., Cristofano, A. D., Maehama, T., Shi, Y., Dixon, J. E., Pandolfi, P., & Pavletich, N. P. (1999). Crystal Structure of the PTEN Tumor Suppressor: Implications for Its Phosphoinositide Phosphatase Activity and Membrane Association. *Cell*, *99*(3), 323–334. https://doi.org/10.1016/S0092-8674(00)81663-3

Lee, S., Kruglikov, I., Huang, Z. J., Fishell, G., & Rudy, B. (2013). A disinhibitory circuit mediates motor integration in the somatosensory cortex. *Nature Neuroscience*, *16*(11), 1662–1670. https://doi.org/10.1038/nn.3544

Letzkus, J. J., Wolff, S. B. E., Meyer, E. M. M., Tovote, P., Courtin, J., Herry, C., & Lüthi, A. (2011). A disinhibitory microcircuit for associative fear learning in the auditory cortex. *Nature*, *480*(7377), 331–335. https://doi.org/10.1038/nature10674

Lewis, D. A., Hashimoto, T., & Volk, D. W. (2005). Cortical inhibitory neurons and schizophrenia. *Nature Reviews Neuroscience*, *6*(4), 312–324. https://doi.org/10.1038/nrn1648

Li, D.-M., & Sun, H. (1997). TEP1, Encoded by a Candidate Tumor Suppressor Locus, Is a Novel Protein Tyrosine Phosphatase Regulated by Transforming Growth Factor β. *Cancer Research*, *57*(11), 2124–2129.

Li, G., Robinson, G. W., Lesche, R., Martinez-Diaz, H., Jiang, Z., Rozengurt, N., Wagner, K.-U., Wu, D.-C., Lane, T. F., Liu, X., Hennighausen, L., & Wu, H. (2002). Conditional loss of PTEN leads to precocious development and neoplasia in the mammary gland. *Development (Cambridge, England)*, *129*(17), 4159–4170.

Li, H., Penzo, M. A., Taniguchi, H., Kopec, C. D., Huang, Z. J., & Li, B. (2013). Experience-dependent modification of a central amygdala fear circuit. *Nature Neuroscience*, *16*(3), 332–339. https://doi.org/10.1038/nn.3322

Li, J., Yen, C., Liaw, D., Podsypanina, K., Bose, S., Wang, S. I., Puc, J., Miliaresis, C., Rodgers, L., McCombie, R., Bigner, S. H., Giovanella, B. C., Ittmann, M., Tycko, B., Hibshoosh, H., Wigler, M. H., & Parsons, R. (1997). PTEN, a Putative Protein Tyrosine Phosphatase Gene Mutated in Human Brain, Breast, and Prostate Cancer. *Science*, *275*(5308), 1943–1947. https://doi.org/10.1126/science.275.5308.1943

Liaw, D., Marsh, D. J., Li, J., Dahia, P. L. M., Wang, S. I., Zheng, Z., Bose, S., Call, K. M., Tsou, H. C., Peacoke, M., Eng, C., & Parsons, R. (1997). Germline mutations of the PTEN gene in Cowden disease, an inherited breast and thyroid cancer syndrome. *Nature Genetics*, *16*(1), 64–67. https://doi.org/10.1038/ng0597-64

Lindley, P., Marks, I., Philpott, R., & Snowden, J. (1977). Treatment of Obsessive-Compulsive Neurosis with History of Childhood Autism. *The British Journal of Psychiatry*, *130*(6), 592–597. https://doi.org/10.1192/bjp.130.6.592

Liu, K., Lu, Y., Lee, J. K., Samara, R., Willenberg, R., Sears-Kraxberger, I., Tedeschi, A., Park, K. K., Jin, D., Cai, B., Xu, B., Connolly, L., Steward, O., Zheng, B., & He, Z. (2010). PTEN deletion enhances the regenerative ability of adult corticospinal neurons. *Nature Neuroscience*, *13*(9), 1075–1081. https://doi.org/10.1038/nn.2603

Luikart, B. W., Schnell, E., Washburn, E. K., Bensen, A. L., Tovar, K. R., & Westbrook, G. L. (2011). Pten Knockdown In Vivo Increases Excitatory Drive onto Dentate Granule Cells. *Journal of Neuroscience*, *31*(11), 4345–4354. https://doi.org/10.1523/JNEUROSCI.0061-11.2011

Madsen, K. M., Hviid, A., Vestergaard, M., Schendel, D., Wohlfahrt, J., Thorsen, P., Olsen, J., & Melbye, M. (2002). A population-based study of measles, mumps, and rubella vaccination and autism. *The New England Journal of Medicine*, *347*(19), 1477–1482. https://doi.org/10.1056/NEJMoa021134

Maehama, T., & Dixon, J. E. (1998). The tumor suppressor, PTEN/MMAC1, dephosphorylates the lipid second messenger, phosphatidylinositol 3,4,5-trisphosphate. *The Journal of Biological Chemistry*, *273*(22), 13375–13378. https://doi.org/10.1074/jbc.273.22.13375

Maenner, M. J. (2020). Prevalence of Autism Spectrum Disorder Among Children Aged 8 Years—Autism and Developmental Disabilities Monitoring Network, 11 Sites, United States, 2016. *MMWR. Surveillance Summaries*, *69*. https://doi.org/10.15585/mmwr.ss6904a1

Manning, B. D., & Cantley, L. C. (2007). AKT/PKB Signaling: Navigating Downstream. *Cell*, *129*(7), 1261–1274. https://doi.org/10.1016/j.cell.2007.06.009

Manning, B. D., Tee, A. R., Logsdon, M. N., Blenis, J., & Cantley, L. C. (2002). Identification of the Tuberous Sclerosis Complex-2 Tumor Suppressor Gene Product Tuberin as a Target of the Phosphoinositide 3-Kinase/Akt Pathway. *Molecular Cell*, *10*(1), 151–162. https://doi.org/10.1016/S1097-2765(02)00568-3

Marek, R., Jin, J., Goode, T. D., Giustino, T. F., Wang, Q., Acca, G. M., Holehonnur, R., Ploski, J. E., Fitzgerald, P. J., Lynagh, T., Lynch, J. W., Maren, S., & Sah, P. (2018). Hippocampus-driven feed-forward inhibition of the prefrontal cortex mediates relapse of extinguished fear. *Nature Neuroscience*, *21*(3), 384–392. https://doi.org/10.1038/s41593-018-0073-9

Markram, K., & Markram, H. (2010). The Intense World Theory – A Unifying Theory of the Neurobiology of Autism. *Frontiers in Human Neuroscience*, *4*. https://doi.org/10.3389/fnhum.2010.00224

Marsh, D. J., Coulon, V., Lunetta, K. L., Rocca-Serra, P., Dahia, P. L. M., Zheng, Z., Liaw, D., Caron, S., Duboué, B., Lin, A. Y., Richardson, A.-L., Bonnetblanc, J.-M., Bressieux, J.-M., Cabarrot-Moreau, A., Chompret, A., Demange, L., Eeles, R. A., Yahanda, A. M., Fearon, E. R., … Eng, C. (1998). Mutation Spectrum and Genotype-Phenotype Analyses in Cowden Disease and Bannayan-Zonana Syndrome, Two Hamartoma Syndromes With Germline PTEN Mutation. *Human Molecular Genetics*, *7*(3), 507–515. https://doi.org/10.1093/hmg/7.3.507

Marsh, D. J., Dahia, P. L., Caron, S., Kum, J. B., Frayling, I. M., Tomlinson, I. P., Hughes, K. S., Eeles, R. A., Hodgson, S. V., Murday, V. A., Houlston, R., & Eng, C. (1998).

Germline PTEN mutations in Cowden syndrome-like families. *Journal of Medical Genetics*, *35*(11), 881–885.

Marsh, D. J., Dahia, P. L. M., Zheng, Z., Liaw, D., Parsons, R., Gorlin, R. J., & Eng, C. (1997). Germline mutations in PTEN are present in Bannayan-Zonana syndrome. *Nature Genetics*, *16*(4), 333–334. https://doi.org/10.1038/ng0897-333

McBride, K. L., Varga, E. A., Pastore, M. T., Prior, T. W., Manickam, K., Atkin, J. F., & Herman, G. E. (2010). Confirmation study of PTEN mutations among individuals with autism or developmental delays/mental retardation and macrocephaly. *Autism Research*, *3*(3), 137–141. https://doi.org/10.1002/aur.132

McCary, L. M., & Roberts, J. E. (2013). Early identification of autism in fragile X syndrome: A review. *Journal of Intellectual Disability Research : JIDR*, *57*(9), 803–814. https://doi.org/10.1111/j.1365-2788.2012.01609.x

Megías, M., Emri, Z., Freund, T. F., & Gulyás, A. I. (2001). Total number and distribution of inhibitory and excitatory synapses on hippocampal CA1 pyramidal cells. *Neuroscience*, *102*(3), 527–540. https://doi.org/10.1016/S0306-4522(00)00496-6

Mei, Y., Monteiro, P., Zhou, Y., Kim, J.-A., Gao, X., Fu, Z., & Feng, G. (2016). Adult restoration of Shank3 expression rescues selective autistic-like phenotypes. *Nature*, *530*(7591), 481–484. https://doi.org/10.1038/nature16971

Morgan, J. T., Barger, N., Amaral, D. G., & Schumann, C. M. (2014). Stereological Study of Amygdala Glial Populations in Adolescents and Adults with Autism

Spectrum Disorder. *PLoS ONE*, *9*(10), e110356. https://doi.org/10.1371/journal.pone.0110356

Muller, J. F., Mascagni, F., & McDonald, A. J. (2007). Postsynaptic targets of somatostatin-containing interneurons in the rat basolateral amygdala. *Journal of Comparative Neurology*, *500*(3), 513–529. https://doi.org/10.1002/cne.21185

Nadler, J. J., Moy, S. S., Dold, G., Simmons, N., Perez, A., Young, N. B., Barbaro, R. P., Piven, J., Magnuson, T. R., & Crawley, J. N. (2004). Automated apparatus for quantitation of social approach behaviors in mice. *Genes, Brain and Behavior*, *3*(5), 303–314. https://doi.org/10.1111/j.1601-183X.2004.00071.x

Nagel, G., Brauner, M., Liewald, J. F., Adeishvili, N., Bamberg, E., & Gottschalk, A. (2005). Light Activation of Channelrhodopsin-2 in Excitable Cells of Caenorhabditis elegans Triggers Rapid Behavioral Responses. *Current Biology*, *15*(24), 2279–2284. https://doi.org/10.1016/j.cub.2005.11.032

Nagel, G., Szellas, T., Huhn, W., Kateriya, S., Adeishvili, N., Berthold, P., Ollig, D., Hegemann, P., & Bamberg, E. (2003). Channelrhodopsin-2, a directly light-gated cation-selective membrane channel. *Proceedings of the National Academy of Sciences of the United States of America*, *100*(24), 13940–13945. https://doi.org/10.1073/pnas.1936192100

Nelen, M. R., van Staveren, W. C. G., Peeters, E. A. J., Ben Hassel, M., Gorlin, R. J., Hamm, H., Lindboe, C. F., Fryns, J.-P., Sijmons, R. H., Woods, D. G., Mariman, E. C. M., Padberg, G. W., & Kremer, H. (1997). Germline Mutations in the

PTEN/MMAC1 Gene in Patients With Cowden Disease. *Human Molecular Genetics*, *6*(8), 1383–1387. https://doi.org/10.1093/hmg/6.8.1383

Nelson, K. B., & Bauman, M. L. (2003). Thimerosal and Autism? *Pediatrics*, *111*(3), 674–679. https://doi.org/10.1542/peds.111.3.674

Nicolini, C., & Fahnestock, M. (2018). The valproic acid-induced rodent model of autism. *Experimental Neurology*, *299*, 217–227. https://doi.org/10.1016/j.expneurol.2017.04.017

Nienborg, H., Hasenstaub, A., Nauhaus, I., Taniguchi, H., Huang, Z. J., & Callaway, E. M. (2013). Contrast Dependence and Differential Contributions from Somatostatin- and Parvalbumin-Expressing Neurons to Spatial Integration in Mouse V1. *The Journal of Neuroscience*, *33*(27), 11145–11154. https://doi.org/10.1523/JNEUROSCI.5320-12.2013

Ning, K., Pei, L., Liao, M., Liu, B., Zhang, Y., Jiang, W., Mielke, J. G., Li, L., Chen, Y., El-Hayek, Y. H., Fehlings, M. G., Zhang, X., Liu, F., Eubanks, J., & Wan, Q. (2004). Dual Neuroprotective Signaling Mediated by Downregulating Two Distinct Phosphatase Activities of PTEN. *Journal of Neuroscience*, *24*(16), 4052–4060. https://doi.org/10.1523/JNEUROSCI.5449-03.2004

O'Roak, B. J., Deriziotis, P., Lee, C., Vives, L., Schwartz, J. J., Girirajan, S., Karakoc, E., MacKenzie, A. P., Ng, S. B., Baker, C., Rieder, M. J., Nickerson, D. A., Bernier, R., Fisher, S. E., Shendure, J., & Eichler, E. E. (2011). Exome sequencing in sporadic autism spectrum disorders identifies severe de novo mutations. *Nature Genetics*, *43*(6), 585–589. https://doi.org/10.1038/ng.835

O'Roak, B. J., & State, M. W. (2008). Autism genetics: Strategies, challenges, and opportunities. *Autism Research*, *1*(1), 4–17. https://doi.org/10.1002/aur.3

O'Roak, B. J., Vives, L., Fu, W., Egertson, J. D., Stanaway, I. B., Phelps, I. G., Carvill, G., Kumar, A., Lee, C., Ankenman, K., Munson, J., Hiatt, J. B., Turner, E. H., Levy, R., O'Day, D. R., Krumm, N., Coe, B. P., Martin, B. K., Borenstein, E., … Shendure, J. (2012). Multiplex Targeted Sequencing Identifies Recurrently Mutated Genes in Autism Spectrum Disorders. *Science*, *338*(6114), 1619–1622. https://doi.org/10.1126/science.1227764

Papp, E., Leinekugel, X., Henze, D. A., Lee, J., & Buzsáki, G. (2001). The apical shaft of CA1 pyramidal cells is under GABAergic interneuronal control. *Neuroscience*, *102*(4), 715–721. https://doi.org/10.1016/S0306-4522(00)00584-4

Parisi, M., DINULOS, M. B., LEPPIG, K., SYBERT, V., ENG, C., & HUDGINS, L. (2001). The spectrum and evolution of phenotypic findings in PTEN mutation positive cases of Bannayan-Riley-Ruvalcaba syndrome. *Journal of Medical Genetics*, *38*(1), 52–58. https://doi.org/10.1136/jmg.38.1.52

Park, K. K., Liu, K., Hu, Y., Smith, P. D., Wang, C., Cai, B., Xu, B., Connolly, L., Kramvis, I., Sahin, M., & He, Z. (2008). Promoting Axon Regeneration in the Adult CNS by Modulation of the PTEN/mTOR Pathway. *Science*, *322*(5903), 963–966. https://doi.org/10.1126/science.1161566

Patterson, P. H. (2011). MATERNAL INFECTION AND IMMUNE INVOLVEMENT IN AUTISM. *Trends in Molecular Medicine*, *17*(7), 389–394. https://doi.org/10.1016/j.molmed.2011.03.001

Peça, J., Feliciano, C., Ting, J. T., Wang, W., Wells, M. F., Venkatraman, T. N., Lascola, C. D., Fu, Z., & Feng, G. (2011). Shank3 mutant mice display autistic-like behaviours and striatal dysfunction. *Nature*, *472*(7344), 437–442. https://doi.org/10.1038/nature09965

Peñagarikano, O., Abrahams, B. S., Herman, E. I., Winden, K. D., Gdalyahu, A., Dong, H., Sonnenblick, L. I., Gruver, R., Almajano, J., Bragin, A., Golshani, P., Trachtenberg, J. T., Peles, E., & Geschwind, D. H. (2011). Absence of CNTNAP2 Leads to Epilepsy, Neuronal Migration Abnormalities, and Core Autism-Related Deficits. *Cell*, *147*(1), 235–246. https://doi.org/10.1016/j.cell.2011.08.040

Penzo, M. A., Robert, V., & Li, B. (2014). Fear Conditioning Potentiates Synaptic Transmission onto Long-Range Projection Neurons in the Lateral Subdivision of Central Amygdala. *The Journal of Neuroscience*, *34*(7), 2432–2437. https://doi.org/10.1523/JNEUROSCI.4166-13.2014

Perry, W., Minassian, A., Lopez, B., Maron, L., & Lincoln, A. (2007). Sensorimotor Gating Deficits in Adults with Autism. *Biological Psychiatry*, *61*(4), 482–486. https://doi.org/10.1016/j.biopsych.2005.09.025

Pfeffer, C. K., Xue, M., He, M., Huang, Z. J., & Scanziani, M. (2013). Inhibition of inhibition in visual cortex: The logic of connections between molecularly distinct interneurons. *Nature Neuroscience*, *16*(8), 1068–1076. https://doi.org/10.1038/nn.3446

Phelps, E. A., & LeDoux, J. E. (2005). Contributions of the Amygdala to Emotion Processing: From Animal Models to Human Behavior. *Neuron*, *48*(2), 175–187. https://doi.org/10.1016/j.neuron.2005.09.025

Pi, H.-J., Hangya, B., Kvitsiani, D., Sanders, J. I., Huang, Z. J., & Kepecs, A. (2013). Cortical interneurons that specialize in disinhibitory control. *Nature*, *503*(7477), 521–524. https://doi.org/10.1038/nature12676

Podsypanina, K., Ellenson, L. H., Nemes, A., Gu, J., Tamura, M., Yamada, K. M., Cordon-Cardo, C., Catoretti, G., Fisher, P. E., & Parsons, R. (1999). Mutation of Pten/Mmac1 in mice causes neoplasia in multiple organ systems. *Proceedings of the National Academy of Sciences of the United States of America*, *96*(4), 1563–1568. https://doi.org/10.1073/pnas.96.4.1563

Poliak, S., Salomon, D., Elhanany, H., Sabanay, H., Kiernan, B., Pevny, L., Stewart, C. L., Xu, X., Chiu, S.-Y., Shrager, P., Furley, A. J. W., & Peles, E. (2003). Juxtaparanodal clustering of Shaker-like K+ channels in myelinated axons depends on Caspr2 and TAG-1. *The Journal of Cell Biology*, *162*(6), 1149–1160. https://doi.org/10.1083/jcb.200305018

Potter, C. J., Pedraza, L. G., & Xu, T. (2002). Akt regulates growth by directly phosphorylating Tsc2. *Nature Cell Biology*, *4*(9), 658–665. https://doi.org/10.1038/ncb840

Powell, S. B., Zhou, X., & Geyer, M. A. (2009). Prepulse inhibition and genetic mouse models of schizophrenia. *Behavioural Brain Research*, *204*(2), 282–294. https://doi.org/10.1016/j.bbr.2009.04.021

Puc, J., & Parsons, R. (2005). PTEN Loss Inhibits CHK1 to Cause Double Stranded-DNA Breaks in Cells. *Cell Cycle*, *4*(7), 927–929. https://doi.org/10.4161/cc.4.7.1795

Puścian, A., Łęski, S., Kasprowicz, G., Winiarski, M., Borowska, J., Nikolaev, T., Boguszewski, P. M., Lipp, H.-P., & Knapska, E. (2016). Eco-HAB as a fully automated and ecologically relevant assessment of social impairments in mouse models of autism. *ELife*, *5*, e19532. https://doi.org/10.7554/eLife.19532

Raftopoulou, M., Etienne-Manneville, S., Self, A., Nicholls, S., & Hall, A. (2004). Regulation of Cell Migration by the C2 Domain of the Tumor Suppressor PTEN. *Science*, *303*(5661), 1179–1181. https://doi.org/10.1126/science.1092089

Rausch, A., Zhang, W., Haak, K. V., Mennes, M., Hermans, E. J., van Oort, E., van Wingen, G., Beckmann, C. F., Buitelaar, J. K., & Groen, W. B. (2016). Altered functional connectivity of the amygdaloid input nuclei in adolescents and young adults with autism spectrum disorder: A resting state fMRI study. *Molecular Autism*, *7*, 13. https://doi.org/10.1186/s13229-015-0060-x

Rippon, G., Brock, J., Brown, C., & Boucher, J. (2007). Disordered connectivity in the autistic brain: Challenges for the 'new psychophysiology.' *International Journal of Psychophysiology*, *63*(2), 164–172. https://doi.org/10.1016/j.ijpsycho.2006.03.012

Risinger, J. I., Hayes, A. K., Berchuck, A., & Barrett, J. C. (1997). PTEN/MMAC1 Mutations in Endometrial Cancers. *Cancer Research*, *57*(21), 4736–4738.

Rubenstein, E., Young, J. C., Croen, L. A., DiGuiseppi, C., Dowling, N. F., Lee, L.-C., Schieve, L., Wiggins, L. D., & Daniels, J. (2019). Brief Report: Maternal Opioid Prescription from Preconception Through Pregnancy and the Odds of Autism Spectrum Disorder and Autism Features in Children. *Journal of Autism and Developmental Disorders*, *49*(1), 376–382. https://doi.org/10.1007/s10803-018-3721-8

Rubenstein, J. L. R., & Merzenich, M. M. (2003). Model of autism: Increased ratio of excitation/inhibition in key neural systems. *Genes, Brain and Behavior*, *2*(5), 255–267. https://doi.org/10.1034/j.1601-183X.2003.00037.x

Samson, A. C., Oswald, H., & Gross, J. J. (2012). Emotion regulation in Asperger's syndrome and high-functioning autism. *Emotion*, *12*(4), 659–665.

Sancak, Y., Thoreen, C. C., Peterson, T. R., Lindquist, R. A., Kang, S. A., Spooner, E., Carr, S. A., & Sabatini, D. M. (2007). PRAS40 Is an Insulin-Regulated Inhibitor of the mTORC1 Protein Kinase. *Molecular Cell*, *25*(6), 903–915. https://doi.org/10.1016/j.molcel.2007.03.003

Sarbassov, D. D., Guertin, D. A., Ali, S. M., & Sabatini, D. M. (2005). Phosphorylation and Regulation of Akt/PKB by the Rictor-mTOR Complex. *Science*, *307*(5712), 1098–1101. https://doi.org/10.1126/science.1106148

Scarani, P., Neroni, S., Giangaspero, F., Orcioni, G. F., & Eusebi, V. (1996). [Carlo Martinotti: The real discoverer of Martinotti's cells]. *Pathologica*, *88*(6), 506–510.

Schmidt, M. J., Horvath, S., Ebert, P., Norris, J. L., Seeley, E. H., Brown, J., Gellert, L., Everheart, M., Garbett, K. A., Grice, T. W., Caprioli, R. M., & Mirnics, K. (2014).

Modulation of behavioral networks by selective interneuronal inactivation. *Molecular Psychiatry*, *19*(5), 580–587. https://doi.org/10.1038/mp.2013.167

Schumann, C. M., & Amaral, D. G. (2006). Stereological Analysis of Amygdala Neuron Number in Autism. *The Journal of Neuroscience*, *26*(29), 7674–7679. https://doi.org/10.1523/JNEUROSCI.1285-06.2006

Selby, L., Zhang, C., & Sun, Q.-Q. (2007). Major defects in neocortical GABAergic inhibitory circuits in mice lacking the fragile X mental retardation protein. *Neuroscience Letters*, *412*(3), 227–232. https://doi.org/10.1016/j.neulet.2006.11.062

Shattuck, P. T. (2006). The Contribution of Diagnostic Substitution to the Growing Administrative Prevalence of Autism in US Special Education. *Pediatrics*, *117*(4), 1028–1037. https://doi.org/10.1542/peds.2005-1516

Shemesh, Y., Sztainberg, Y., Forkosh, O., Shlapobersky, T., Chen, A., & Schneidman, E. (2013). High-order social interactions in groups of mice. *ELife*, *2*, e00759. https://doi.org/10.7554/eLife.00759

Shen, W. H., Balajee, A. S., Wang, J., Wu, H., Eng, C., Pandolfi, P. P., & Yin, Y. (2007). Essential Role for Nuclear PTEN in Maintaining Chromosomal Integrity. *Cell*, *128*(1), 157–170. https://doi.org/10.1016/j.cell.2006.11.042

Sholl, D. A. (1953). Dendritic organization in the neurons of the visual and motor cortices of the cat. *Journal of Anatomy*, *87*(Pt 4), 387-406.1.

Silverman, J. L., Yang, M., Lord, C., & Crawley, J. N. (2010). Behavioural phenotyping assays for mouse models of autism. *Nature Reviews. Neuroscience*, *11*(7), 490–502. https://doi.org/10.1038/nrn2851

Simonoff, E., Jones, C. R. G., Pickles, A., Happé, F., Baird, G., & Charman, T. (2012). Severe mood problems in adolescents with autism spectrum disorder. *Journal of Child Psychology and Psychiatry*, *53*(11), 1157–1166. https://doi.org/10.1111/j.1469-7610.2012.02600.x

Singh, B., Singh, V., Krishnan, A., Koshy, K., Martinez, J. A., Cheng, C., Almquist, C., & Zochodne, D. W. (2014). Regeneration of diabetic axons is enhanced by selective knockdown of the PTEN gene. *Brain*, *137*(4), 1051–1067. https://doi.org/10.1093/brain/awu031

Song, M. S., Salmena, L., & Pandolfi, P. P. (2012). The functions and regulation of the PTEN tumour suppressor. *Nature Reviews Molecular Cell Biology*, *13*(5), 283–296. https://doi.org/10.1038/nrm3330

Sørensen, E. M., Bertelsen, F., Weikop, P., Skovborg, M. M., Banke, T., Drasbek, K. R., & Scheel-Krüger, J. (2015). Hyperactivity and lack of social discrimination in the adolescent Fmr1 knockout mouse. *Behavioural Pharmacology*, *26*(8 Special Issue Pharmacological Approaches To The Study Of Social Behaviour-Part 3: Drug Effects O), 733–740. https://doi.org/10.1097/FBP.0000000000000152

Soria, J.-C., Lee, H.-Y., Lee, J. I., Wang, L., Issa, J.-P., Kemp, B. L., Liu, D. D., Kurie, J. M., Mao, L., & Khuri, F. R. (2002). Lack of PTEN Expression in Non-Small Cell Lung Cancer Could Be Related to Promoter Methylation. *Clinical Cancer Research*, *8*(5), 1178–1184.

Sotres-Bayon, F., Sierra-Mercado, D., Pardilla-Delgado, E., & Quirk, G. J. (2012). Gating of Fear in Prelimbic Cortex by Hippocampal and Amygdala Inputs. *Neuron*, *76*(4), 804–812. https://doi.org/10.1016/j.neuron.2012.09.028

Spencer, C. M., Alekseyenko, O., Serysheva, E., Yuva-Paylor, L. A., & Paylor, R. (2005). Altered anxiety-related and social behaviors in the Fmr1 knockout mouse model of fragile X syndrome. *Genes, Brain and Behavior*, *4*(7), 420–430. https://doi.org/10.1111/j.1601-183X.2005.00123.x

Sperow, M., Berry, R. B., Bayazitov, I. T., Zhu, G., Baker, S. J., & Zakharenko, S. S. (2012). Phosphatase and tensin homologue (PTEN) regulates synaptic plasticity independently of its effect on neuronal morphology and migration. *The Journal of Physiology*, *590*(Pt 4), 777–792. https://doi.org/10.1113/jphysiol.2011.220236

Steck, P. A., Pershouse, M. A., Jasser, S. A., Yung, W. K. A., Lin, H., Ligon, A. H., Langford, L. A., Baumgard, M. L., Hattier, T., Davis, T., Frye, C., Hu, R., Swedlund, B., Teng, D. H. R., & Tavtigian, S. V. (1997). Identification of a candidate tumour suppressor gene, MMAC1 , at chromosome 10q23.3 that is mutated in multiple advanced cancers. *Nature Genetics*, *15*(4), 356–362. https://doi.org/10.1038/ng0497-356

Sun, F., Park, K. K., Belin, S., Wang, D., Lu, T., Chen, G., Zhang, K., Yeung, C., Feng, G., Yankner, B. A., & He, Z. (2011). Sustained axon regeneration induced by co-deletion of PTEN and SOCS3. *Nature*, *480*(7377), 372–375. https://doi.org/10.1038/nature10594

Suzuki, A., de la Pompa, J. L., Stambolic, V., Elia, A. J., Sasaki, T., Barrantes, I. del B., Ho, A., Wakeham, A., ltie, A., Khoo, W., Fukumoto, M., & Mak, T. W. (1998). High cancer susceptibility and embryonic lethality associated with mutation of the PTEN tumor suppressor gene in mice. *Current Biology*, *8*(21), 1169–1178. https://doi.org/10.1016/S0960-9822(07)00488-5

Tamburini, J., Chapuis, N., Bardet, V., Park, S., Sujobert, P., Willems, L., Ifrah, N., Dreyfus, F., Mayeux, P., Lacombe, C., & Bouscary, D. (2008). Mammalian target of rapamycin (mTOR) inhibition activates phosphatidylinositol 3-kinase/Akt by up-regulating insulin-like growth factor-1 receptor signaling in acute myeloid leukemia: Rationale for therapeutic inhibition of both pathways. *Blood*, *111*(1), 379–382. https://doi.org/10.1182/blood-2007-03-080796

Tomioka, R., Okamoto, K., Furuta, T., Fujiyama, F., Iwasato, T., Yanagawa, Y., Obata, K., Kaneko, T., & Tamamaki, N. (2005). Demonstration of long-range GABAergic connections distributed throughout the mouse neocortex. *European Journal of Neuroscience*, *21*(6), 1587–1600. https://doi.org/10.1111/j.1460-9568.2005.03989.x

Tremblay, R., Lee, S., & Rudy, B. (2016). GABAergic Interneurons in the Neocortex: From Cellular Properties to Circuits. *Neuron*, *91*(2), 260–292. https://doi.org/10.1016/j.neuron.2016.06.033

Trimboli, A. J., Cantemir-Stone, C. Z., Li, F., Wallace, J. A., Merchant, A., Creasap, N., Thompson, J. C., Caserta, E., Wang, H., Chong, J.-L., Naidu, S., Wei, G., Sharma, S. M., Stephens, J. A., Fernandez, S. A., Gurcan, M. N., Weinstein, M. B., Barsky, S.

H., Yee, L., … Leone, G. (2009). Pten in Stromal Fibroblasts Suppresses Mammary Epithelial Tumors. *Nature*, *461*(7267), 1084–1091. https://doi.org/10.1038/nature08486

Tye, K. M., & Deisseroth, K. (2012). Optogenetic investigation of neural circuits underlying brain disease in animal models. *Nature Reviews Neuroscience*, *13*(4), 251–266. https://doi.org/10.1038/nrn3171

Ünal, Ç. T., Ünal, B., & Bolton, M. M. (2020). Low-threshold spiking interneurons perform feedback inhibition in the lateral amygdala. *Brain Structure & Function*, *225*(3), 909–923. https://doi.org/10.1007/s00429-020-02051-4

Unal, G., Paré, J.-F., Smith, Y., & Paré, D. (2014). CORTICAL INPUTS INNERVATE CALBINDIN-IMMUNOREACTIVE INTERNEURONS OF THE RAT BASOLATERAL AMYGDALOID COMPLEX. *The Journal of Comparative Neurology*, *522*(8), 1915–1928. https://doi.org/10.1002/cne.23511

Varga, E. A., Pastore, M., Prior, T., Herman, G. E., & McBride, K. L. (2009). The prevalence of PTEN mutations in a clinical pediatric cohort with autism spectrum disorders, developmental delay, and macrocephaly. *Genetics in Medicine*, *11*(2), 111–117. https://doi.org/10.1097/GIM.0b013e31818fd762

Vogel, E., Krabbe, S., Gründemann, J., Wamsteeker Cusulin, J. I., & Lüthi, A. (2016). Projection-Specific Dynamic Regulation of Inhibition in Amygdala Micro-Circuits. *Neuron*, *91*(3), 644–651. https://doi.org/10.1016/j.neuron.2016.06.036

Vogt, D., Cho, K. K. A., Lee, A. T., Sohal, V. S., & Rubenstein, J. L. R. (2015). The Parvalbumin/Somatostatin Ratio Is Increased in Pten Mutant Mice and by

Human PTEN ASD Alleles. *Cell Reports*, *11*(6), 944–956. https://doi.org/10.1016/j.celrep.2015.04.019

Wan, X., Harkavy, B., Shen, N., Grohar, P., & Helman, L. J. (2007). Rapamycin induces feedback activation of Akt signaling through an IGF-1R-dependent mechanism. *Oncogene*, *26*(13), 1932–1940. https://doi.org/10.1038/sj.onc.1209990

Wang, H., Douglas, W., Lia, M., Edelmann, W., Kucherlapati, R., Podsypanina, K., Parsons, R., & Ellenson, L. H. (2002). DNA Mismatch Repair Deficiency Accelerates Endometrial Tumorigenesis in Pten Heterozygous Mice. *The American Journal of Pathology*, *160*(4), 1481–1486.

Wang, S. I., Puc, J., Li, J., Bruce, J. N., Cairns, P., Sidransky, D., & Parsons, R. (1997). Somatic Mutations of PTEN in Glioblastoma Multiforme. *Cancer Research*, *57*(19), 4183–4186.

Wegiel, J., Flory, M., Kuchna, I., Nowicki, K., Ma, S. Y., Imaki, H., Wegiel, J., Cohen, I. L., London, E., Brown, W. T., & Wisniewski, T. (2014). Brain-region–specific alterations of the trajectories of neuronal volume growth throughout the lifespan in autism. *Acta Neuropathologica Communications*, *2*, 28. https://doi.org/10.1186/2051-5960-2-28

Weiskrantz, L. (1956). Behavioral changes associated with ablation of the amygdaloid complex in monkeys. *Journal of Comparative and Physiological Psychology*, *49*(4), 381–391. https://doi.org/10.1037/h0088009

Whissell, P. D., Bang, J. Y., Khan, I., Xie, Y.-F., Parfitt, G. M., Grenon, M., Plummer, N. W., Jensen, P., Bonin, R. P., & Kim, J. C. (2019). Selective Activation of

Cholecystokinin-Expressing GABA (CCK-GABA) Neurons Enhances Memory and Cognition. *ENeuro*, *6*(1). https://doi.org/10.1523/ENEURO.0360-18.2019

Williams, M. R., DeSpenza, T., Li, M., Gulledge, A. T., & Luikart, B. W. (2015). Hyperactivity of Newborn Pten Knock-out Neurons Results from Increased Excitatory Synaptic Drive. *The Journal of Neuroscience*, *35*(3), 943–959. https://doi.org/10.1523/JNEUROSCI.3144-14.2015

Wolff, S. B. E., Gründemann, J., Tovote, P., Krabbe, S., Jacobson, G. A., Müller, C., Herry, C., Ehrlich, I., Friedrich, R. W., Letzkus, J. J., & Lüthi, A. (2014). Amygdala interneuron subtypes control fear learning through disinhibition. *Nature*, *509*(7501), 453–458. https://doi.org/10.1038/nature13258

Wu, X., Hepner, K., Castelino-Prabhu, S., Do, D., Kaye, M. B., Yuan, X.-J., Wood, J., Ross, C., Sawyers, C. L., & Whang, Y. E. (2000). Evidence for regulation of the PTEN tumor suppressor by a membrane-localized multi-PDZ domain containing scaffold protein MAGI-2. *Proceedings of the National Academy of Sciences of the United States of America*, *97*(8), 4233–4238.

Yanagi, S., Kishimoto, H., Kawahara, K., Sasaki, T., Sasaki, M., Nishio, M., Yajima, N., Hamada, K., Horie, Y., Kubo, H., Whitsett, J. A., Mak, T. W., Nakano, T., Nakazato, M., & Suzuki, A. (2007). Pten controls lung morphogenesis, bronchioalveolar stem cells, and onset of lung adenocarcinomas in mice. *The Journal of Clinical Investigation*, *117*(10), 2929–2940. https://doi.org/10.1172/JCI31854

Yao, Y. J., Ping, X. L., Zhang, H., Chen, F. F., Lee, P. K., Ahsan, H., Chen, C.-J., Lee, P.-H., Peacocke, M., Santella, R. M., & Tsou, H. C. (1999). PTEN/MMAC1 mutations in hepatocellular carcinomas. *Oncogene*, *18*(20), 3181–3185. https://doi.org/10.1038/sj.onc.1202659

Yavorska, I., & Wehr, M. (2016). Somatostatin-Expressing Inhibitory Interneurons in Cortical Circuits. *Frontiers in Neural Circuits*, *10*. https://doi.org/10.3389/fncir.2016.00076

Yizhar, O., Fenno, L. E., Prigge, M., Schneider, F., Davidson, T. J., O'Shea, D. J., Sohal, V. S., Goshen, I., Finkelstein, J., Paz, J. T., Stehfest, K., Fudim, R., Ramakrishnan, C., Huguenard, J. R., Hegemann, P., & Deisseroth, K. (2011). Neocortical excitation/inhibition balance in information processing and social dysfunction. *Nature*, *477*(7363), 171–178. https://doi.org/10.1038/nature10360

Yu, K., Ahrens, S., Zhang, X., Schiff, H., Ramakrishnan, C., Fenno, L., Deisseroth, K., Zhao, F., Luo, M.-H., Gong, L., He, M., Zhou, P., Paninski, L., & Li, B. (2017). The central amygdala controls learning in the lateral amygdala. *Nature Neuroscience*, *20*(12), 1680–1685. https://doi.org/10.1038/s41593-017-0009-9

Zablotsky, B., Black, L. I., Maenner, M. J., Schieve, L. A., Danielson, M. L., Bitsko, R. H., Blumberg, S. J., Kogan, M. D., & Boyle, C. A. (2019). Prevalence and Trends of Developmental Disabilities among Children in the United States: 2009–2017. *Pediatrics*, *144*(4). https://doi.org/10.1542/peds.2019-0811

Zhang, J., Wang, J., Zhao, F., Liu, Q., Jiang, K., & Yang, G. (2010). MicroRNA-21 (miR-21) represses tumor suppressor PTEN and promotes growth and invasion in non-small cell lung cancer (NSCLC). *Clinica Chimica Acta*, *411*(11), 846–852. https://doi.org/10.1016/j.cca.2010.02.074

Zoncu, R., Efeyan, A., & Sabatini, D. M. (2011). mTOR: From growth signal integration to cancer, diabetes and ageing. *Nature Reviews. Molecular Cell Biology*, *12*(1), 21–35. https://doi.org/10.1038/nrm3025

Zori, R. T., Marsh, D. J., Graham, G. E., Marliss, E. B., & Eng, C. (1998). Germline PTEN mutation in a family with Cowden syndrome and Bannayan-Riley-Ruvalcaba syndrome. *American Journal of Medical Genetics*, *80*(4), 399–402.

Zukor, K., Belin, S., Wang, C., Keelan, N., Wang, X., & He, Z. (2013). Short Hairpin RNA against PTEN Enhances Regenerative Growth of Corticospinal Tract Axons after Spinal Cord Injury. *The Journal of Neuroscience*, *33*(39), 15350–15361. https://doi.org/10.1523/JNEUROSCI.2510-13.2013